CARBON NANOMATERIAL/THERMOPLASTIC POLYURETHANE COMPOSITES FOR SPORTS APPLICATION: PREPARATION, CHARACTERIZATION AND SIMULATION

JING QIFEI

School of Materials Science and Engineering

Nanyang Technological University

&

Wolfson School of Mechanical and Manufacturing Engineering

Loughborough University

2016

CARBON NANOMATERIAL/THERMOPLASTIC POLYURETHANE COMPOSITES FOR SPORTS APPLICATION: PREPARATION, CHARACTERIZATION AND SIMULATION

JING QIFEI

School of Materials Science and Engineering
Nanyang Technological University
&
Wolfson School of Mechanical and Manufacturing Engineering
Loughborough University

A thesis submitted to the Nanyang Technological University and Loughborough University in partial fulfilment of the requirement for the Joint Degree of Doctor of Philosophy

2016

Abstract

Carbon nanomaterials have been widely studied in various fields since their discovery. Their ultrahigh surface-to-volume ratios, low density, as well as outstanding thermal and mechanical properties, make them excellent candidates as nanofillers for high-performance and light-weight polymer composites. The major objectives of this project include two aspects: i) preparation of polyurethane (PU)-based composites reinforced by chemically functionalized multi-walled carbon nanotubes (MWCNTs) and graphene oxide (GO), respectively, with improved mechanical properties and thermal stability; ii) conducting the finite-element analysis (FEA) with Abaqus/Standard to study the mechanical performance of PU and the GO/PU composite under conditions of large-deflection bending typical for shoe soles.

First, MWCNTs were covalently functionalized to fabricate thermoplastic PU-based composites with enhanced performance. Polycaprolactone diol (PCL), as one of PU's monomers in this work, and was selectively used to functionalize MWCNTs to prepare MWCNT-PCL so as to realize a good compatibility between the nanofillers and PU matrix. Besides, the raw MWCNTs and carboxylic acid groups functionalized MWCNTs (MWCNT-COOH) served as control. It was found that both MWCNT-COOH and MWCNT-PCL showed better dispersion states in the PU matrix, as well as improved interfacial interactions with the matrix. In terms of mechanical properties and thermal stability, MWCNT-PCL/PU composite exhibited the greatest extent of improvement with addition of 1 wt% MWCNT-PCL. The achieved remarkable reinforcement effect of MWCNT-PCL was attributed to their homogeneous dispersion in the PU matrix and strong interfacial interactions with the matrix.

Then, GO, with abundant oxygen functional groups, was studied as nanofiller for PU-based composites. To achieve a well exfoliated and stable GO suspension in an organic solvent (dimethylformamide, DMF), 4, 4′- methylenebis (phenyl isocyanate) (MDI) and PCL, two monomers for synthesizing PU, were selectively used to functionalize GO. The obtained functionalized GO (FGO) could form homogeneous dispersions in the DMF

solvent and PU matrix, as well as provide a good compatibility with the PU matrix. The most efficient improvement of mechanical properties was achieved when 0.4 wt% FGO was added into the PU matrix. Regarding the thermal stability, PU filled with 1 wt% FGO showed the largest extent of improvement. The improved dispersion of FGO in the PU matrix and strong interfacial interactions between them could contribute to the improvement in mechanical properties and thermal stability of FGO/PU composites.

Thermoplastic PU elastomers are used as shoe-sole materials due to many excellent properties but their inelastic deformation is a serious deficiency for such applications. Hence, GO was introduced into the synthesized thermoplastic PU to produce a GO/PU composite material with enhanced properties. Plastic behavior of this composite was assessed in cyclic tensile tests, demonstrating reduction of irreversible deformations with the addition of GO. Additionally, in order to evaluate mechanical performance of PU and the GO/PU composite under conditions of large-deflection bending typical for shoe soles, finite-element simulations with Abaqus/Standard were conducted. An elastic-plastic finite-element model was developed to obtain detailed mechanical information for PU and the GO/PU composite. The numerical study demonstrated that the plastic area, final specific plastic dissipation energy and residual height for PU specimens were significantly larger than those for the GO/PU composite. Besides, the addition of GO into the PU matrix greatly delayed the onset of plastic deformation in PU in a large-deflection bending process. The finite-element analysis provided quantification of the effect of GO enhancement on the large-deflection bending performance of PU for regimes typical for shoe soles and can be used as a basis for optimization of real composite products.

Acknowledgements

I would like to express my sincere gratitude and appreciation to my supervisors, Prof. Dong Zhili and Prof. Li Lin from NTU, Singapore, and Prof. Vadim V. Silberschmidt from LU, UK, for their great support, encouragement and patient instruction in the course of my Ph.D. study.

My gratitude also goes to my research group members for their inspiration and assistance, especially Dr. Pan Yongzheng, Dr. Liu Qiang, Zhang Lizhi, Yao Lei, Lua Shun Kuang, Wang Jingxian, Xia Jing, Gao Xing, Gayan Aravinda Abeygunawardane, Emrah Sozumert, Laurence Coles, Osman Bayrak and Alessandro Schiavone. Besides, I would like to thank Dr. Tang Xiuzhi, Dr. Law Jiayan, Dr. Liu Wanshuang, Dr. Phua Silei, Chen Xuelong, and Li Linlin for their kind sharing of knowledge. Also, I thank Prof. Tan Lay Poh's group and Prof. Lu Xuehong's group for their experimental assistance.

I would like to acknowledge Institute for Sports Research (ISR), NTU, for providing me the opportunity to join the NTU-LU Joint Ph.D. Program.

Finally, I would like to express my gratitude to all my friends for their company and sharing of experience. Most importantly, this work is dedicated to my family and girlfriend, Miss Liao Yanwan, for their continuous support and encouragement.

Table of Contents

Table Captions

Figure Captions

Abbreviations

1,4-BD	1,4-butanediol
AmimCl	1-allyl-methylimidazolium chloride
ASTM	American society for testing and materials
ATR	Attenuated total reflectance
BEI	Backscatter electron images
BSE	Backscattered electron
CNTs	Carbon nanotubes
CS	Chitosan
CVD	Chemical vapor decomposition
DBTDL	Dibutyltin dilaurate
DI	water Deionized water
DMA	Dynamic mechanical analysis
DMF	N, N-dimethylformamide
EDA	Ethylenediamine
EDS	Energy dispersive X-ray spectroscopy
FEA	Finite-element analysis
FESEM	Field-emission scanning electron microscopy
FTIR	Fourier transform infrared spectroscopy
G"	Loss modulus
G'	Storage modulus
GO	Graphene oxide

MDI	4, 4′-methylenebis (phenyl isocyanate)
MOCA	Methylene-bis-ortho-chloroanilline
MWCNTs	Multi-walled carbon nanotubes
PA	Polyamide
PCL	Polycaprolactone diol
PET	Poly(ethylene terephthalate)
PMMA	Poly(methyl methacrylate)
PP	Polypropylene
PS	Polystyrene
PU	Polyurethane
PVA	Poly(vinyl alcohol)
SAED	Selected area electron diffraction
SEI	Secondary electron images
SEM	Scanning electron microscopy
SMP	Shape memory polymer
SWCNTs	Single-walled carbon nanotubes
TEM	Transmission electron microscopy
TGA	Thermogravimetric analysis
TPU	Thermoplastic polyurethane
XRD	X-ray diffraction
ε	Strain
σ	Stress

Chapter 1 Introduction

1.1 Background

Polymer composites reinforced by carbon nanomaterial have attracted tremendous attention in recent decades. The incorporation of carbon nanomaterial could usually modify the properties of polymer matrixes and greatly broaden their applications in various fields, such as magnetic manipulation and targeting [1], water treatment [2], fuel cell [3], sensitive detection [4], electromagnetic interference shielding [5], shape memory applications [6], drug delivery [7], enhancement of mechanical properties [8], thermal stability [9]. Nanomaterials are particles with at least one dimension at nanometer scale. As an important class of nanomaterials, carbon nanomaterials, including fullerenes, nanodiamonds, carbon nanofibers, carbon nanotubes (CNTs), graphene, carbon nanocones-disks and nanohorns, have been widely studied since their discovery [10]. Their ultrahigh surface-to-volume ratios, low density, as well as outstanding thermal and mechanical properties, make them promising candidates as nanofillers for high-performance and light-weight polymer composite materials.

Among them, CNTs are one of the most promising nanofillers. With a cylindrical nanostructure, CNTs own a high aspect ratio of typically 300-1000, and a large specific surface area of approximate 1000 m^2/g [11]. The remarkable mechanical properties of CNTs were demonstrated experimentally, with the elastic moduli of multi-walled carbon nanotubes (MWCNTs) reported to be as high as 1.8 TPa [12] and the tensile strength of

individual multi-walled carbon nanotube being in the range of 11-63 GPa [13]. Moreover, CNTs show superior thermal properties. The room-temperature thermal conductivity of a single-walled carbon nanotube along the axis was tested to be about 3500 $W \cdot m^{-1} \cdot K^{-1}$ [14], which is about ten times as large as that of copper. Also, its thermal stability could reach approximately 750 ℃ in air and 2800 ℃ in vacuum [15]. High stiffness and strength, low density, and high thermal conductivity and stability of CNTs make them very attractive for preparation of composite materials.

Since the single-layer graphene was obtained by Geim and Novoselov in 2004 [16], research into graphene has been one of the fastest growing areas. Graphene, a one-atom-thick hexagonal lattice of sp^2 carbon atoms, exhibits a two-dimensional sheet-like structure. It was proven experimentally to be the strongest material developed so far [17], with a large specific surface area (theoretical value 2630 m^2/g) [18]. For fabrication of polymer composites, bulk quantities of nanofillers are necessary. Under this circumstance, graphene oxide (GO) has been extensively studied as an alternative to graphene. The established advantages of GO in production yield and cost make it a very promising candidate as the nanofiller. In addition, massive oxygen functional groups on its surfaces and edges enable it to be easily modified for better compatibility with the polymer matrix.

Polyurethane (PU) is an important class of polymers, which has been widely used in various applications such as foams, coatings, elastomers and adhesives. Thermoplastic PU elastomers have been used in many sporting applications such as ski tips, ski boots, fins for surfboards, goggles and inline skates. Besides, they have been introduced in

athletic footwear since 1970's, and are mostly used as outsole materials for rugby, American football, golf and soccer shoes, and so on [19]. In this study, thermoplastic PU elastomer was chosen as the polymer matrix to prepare PU-based composite.

1.2 Problem statement and motivation

To produce high-performance polymer composites reinforced with carbon nanomaterials, it is widely acknowledged that the following two factors should be addressed: first, carbon nanomaterials tend to aggregate because of van der Waals forces, preventing homogeneous dispersion in polymer matrices; second, a lack of sufficient interfacial interaction between the nanomaterials and polymer matrices greatly compromises the reinforcing effect of the nanomaterials. In this situation, specific functionalization of the carbon nanomaterials according to the target polymer matrix becomes necessary.

Besides, studying the performance of materials in real-life applications is much more complicated than analysis of their basic properties in experiments. Extending analysis of material's behavior to cases of in-service conditions typical to those of real-life products is very challenging, especially when non-linear factors are considered. Therefore, the numerical simulation method is applied in this study, owning to its advantages in terms of comprehensive information presented and low costs when compared to parametric experimental studies.

1.3 Scope and objective of the project

This project includes two aspects: first, preparing PU-based composites reinforced by functionalized MWCNTs and GO, respectively, with improved mechanical properties and thermal stability. In order to achieve better compatibility between the nanofillers and PU matrix, the MWCNTs and GO will be specifically functionalized based on their particular physical structures and chemical properties, as well as the PU matrix. The effect of the studied functionalization approach on the dispersion of nanofillers in the PU matrix is to be investigated together with the derived mechanical properties and thermal stability of the composites; second, conducting finite-element analysis (FEA) with Abaqus/Standard software to study the mechanical performance of PU and its composite under conditions of large-deflection bending typical for shoe soles. Detailed mechanical information obtained from the FEA will be used to quantitatively reveal the effect of nano-enhancement on the large-deflection bending performance of PU.

The objective of this project consists of three parts of research work as follows:

(1) To obtain PU-based composites with specifically functionalized MWCNTs. In order to achieve a better compatibility between MWCNTs and the PU matrix, raw MWCNTs are to be chemically functionalized with carboxylic acid groups and polycaprolactone diol (PCL) (one of PU's monomers). The dispersion of the functionalized MWCNTs in the PU matrix, as well as the interfacial interactions between them, are expected to

improve. The mechanical properties and thermal stability of the obtained composites will also be investigated.

(2) To improve the dispersions of GO in the organic solvent and PU matrix through chemical functionalization. The high hydrophilicity of GO does not favor the exfoliation in organic solvents, e.g. DMF. Considering the abundant oxygen functional groups of GO, 4, 4′-methylenebis (phenyl isocyanate) (MDI) and PCL are to be sequentially grafted onto GO to obtain the functionalized GO (FGO). The FGO is expected to show better dispersions in both DMF solvent and the PU matrix, as well as to improve the mechanical properties and thermal stability of PU.

(3) To reveal the effect of GO enhancement on the large-deflection bending performance of PU through numerical simulations. Based on the study in part (2), GO will be added into the PU matrix to fabricate a GO/PU composite. The effect of GO on plastic properties of PU is to be investigated experimentally by means of cyclic tensile tests. Then, an elastic-plastic finite-element model will be developed to obtain the detailed mechanical information for PU and the GO/PU composite under conditions of large-deflection bending typical for shoe soles. Results of numerical analysis for the in-service behavior of the studied materials are expected to be useful for the real product optimization.

1.4 Structure of the thesis

The thesis consists of six chapters. Chapter 1 provides an introduction to the thesis. Chapter 2 reviews the literature concerning the fundamentals of CNTs and GO, and corresponding polymer-based composites. The elastic-plastic behavior of a material is also reviewed. In Chapter 3, the effect of chemical functionalization of MWCNTs on mechanical properties and thermal stability of PU is studied. In Chapter 4, dispersions of GO after functionalization with MDI and PCL in both DMF solvent and the PU matrix are studied. Then, mechanical properties and thermal stability of FGO/PU composites with different loading contents are discussed. Chapter 3 and 4 study the enhancing effect of nanomaterials in PU by experiments. In Chapter 5, FEA with Abaqus/Standard is conducted to assess the effect of GO enhancement on the large-deflection bending performance of PU for regimes typical for shoe soles. At last, Chapter 6 summarizes the important findings of this project and proposes recommendations for future research.

References

[1] Quyen Chau ND, Ménard-Moyon C, Kostarelos K, Bianco A. Multifunctional carbon nanomaterial hybrids for magnetic manipulation and targeting. Biochemical and Biophysical Research Communications. (0).

[2] Yin J, Deng B. Polymer-matrix nanocomposite membranes for water treatment. Journal of Membrane Science. 2015;479(0):256-75.

[3] Kim DJ, Jo MJ, Nam SY. A review of polymer–nanocomposite electrolyte membranes for fuel cell application. Journal of Industrial and Engineering Chemistry. 2015;21(0):36-52.

[4] Ma Y, Xu S, Wang S, Wang L. Luminescent molecularly-imprinted polymer nanocomposites for sensitive detection. TrAC Trends in Analytical Chemistry. 2015;67(0):209-16.

[5] Moon Y-E, Yun J, Kim H-I. Synergetic improvement in electromagnetic interference shielding characteristics of polyaniline-coated graphite oxide/γ-Fe2O3/BaTiO3 nanocomposites. Journal of Industrial and Engineering Chemistry. 2013;19(2):493-7.

[6] Meng H, Li G. A review of stimuli-responsive shape memory polymer composites. Polymer. 2013;54(9):2199-221.

[7] Iliescu RI, Andronescu E, Ghitulica CD, Voicu G, Ficai A, Hoteteu M. Montmorillonite–alginate nanocomposite as a drug delivery system – incorporation and in vitro release of irinotecan. International Journal of Pharmaceutics. 2014;463(2):184-92.

[8] Xiong QL, Meguid SA. Atomistic investigation of the interfacial mechanical characteristics of carbon nanotube reinforced epoxy composite. European Polymer Journal. 2015;69(0):1-15.

[9] Amirian M, Nabipour Chakoli A, Cai W, Sui J. Effect of functionalized multiwalled carbon nanotubes on thermal stability of poly (L-LACTIDE) biodegradable polymer. Scientia Iranica. 2013;20(3):1023-7.

[10] Zhang B-T, Zheng X, Li H-F, Lin J-M. Application of carbon-based nanomaterials in sample preparation: A review. Analytica Chimica Acta. 2013;784(0):1-17.

[11] Yamabe T, Fukui K, Tanaka K. The science and technology of carbon nanotubes: Elsevier; 1999.

[12] Treacy MJ, Ebbesen T, Gibson J. Exceptionally high Young's modulus observed for individual carbon nanotubes. 1996.

[13] Yu M-F, Files BS, Arepalli S, Ruoff RS. Tensile loading of ropes of single wall carbon nanotubes and their mechanical properties. Physical review letters. 2000;84(24):5552.

[14] Pop E, Mann D, Wang Q, Goodson K, Dai H. Thermal conductance of an individual single-wall carbon nanotube above room temperature. Nano letters. 2006;6(1):96-100.

[15] Thostenson ET, Li C, Chou T-W. Nanocomposites in context. Composites Science and Technology. 2005;65(3–4):491-516.

[16] Novoselov KS, Geim AK, Morozov S, Jiang D, Zhang Y, Dubonos Sa, et al. Electric field effect in atomically thin carbon films. Science. 2004;306(5696):666-9.

[17] Lee C, Wei X, Kysar JW, Hone J. Measurement of the elastic properties and intrinsic strength of monolayer graphene. Science. 2008;321(5887):385-8.

[18] Liu Q, Shi J, Zeng L, Wang T, Cai Y, Jiang G. Evaluation of graphene as an advantageous adsorbent for solid-phase extraction with chlorophenols as model analytes. Journal of Chromatography A. 2011;1218(2):197-204.

[19] Ames KA. Elastomers for shoe applications. Rubber chemistry and technology. 2004;77(3):413-75.

Chapter 2 Literature Review

2.1 Carbon nanotubes

2.1.1 Properties of CNTs

Since first reported by Iijima in 1991 [1], carbon nanotubes (CNTs) have become a research focus because of their unique structure and remarkable properties. CNTs are allotropes of carbon with a cylindrical nanostructure, consisting of a sp^2 carbon-bonding network that contributes to their extraordinary properties. Based on the number of walls, CNTs could be divided into two types: single-walled carbon nanotubes (SWCNTs) and multi-walled carbon nanotubes (MWCNTs). Their structures are presented in Figure 2.1. SWCNT could be viewed as a one-atom-thick single layer of graphite which is wrapped into a cylinder structure, while MWCNT could be considered as multiple layers of graphite with concentric tubes. The typical diameters for SWCNTs and MWCNTs are several nanometers and 10-50 nm, respectively, while the typical length of CNTs could range from one micron to tens of microns.

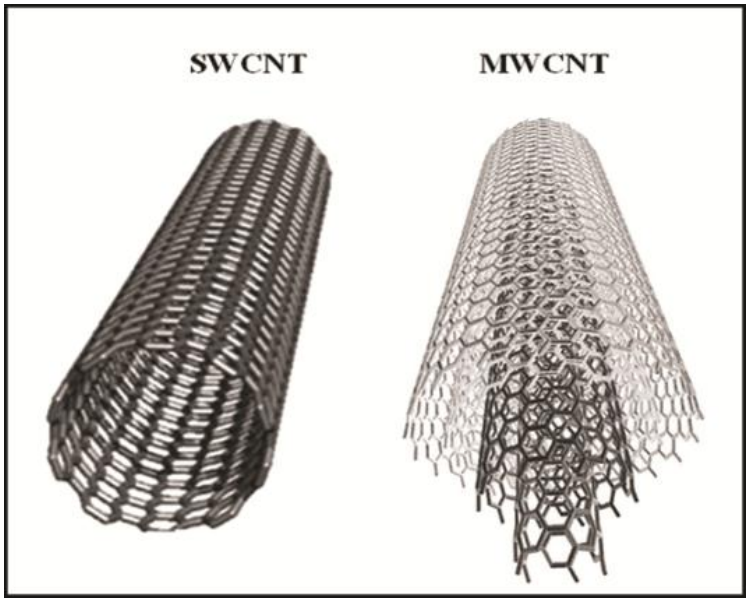

Figure 2.1 Structures of SWCNT and MWCNT [2]

With a cylindrical nanostructure, CNTs have a high aspect ratio of typically 300-1000, and a large specific surface area of approximate 1000 m^2/g [3]. The remarkable mechanical properties of CNTs were demonstrated experimentally, with the elastic moduli of multi-walled carbon nanotubes (MWCNTs) reported to be as high as 1.8 TPa [4] and the tensile strength of individual multi-walled carbon nanotube being in the range of 11-63 GPa [5]. Additionally, CNTs show superior thermal properties. Room-temperature thermal conductivity of a SWCNT along the axis was tested to be about 3500 $W\ m^{-1}\ K^{-1}$ [6], which is about ten times as large as that of copper (385 $W\ m^{-1}\ K^{-1}$). On the other hand, its room-temperature thermal conductivity across the axis is only 1.64 $W\ m^{-1}\ K^{-1}$ [7], almost as low as soil. Also, its thermal stability could reach approximately 750 ℃ in air and 2800 ℃ in vacuum [8]. High stiffness and strength, low

density, and high thermal conductivity and stability of CNTs make them very attractive in preparing reinforced composite materials.

2.1.2 Synthesis of CNTs

There are three main methods widely applied to synthesize CNTs: arc discharge [9], laser ablation [10] and chemical vapor deposition (CVD) [11]. Each method has its own strengths and weaknesses in terms of quality and cost of products. Among them, the CVD method is the most popular one, especially for commercial purpose, attributed to its low cost and large-scale production ranging from kilograms to tons. The classical CVD method to synthesize CNTs is usually conducted in a high-temperature tube furnace, with hydrocarbons serving as feedstock. Many kinds of hydrocarbons have been studied as the feedstock, such as benzene [12], carbon monoxide [13], ethylene [14] and methane [11]. Transition metal nanoparticles with high surface areas are often utilized as the catalysts [15]. The growth mechanism of the CVD method could be briefly explained in three steps: firstly, hydrocarbon molecules are dissociated with the transition metal nanoparticles as catalysts; secondly, the carbon atoms are dissolved and saturated in the transition metal nanoparticles; thirdly, tubular carbon solid in the form of sp^2-bonding structure is generated as the carbon atoms precipitate from the saturated transition metal nanoparticles. It is noteworthy that the properties of the synthesized CNTs, such as lengths, diameters, defects and chirality, vary greatly with the synthesis process.

2.2 Graphene oxide

2.2.1 Properties of graphene and graphene oxide

Graphene, a one-atom-thick hexagonal lattice of sp^2 carbon atoms, has been widely studied as nanofiller used to prepare polymer-based composites. Compared to CNTs, extensive attention was only paid to graphene recently. Especially after the single-layer graphene was obtained by Geim and Novoselov in 2004 [16], research on graphene has been one of the fastest growing areas. Its lower cost and naturally abundant source make it a competitive candidate as nanofiller. Graphene exhibits a two-dimensional sheet-like structure. A typical interlayer spacing between graphene layers is 3.35Å, and the length of carbon-carbon bond in the graphene layer is approximate 0.14 nm. Besides, graphene was proven experimentally to be the strongest material developed so far (breaking strength of 42 N/m) [17], with a large specific surface area (theoretical value - 2630 m^2/g) [18]. Its thermal conductivity could be as high as about 5000 $W\ m^{-1}\ K^{-1}$.

For the purpose of preparing polymer composites reinforced with graphene, bulk quantities of nanofillers are necessary. Under this circumstance, graphene oxide (GO) has been extensively investigated as an alternative to graphene. The established advantages of GO in production yield and cost make it very attractive as nanofiller. GO, having the same framework as graphene, contains massive oxygen functional groups such as epoxide, hydroxyl, carboxyl and carbonyl groups located at its edges and basal planes [19-22], as illustrated in Figure 2.2. The presence of these massive oxygen functional

groups makes GO highly hydrophilic. Hence, GO can be readily dispersed in water and form a stable colloidal suspension. However, the strong hydrophilicity of GO was found to prevent its full exfoliation in organic solvents. In addition, the oxygen functional groups on the surfaces and edges of GO could act as active reaction sites for further chemical functionalization, thus opening a promising route for obtaining functionalized GO with desired properties, as well as corresponding polymer composites.

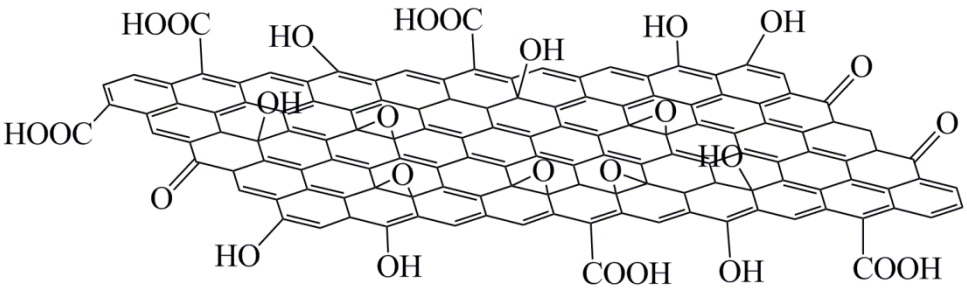

Figure 2.2 Schematic model of GO

2.2.2 Synthesis of graphene oxide

The widely used methods to synthesize GO from graphite are the Staudenmaier method [23], Hummers method [24] and some slightly modified versions based on these methods. Despite different reagents used in the reaction process, all these methods involve the oxidation of graphite in the presence of oxidants and strong acids. The oxidation level of graphite varies significantly with the reaction process and the amounts of reagents. To be more specific, the Staudenmaier method applies a mixture of nitric acid (HNO_3) and potassium chlorate ($KClO_3$) to treat graphite, while a combination of sulfuric acid

(H_2SO_4), sodium nitrate ($NaNO_3$) and potassium permanganate ($KMnO_4$) is used to oxidize graphite in the Hummers method. The Hummers method is safer as it produces nitric acid *in situ*, and thus the usage of highly corrosive fuming nitric acid could be avoided. Despite the absence of fuming nitric acid, the combination of $KMnO_4$ and $NaNO_3$ results in a more heavily oxygenated form of graphite oxide. As a result, the Hummers method has been very well accepted and adopted by many researchers. It should be noted that properties of the synthesized GO have been demonstrated to be dependent on not only the reaction conditions and oxidants utilized but also the graphite source [25].

2.3 Polyurethane

Polyurethane (PU) is a polymer consisting of chains of organic units by urethane links (-RNHCOOR′-). To fabricate PU, isocyanates (R-(N=C=O) $_{n \geq 2}$) and polyols (R′-(OH) $_{n \geq 2}$) are reacted (as illustrated in Figure 2.3), with the addition of certain catalysts, chain extender and/or surfactants. Based on the polyols used, PU could be divided into two types: polyester PU and polyether PU. The types of isocyanates and polyols have a significant influence on the final properties of the PU product. PU is described to contain alternating hard and soft segments. The soft segment is contributed by polyols, while the hard segment is composed of isocyanates and chain extender molecules, etc. Due to the thermodynamic incompatibility of these two segments, PU usually presents a two-phase morphology. In general, the hard segment primarily influences the stiffness and determines the upper-use temperature of PU due to its capability to keep associated along

with the rising temperature, while the soft segment mainly affects the elasticity and low-temperature performance of PU [26, 27]. The properties of PU could be easily tailored by alternating different hard and soft segments.

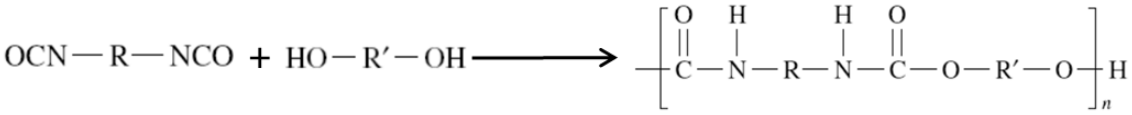

Figure 2.3 Generalized reaction between isocyanate and polyol

PU is one of the most versatile polymers with a wide range of chemical and physical properties. It provides a unique combination of the elasticity of rubber materials with the durability and toughness of metal materials [28]. Besides, most manufacturing techniques in the polymer processing field could be applied to PU, which contributes to PU's broad range of applications. For example, PU is applied to fabricate durable elastomeric wheels and tires, surface sealants and coatings, hoses, carpet underlay, condoms, high-performance adhesives, automotive suspension bushings, flexible and high-resilience foam seating, microcellular foam gaskets, electrical potting compounds, synthetic fibers and rigid foam insulation panels, etc. In addition, PU has been employed in the sport industry for many years. Many sporting applications use PU elastomers, including ski tips, ski boots, fins for surfboards, goggles and inline skates. Also, since the 1970's PU elastomers were introduced in athletic footwear, and are mostly used as outsole materials for rugby, American football, golf and soccer shoes, and so on [29].

2.4 Preparation methods of carbon nanomaterials/polymer composites

In order to obtain carbon nanomaterials/polymer composites with significantly improved properties, a lot of efforts have been spent on different preparation methods since they could greatly influence the dispersion status of nanomaterials in the polymer matrix. There are mainly three methods used for the preparation of carbon nanomaterials/polymer composites, as introduced below.

2.4.1 Melt processing

This melt processing method is widely applied to a broad range of commercial polymers, from high-polarity nylon to slightly polar poly (ethylene terephthalate) and to essentially non-polar polystyrene. During the melt processing, an applied high shear force expedites the dispersion of carbon nanomaterials under high temperature above the melting point of polymers. This method is quite popular in the industrial field because it is environmentally friendly and economical due to the absence of solvents. However, it's found that the melt processing is not very effective at dispersing the carbon nanomaterials in the polymer matrix. Also, it is limited to low loading contents of nanomaterials. The melt processing conditions have been studied to obtain optimized dispersion and properties of the polymer composites. For example, in Krause's work [30], polyamide (PA)/MWCNTs composites were prepared via a small-scale melt processing method with different conditions, such as mixing time, rotation speed and processing temperature. It was found that dispersion of MWCNTs and electrical volume resistivity of the obtained

composites varied significantly with different mixing conditions. A long mixing time, a low rotation speed and a high processing temperature were demonstrated to be the best conditions, leading to minimum electrical volume resistivity of the 5 wt% PA/MWCNTs composites.

2.4.2 Solution mixing

The solution mixing is probably the most popular method for various polymers, which could be dissolved in certain solvents. In this method, a large amount of solvent is used to disperse nanomaterials and dissolve polymers, while different mechanical agitations are adopted to facilitate the dispersion of nanomaterials in the polymer matrix. Generally, these mechanical agitations include mechanical shearing, magnetic stirring and ultrasonication, which are effective at breaking up the aggregations of nanomaterials. In terms of homogeneously dispersing the nanomaterials in the polymer matrix, the solution mixing method is proven to be very efficient and effective. But the need of a large amount of solvent for this method leads to a high cost and harms to environment, making it not favorable for large-scale industrial production of nanomaterials/polymer composites. Considering that nanomaterials need to be dispersed in a certain solvent prior to blending with the polymer solution, the solubility and stability of nanomaterials in the solvent turn to be of great importance. As a result, functionalization (covalent or non-covalent) of nanomaterials has become a promising route to produce homogeneous dispersion. As discussed above, GO is highly hydrophilic, and can be readily dispersed in water and form a stable colloidal suspension. Thus GO is an attractive nanofiller for

water-soluble polymers such as PVA and chitosan (CS). For example, Liang *et al.* [31] prepared GO/PVA composites using the simple solution mixing method with water serving as solvent. The GO sheets were observed finely-dispersed in the PVA matrix, and efficient stress transfer was found between the GO and PVA matrix. Mechanical properties of the prepared GO/PVA composites were significantly improved, with a 76% increase (from 49.9 to 87.6 MPa) in tensile strength and a 62% increase (from 2.13 to 3.45 GPa) in Young's modulus at only 0.7 wt% loading content of GO.

2.4.3 *In situ* polymerization

The *in-situ* polymerization method is reported to be applicable to fabricate polymer composites with high loading contents of nanomaterials, such as polypropylene, epoxy, etc. [32, 33]. This method often involves mixing nanomaterials with a monomer, prepolymer or their solutions so that the nanomaterials will participate in the polymerization process of polymers. Covalent linkages are generally produced between the nanomaterials and polymer matrix in this method, offering strong interfacial interactions between them. Besides, thanks to low viscosity of the monomer or monomer solution, it is easier to obtain a more homogeneous dispersion of nanomaterials compared to that in the solution mixing method. However, the incorporation of nanomaterials in the synthesis process of polymers may have a detrimental effect on the synthesis, resulting in a decrease of molecular weight of polymer chains. Thus, this method requires highly stringent synthesis conditions. In order to form covalent linkages with the polymer matrix, the nanomaterials are usually functionalized prior to blending. For example, Tseng *et al.*

[34] reported MWCNTs/epoxy composites prepared via the *in-situ* polymerization method. The MWCNTs were functionalized with maleic anhydride (MA), which was shown to be grafted on their surfaces. Owing to the reaction between the MA-functionalized MWCNTs and diamine curing agent, the MA-functionalized MWCNTs were covalently bonded to the epoxy matrix. The final MWCNTs/epoxy composite presented great improvements in both mechanical properties and electrical conductivity. With only 1 wt% loading of the MA-functionalized MWCNTs, the tensile strength and modulus of the composite were increased by more than 50% and 100%, respectively. Also, the electrical conductivity of the composite with 1 wt% MA-functionalized MWCNTs was increased to 2.6×10^{-4} S/m, which was two orders higher than that of pristine epoxy.

2.5 Carbon nanomaterials/polyurethane composites

Carbon nanomaterials exhibit outstanding mechanical and thermal properties, which make them very attractive as nanofillers for preparing polymer-based composites. Both CNTs and GO could be used as excellent nanofillers to fabricate polymer-based composites with improved mechanical and thermal properties. In general, the reinforcing effect introduced by carbon nanomaterials is mainly influenced by the dispersion state of carbon nanomaterials in the polymer matrix and the interfacial interactions between them. The carbon nanomaterials tend to aggregate due to van der Waals forces, leading to a decrease of the contact areas between the nanofillers and polymer matrix, which would induce stress concentration in the matrix and even deteriorate mechanical properties of

the polymer matrix. Besides, a lack of sufficient interfacial interactions between nanofillers and the polymer matrix allows nanofillers to slide easily in the matrix under external forces, limiting the effective stress transfer between them. In this situation, functionalization (covalent or non-covalent) of carbon nanomaterials became a promising route to obtain effectively reinforced polymer composites. Xiong and co-workers [35] covalently functionalized MWCNTs with methylene-bis-ortho-chloroanilline (MOCA) to obtain amide-terminated MWCNTs. The amide-terminated MWCNTs reacted with monomers of PU to prepare a pre-polymer. Then, a certain stoichiometric number of chain extender, depending on the amount of isocyanate groups ascertained by titration, was added into the pre-polymer to fabricate MWCNTs/PU composites. The obtained results showed that the MOCA-functionalized MWCNTs were linked with PU chains by chemical bonds, and they could homogeneously disperse in the matrix at a content of 2 wt%. The 2 wt% MOCA-functionalized MWCNTs/PU composite, prepared by the *in-situ* polymerization method, demonstrated significantly improved mechanical properties and thermal stability. Non-covalent functionalization of graphene was also reported. Ma *et al*. [36] found that reduced GO could be non-covalent functionalized with 1-allyl-methylimidazolium chloride (AmimCl) through π-π and cation-π interactions, which benefited the dispersion of reduced GO in the PU matrix and interfacial interaction between them.

The *in-situ* polymerization method requires highly stringent synthesis conditions to avoid a possible detrimental effect of nanomaterials on the synthesis of polymers. And, the non-covalent functionalization usually provides a weak interaction, leading to a poor

reinforcing effect of nanomaterials. So, it is of great interest to develop an efficient and effective way to prepare polyurethane composites reinforced by nanomaterials. In general, a good compatibility between the nanofiller and polymer matrix is crucial for high-performance composites. Considering that the monomer of a polymer is generally well compatible with the polymer itself due to their structural similarity, the approach based on the use of monomer-functionalized nanomaterials is expected to be very promising in enhancing the performance of composites, such as mechanical and thermal properties.

2.6 Elastic-plastic behavior

In physics and materials science, elastic deformation is used to describe the phenomenon when a material deforms under an applied force and returns to its original shape after a force removal. The material behaves elastically until the applied force rises beyond the elastic limit, which is also known as the *yield stress*, indicated by point 2 in Figure 2.4. Beyond the yield stress, the material experiences permanent deformation and fails to return to its original shape when the force is removed, termed *plastic deformation*. In the plastic deformation region, the strain (ε) at a certain point on the curve (i.e. point 3) could be decomposed into two parts: elastic strain (ε_e) and plastic strain (ε_p), as shown in the following relation [37]:

$$\varepsilon = \varepsilon_e + \varepsilon_p \tag{1}$$

It's notable that the elastic modulus (E) of the material will remain the same in both elastic and plastic regions.

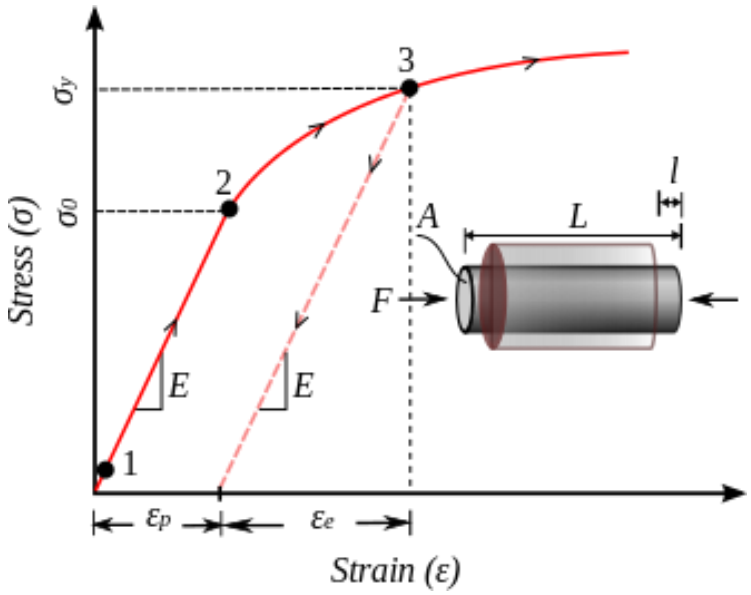

Figure 2.4 Typical uniaxial stress-strain curve showing an elastic-plastic behavior

Currently, there are several classical theoretical models to describe the elastic-plastic behaviors, as shown in Figure 2.5. Figure 2.5 (1) presents a pure linear elastic behavior, while Figures 2.5 (2), (3) and (4) demonstrate different elastic-plastic behaviors. Figure 2.5 (2) shows an elastic-perfect plastic behavior, indicating that the material experiences irreversible deformation under a constant stress in the plastic region. Figure 2.5 (3) exhibits a linear hardening in the plastic deformation region, while the stress-strain relationship of the plastic deformation in Figure 2.5 (4) is described by a power function.

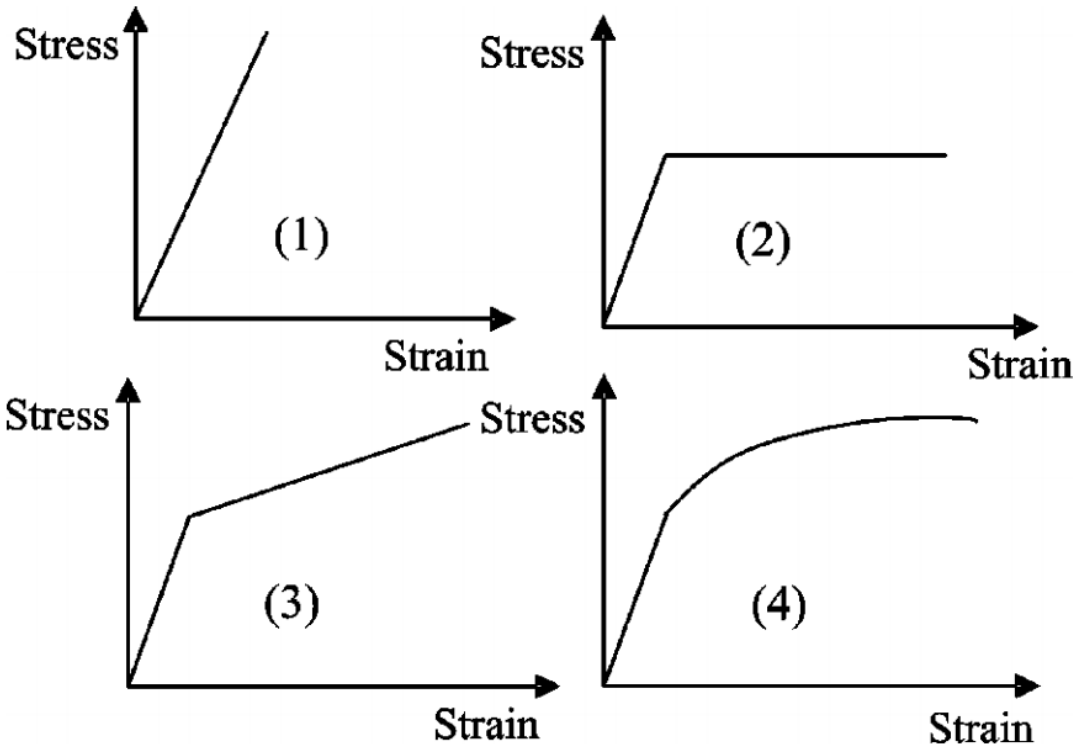

Figure 2.5 Stress-strain relationships: pure linear elastic (1); elastic-perfect plastic (2); linear hardening (3); power law hardening (4) [38]

2.7 Summary

In this chapter, the fundamentals of CNTs, GO and PU were reviewed. The preparation of carbon nanomaterials/polymer composites and the elastic-plastic behavior of a material were also introduced. The remarkable properties of CNTs and GO, such as their high aspect ratio, excellent mechanical and thermal properties, make them very attractive as nanofillers for preparing polymer-based composites. In general, the reinforcing effect of nanomaterials is greatly affected by their dispersion states in the polymer matrix and the interfacial interactions between them. Still, due to the incompatibility between the

nanomaterials and polymer matrix, it still remains challenging to achieve the theoretical values of properties of nanomaterials in the polymer-based composites. As a result, it is of great interest to develop an effective functionalization method for nanomaterials to provide good compatibility with the polymer matrix, thus contributing to the reinforcing effect of nanomaterials.

References

[1] Iijima S. Helical microtubules of graphitic carbon. nature. 1991;354(6348):56-8.

[2] Choudhary V, Gupta A. Polymer/Carbon Nanotube Nanocomposites2011.

[3] Yamabe T, Fukui K, Tanaka K. The science and technology of carbon nanotubes: Elsevier; 1999.

[4] Treacy MJ, Ebbesen T, Gibson J. Exceptionally high Young's modulus observed for individual carbon nanotubes. 1996.

[5] Yu M-F, Files BS, Arepalli S, Ruoff RS. Tensile loading of ropes of single wall carbon nanotubes and their mechanical properties. Physical review letters. 2000;84(24):5552.

[6] Pop E, Mann D, Wang Q, Goodson K, Dai H. Thermal conductance of an individual single-wall carbon nanotube above room temperature. Nano letters. 2006;6(1):96-100.

[7] Sinha S, Barjami S, Iannacchione G, Schwab A, Muench G. Off-axis thermal properties of carbon nanotube films. Journal of Nanoparticle Research. 2005;7(6):651-7.

[8] Thostenson ET, Li C, Chou T-W. Nanocomposites in context. Composites Science and Technology. 2005;65(3–4):491-516.

[9] Ebbesen T, Ajayan P. Large-scale synthesis of carbon nanotubes. Nature. 1992;358(6383):220-2.

[10] Guo T, Nikolaev P, Thess A, Colbert DT, Smalley RE. Catalytic growth of single-walled manotubes by laser vaporization. Chemical Physics Letters. 1995;243(1–2):49-54.

[11] Kong J, Cassell AM, Dai H. Chemical vapor deposition of methane for single-walled carbon nanotubes. Chemical Physics Letters. 1998;292(4):567-74.

[12] Cheng H, Li F, Su G, Pan H, He L, Sun X, et al. Large-scale and low-cost synthesis of single-walled carbon nanotubes by the catalytic pyrolysis of hydrocarbons. Applied Physics Letters. 1998;72(25):3282-4.

[13] Dai H, Rinzler AG, Nikolaev P, Thess A, Colbert DT, Smalley RE. Single-wall nanotubes produced by metal-catalyzed disproportionation of carbon monoxide. Chemical Physics Letters. 1996;260(3):471-5.

[14] Hafner JH, Bronikowski MJ, Azamian BR, Nikolaev P, Rinzler AG, Colbert DT, et al. Catalytic growth of single-wall carbon nanotubes from metal particles. Chemical Physics Letters. 1998;296(1):195-202.

[15] Su M, Zheng B, Liu J. A scalable CVD method for the synthesis of single-walled carbon nanotubes with high catalyst productivity. Chemical Physics Letters. 2000;322(5):321-6.

[16] Novoselov KS, Geim AK, Morozov S, Jiang D, Zhang Y, Dubonos Sa, et al. Electric field effect in atomically thin carbon films. science. 2004;306(5696):666-9.

[17] Lee C, Wei X, Kysar JW, Hone J. Measurement of the elastic properties and intrinsic strength of monolayer graphene. Science. 2008;321(5887):385-8.

[18] Liu Q, Shi J, Zeng L, Wang T, Cai Y, Jiang G. Evaluation of graphene as an advantageous adsorbent for solid-phase extraction with chlorophenols as model analytes. Journal of Chromatography A. 2011;1218(2):197-204.

[19] Lerf A, He H, Forster M, Klinowski J. Structure of graphite oxide revisited. The Journal of Physical Chemistry B. 1998;102(23):4477-82.

[20] Hontoria-Lucas C, López-Peinado AJ, López-González JdD, Rojas-Cervantes ML, Martín-Aranda RM. Study of oxygen-containing groups in a series of graphite oxides: Physical and chemical characterization. Carbon. 1995;33(11):1585-92.

[21] Stankovich S, Piner RD, Nguyen ST, Ruoff RS. Synthesis and exfoliation of isocyanate-treated graphene oxide nanoplatelets. Carbon. 2006;44(15):3342-7.

[22] Erickson K, Erni R, Lee Z, Alem N, Gannett W, Zettl A. Determination of the local chemical structure of graphene oxide and reduced graphene oxide. Advanced Materials. 2010;22(40):4467-72.

[23] Staudenmaier L. Method for the preparation of graphitic acid. Deutsche Chemische Gesellschaft. 1898;31:1481-7.

[24] William S, Hummers J, Offeman RE. Preparation of graphitic oxide. Journal of the American Chemical Society. 1958;80(6):1339.

[25] Dreyer DR, Park S, Bielawski CW, Ruoff RS. The chemistry of graphene oxide. Chemical Society Reviews. 2010;39(1):228-40.

[26] Gum WF, Riese W, Ulrich H. Reaction polymers : polyurethanes, epoxies, unsaturated polyesters, phenolics, special monomers, and additives : chemistry, technology, applications, markets / edited by Wilson F. Gum, Wolfram Riese, and Henri Ulrich with contributions from the following authors, Lou M. Alberino ... [et al.]:

Munich ; New York : Hanser Publishers ; New York : Distributed in the U.S.A. and Canada by Oxford University Press, c1992.; 1992.

[27] Oertel G, Abele L. Polyurethane handbook : chemistry, raw materials, processing, application, properties / edited by Günter Oertel with contributions from L. Abele ... [et al.]: Munich ; New York : Hanser Publishers ; New York : Distributed in the USA by Macmillan Pub. Co., c1985.; 1985.

[28] Petrović ZS, Ferguson J. Polyurethane elastomers. Progress in Polymer Science. 1991;16(5):695-836.

[29] Ames KA. Elastomers for shoe applications. Rubber chemistry and technology. 2004;77(3):413-75.

[30] Krause B, Pötschke P, Häußler L. Influence of small scale melt mixing conditions on electrical resistivity of carbon nanotube-polyamide composites. Composites Science and Technology. 2009;69(10):1505-15.

[31] Liang J, Huang Y, Zhang L, Wang Y, Ma Y, Guo T, et al. Molecular ‐ level dispersion of graphene into poly (vinyl alcohol) and effective reinforcement of their nanocomposites. Advanced Functional Materials. 2009;19(14):2297-302.

[32] Du K, He AH, Liu X, Han CC. High ‐ Performance Exfoliated Poly (propylene)/Clay Nanocomposites by In Situ Polymerization with a Novel Z ‐ N/Clay Compound Catalyst. Macromolecular Rapid Communications. 2007;28(24):2294-9.

[33] Usuki A, Hasegawa N, Kato M, Kobayashi S. Polymer-clay nanocomposites. Inorganic Polymeric Nanocomposites and Membranes: Springer; 2005. p. 135-95.

[34] Tseng C-H, Wang C-C, Chen C-Y. Functionalizing carbon nanotubes by plasma modification for the preparation of covalent-integrated epoxy composites. Chemistry of Materials. 2007;19(2):308-15.

[35] Xiong J, Zheng Z, Song W, Zhou D, Wang X. Microstructure and properties of polyurethane nanocomposites reinforced with methylene-bis-ortho-chloroanilline-grafted multi-walled carbon nanotubes. Composites Part A: Applied Science and Manufacturing. 2008;39(5):904-10.

[36] Ma W-S, Wu L, Yang F, Wang S-F. Non-covalently modified reduced graphene oxide/polyurethane nanocomposites with good mechanical and thermal properties. Journal of Materials Science. 2014;49(2):562-71.

[37] Dieter GE, Bacon D. Mechanical metallurgy: McGraw-Hill New York; 1986.

[38] Wang F, Keer LM. Numerical Simulation for Three Dimensional Elastic-Plastic Contact with Hardening Behavior. Journal of Tribology. 2005;127(3):494-502.

Chapter 3 Preparation, characterization and properties of polycaprolactone diol-functionalized multi-walled carbon nanotube/polyurethane composite*

Multi-walled carbon nanotubes (MWCNTs) were covalently functionalized to fabricate thermoplastic polyurethane (PU)-based composites with enhanced performance. Polycaprolactone diol (PCL), as one of PU's monomers in this work, and was selectively used to functionalize MWCNTs to prepare MWCNT-PCL so as to realize a good compatibility between the nanofillers and PU matrix. Besides, the raw MWCNTs and carboxylic acid groups functionalized MWCNTs (MWCNT-COOH) served as control. It was found that both MWCNT-COOH and MWCNT-PCL showed a better dispersion in the PU matrix, as well as improved interfacial interactions with the matrix. In terms of mechanical properties and thermal stability, MWCNT-PCL/PU composite exhibited the greatest extent of improvement with addition of 1 wt% MWCNT-PCL. The achieved remarkable reinforcing effect of MWCNT-PCL was attributed to their homogeneous dispersion in the PU matrix and strong interfacial interactions with the matrix.

*The work in Chapter 3 is reprinted (adapted) with permission from Jing Q, Law JY, Tan LP, Silberschmidt VV, Li L, Dong Z. Composites Part A: Applied Science and Manufacturing. 2015;70:8-15. Copyright 2015 Elsevier. Jing Q is the main contributor to this paper, responsible for the project design, experiments and paper writing. Law JY and Tan LP provided assistance during the experiments. Silberschmidt VV, Li L and Dong Z offered guidance and advices on experiments and paper writing.

3.1 Introduction

Since reported in 1991, carbon nanotubes (CNTs) have attracted extensive attention due to their unique physical structures and outstanding properties [1]. In the past decade, enormous effort has been put into applying CNTs in various fields, such as electromechanical actuators [2], nanoprobes for high-resolution imaging [3], nanowires [4], electrochemical biosensors [5, 6] and many other applications [7, 8]. In particular, polymer-based composite reinforced by CNTs is one of the fastest growing fields. Many polymers have been investigated for being used as the composites matrices, e.g. liquid crystalline polymers [9], poly(methyl methacrylate) [10], polystyrene [11], poly(vinyl alcohol) [12] and polypyrrole [13]. The remarkable thermal, electrical and mechanical properties of CNTs, along with their ultra-high aspect ratios, enable them to be used as excellent nanofillers [14-16].

Nevertheless, the reinforcing effect of CNTs in the polymer-based composites is usually limited because of the following two reasons [17, 18]: (i) CNTs have a strong tendency to aggregate due to the van der Waals forces. As a result, it is very challenging to disperse CNTs in the polymer matrix homogeneously. (ii) The interfacial interactions between CNTs and the polymer matrix are generally very weak, which makes CNTs easily slide in the matrix under external forces, leading to an ineffective stress transfer between the two phases. Chemical functionalization of CNTs has been demonstrated to be an effective method to solve these problems [17, 19, 20]. As for CNTs, the acid-treatment method is widely applied for chemical functionalization. Generally, this method involves two steps:

firstly, CNTs are treated with oxidants to introduce carboxylic acid groups onto their surface defect sites [21, 22]; secondly, the grafted carboxylic acid groups can be further converted into other functional groups, such as acyl chloride, amide [9, 23]. Those functional groups on the surfaces of CNTs could directly react with some polymers and/or their monomers, which open a new route for chemical functionalization of CNTs based on different polymers.

Polyurethane (PU), as one of the most versatile polymers, is used widely as foam, adhesive, coating, thermoplastic elastomer, etc. As a block copolymer with alternating hard and soft segments, the molecular structure of PU could be easily tailored to meet specific property requirements [24]. There are mainly three methods to fabricate CNTs/polymer composite including solution mixing, melt processing and *in situ* polymerization. Among them, solution mixing method might be the most popular one because of its feasibility and simplicity. In additional, another advantage of this method is that the de-aggregation and dispersion of CNTs could be significantly improved by agitations, which usually come from shear mixing, ultrasonication, reflux or magnetic stirring [25].

In this work, aiming at achieving a homogeneous dispersion of MWCNTs in the PU matrix, as well as strong interfacial interactions between them, two types of chemical moieties (carboxylic acid groups and polycaprolactone diol (PCL)) were grafted to the surfaces of MWCNTs. Considering PCL is one of the monomers of PU, a good compatibility between PCL-functionalized MWCNTs (MWCNT-PCL) and the PU matrix

is expected due to their structural similarity. Raw MWCNTs, carboxylic acid groups functionalized MWCNTs (MWCNT-COOH) and MWCNT-PCL were added into the PU matrix to fabricate three kinds of MWCNTs/PU composites by the solution mixing method. The functionalized MWCNTs were characterized in detail to confirm the covalent linkage. In addition, the results obtained from FESEM, TEM, TGA and tensile tests were presented and discussed.

3.2 Experimental

3.2.1 Materials

The MWCNTs (95 wt% of purity) were obtained from Cheap Tubes Inc (USA), with an outer diameter of 8-15 nm and length of 10-50 μm. Concentrated nitric acid (HNO_3, 69-70%, Honeywell) and sulfuric acid (H_2SO_4, 95-97%, Honeywell), tetrahydrofuran (THF, Anhydrosolv, Tritech Scientific), anhydrous dimethylformamide (DMF, Tritech Scientific) and Acetone (Aik Moh) were used as received. 4, 4′-methylenebis (phenyl isocyanate) (MDI, molecular weight 250.25 g/mol), PCL (average Mn ~2000 g/mol and ~530 g/mol), dibutyltin dilaurate (DBTDL), thionyl chloride ($SOCl_2$) and 1,4-butanediol (BD, molecular weight 90.12 g/mol) were all purchased from Sigma-Aldrich.

3.2.2 Functionalization of MWCNTs

MWCNT-COOH was prepared through the following process: raw MWCNTs (1g) were dispersed in 100 ml mixture of H_2SO_4/ HNO_3 (volumetric ratio 3:1) with the assistance of

ultrasonication. Afterwards, the mixture was gradually heated to 90 ℃ and remained for 0.5 h with vigorous magnetic stirring under reflux. Then, the reaction system was diluted and filtered via a filter of 0.22 μm Millipore membrane. The obtained powders were subsequently washed, filtered until the filtrate became neutral. At last, the acid-treated MWCNTs were collected and desiccated to a constant weight.

$SOCl_2$ was applied for further functionalization to prepare MWCNT-PCL. The as-prepared MWCNT-COOH was dispersed in $SOCl_2$ with the assistance of ultrasonication. Afterwards, the mixture was kept in a 65 ℃ oil bath under reflux for 24 h. After that, the mixture was filtered via a 0.22 μm polytetrafluoroethylene (PTFE) membrane filter. Dry acetone was used to wash the filter cake to obtain an acyl chloride intermediate MWCNT-COCl solid. The solid was immediately transferred into a solution of PCL (average Mn ~530 g/mol) in dry THF and stirred at 60 ℃ for another 24 h. Then, the reaction mixture was filtered, washed and dried to give MWCNT-PCL. The schematic for preparing MWCNT-COOH and MWCNT-PCL is presented in Figure 3.1.

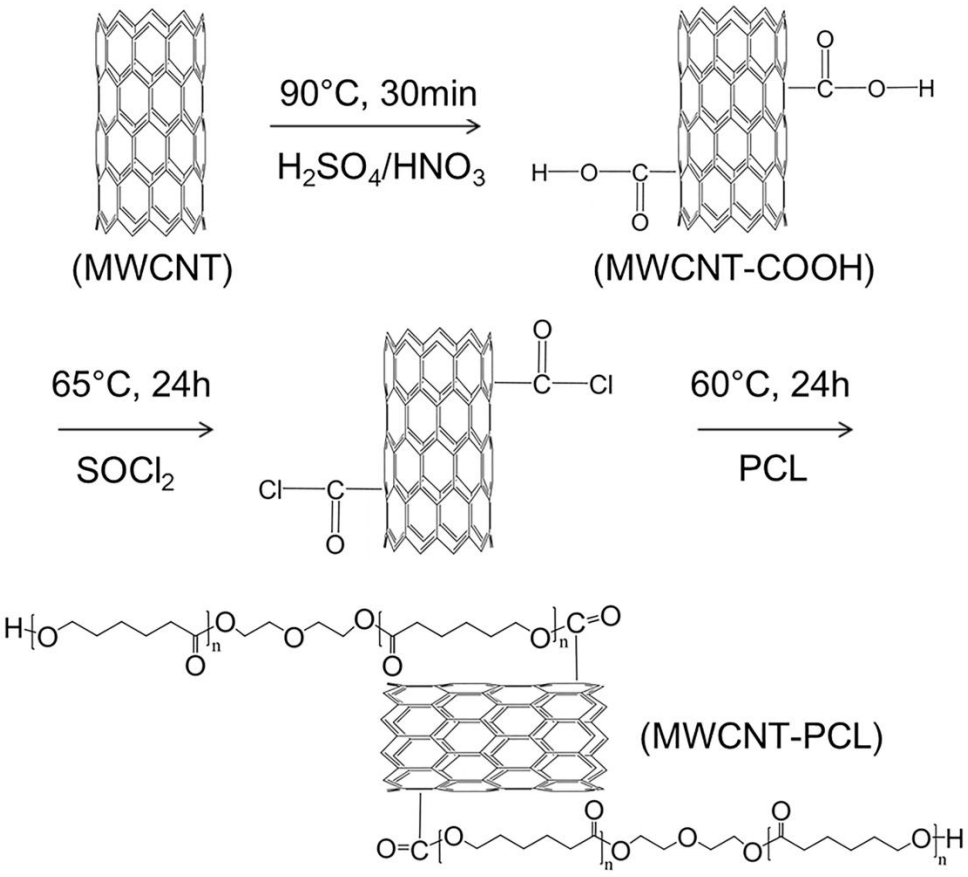

Figure 3.1 Schematic for preparation of MWCNT-COOH and MWCNT-PCL

3.2.3 Fabrication of MWCNTs/PU composites

PU was synthesized by a prepolymerization method using MDI and PCL as two monomers, BD and DBTDL as the chain extender and catalyst, respectively [26]. A molar ratio of 1:6:5 of PCL: MDI: BD was used, leading to 50.6 wt% of soft segment. The MWCNTs/PU composite films were prepared by the solution mixing method. For the MWCNT-PCL/PU composite film, the process was described as follows: MWCNT-PCL was firstly dispersed in DMF solution at a concentration of 0.6 g/L and

ultrasonicated at room temperature for 1.5 h. A certain amount of as-prepared pure PU was added into the solution and dissolved with the aid of magnetic stirring. After PU was completely dissolved, the mixture was continuously stirred at room temperature for 48 h [27], followed by ultrasonication for another 1.5 h. Finally, the MWCNT-PCL/PU composite film was obtained through solution casting. The other two composite films (raw MWCNT/PU and MWCNT-COOH/PU) were fabricated under the same process, while a pure PU film was prepared without adding any MWCNTs. In this work, the loading contents of MWCNTs for all the three kinds of MWCNTs/PU composites were fixed at 1 wt%. The weight percent of functionalized MWCNTs in the composite was calculated based on the weight of MWCNTs before functionalization, which didn't include the amount of grafted functional groups or PCL which was determined by TGA as exhibited later.

3.2.4 Characterization

FTIR spectroscopic measurements were performed using a FTIR Frontier (Perkin Elmer) equipped with an Attenuated Total Reflection (ATR). For the sample preparation, the powder sample was firstly mixed and ground with potassium bromide. Then, the mixture was pressed into a round transparent pellet using a pellet-forming die. ATR was used to obtain the FTIR spectra of film samples. Confocal Raman spectroscopy (Witec alpha300 SR) was employed to investigate the structural change of MWCNTs with a 633 nm laser as the light source. Thermo-gravimetric analysis (TGA) tests were conducted to study the functionalization degrees of MWCNT-COOH and MWCNT-PCL, using a TGA Q500.

The powder samples were heated from 25 ℃ to 900 ℃ at a speed of 10 ℃/min under nitrogen. Besides, the film samples were heated from 25 ℃ to 600 ℃ at a speed of 10 ℃/min under nitrogen using the same TGA equipment to investigate the thermal stability of MWCNTs/PU composites. Field Emission Scanning Electron Microscopy (FESEM, JSM-7600F) was applied to observe the morphological features of composite films. For the sample preparation, the films were broken in liquid nitrogen and sputtered with a thin layer of platinum using a sputter coater. Transmission Electron Microscopy (TEM) observation was conducted with a Carl Zeiss LIBRA®120 in-column energy filter TEM equipped with an integrated OMEGA filter. Leica Ultracut UCT was used to microtome the film samples in order to obtain flakes with a thickness of about 50-100 nm for TEM observation. Tensile Tester Instron 5567 (Instron, USA) was applied to study the mechanical properties of MWCNTs/PU composites based on the ASTM D638 at an extension speed of 100 mm/min. The gauge length of the specimen was 9.5 mm and five specimens were tested for each composite.

3.3 Results and Discussion

3.3.1 Characterization of functionalized MWCNTs

The FTIR spectra of raw MWCNT, MWCNT-COOH, MWCNT-PCL and PCL are shown in Figure 3.2. After acid treatment, one significant peak at 3434 cm^{-1} could be observed, which was attributed to the O-H stretching of carboxylic acid group. In addition, the two peaks at around 1726 cm^{-1} and 1210 cm^{-1} could be associated with the

C=O and C-O stretching, respectively. The results demonstrated that carboxylic acid groups were successfully grafted onto the surfaces of MWCNTs. As can be seen in Figure 3.1, the MWCNT-COOH was further treated with $SOCl_2$ and then reacted with PCL to obtain MWCNT-PCL. Figure 3.2 also reveals that PCL has been grafted onto MWCNTs. Except for the peaks at about 3434 cm^{-1} (O-H stretching), 1726 cm^{-1} (C=O stretching) and 1210 cm^{-1} (C-O stretching), several new peaks appeared for MWCNT-PCL, as compared with MWCNT-COOH. The peaks at approximate 2943 cm^{-1} and 2867 cm^{-1} were associated with the asymmetrical and symmetrical stretching vibrations of the C-H bonds of methylene groups in the alkane chain [28]. The peaks at about 1458 cm^{-1} and 1089 cm^{-1} could be associated with the CH_2 bending and C-O-C stretching modes, respectively [29].

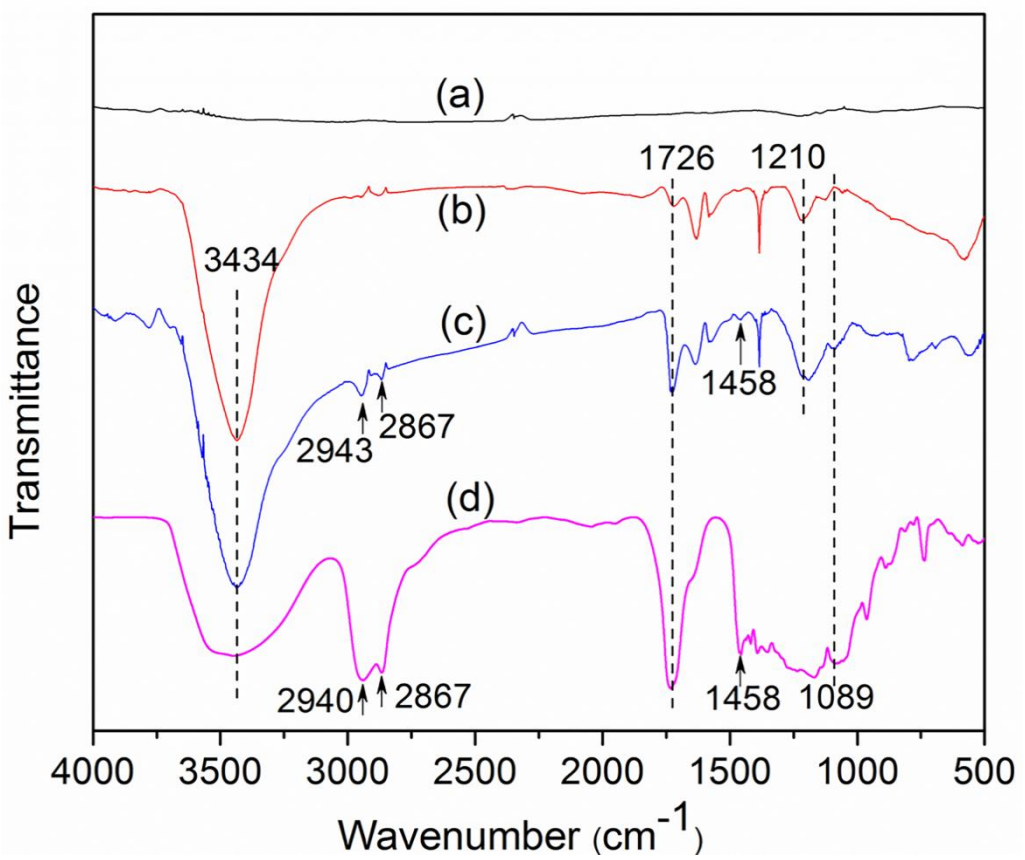

Figure 3.2 FTIR spectra of raw MWCNT (a), MWCNT-COOH (b), MWCNT-PCL (c) and PCL (d)

The functionalization of MWCNTs was studied by Raman tests as well. As presented in Figure 3.3, the band at around 1579 cm^{-1} corresponded to tangential mode (G-band), which was related to the ordered sp^2-hybridized carbon network. The band at around 1360 cm^{-1} corresponded to disorder mode (D-band), which was attributed to surface defects of MWCNTs [30]. The functionalization degree of MWCNTs could be determined by the intensity ratio of the D-band and G-band (I_D/I_G) [31]. It is obvious that I_D and I_G changed greatly after functionalization. The intensity ratios (I_D/I_G) of MWCNT-COOH and MWCNT-PCL were 0.96 and 0.97, respectively, while raw MWCNT's I_D/I_G

was only 0.72. This result showed that defects or functional groups were formed on the surfaces of MWCNTs after chemical functionalization. Additionally, I_D/I_G of MWCNT-PCL was marginally larger than that of MWCNT-COOH, which might be due to the electrical–structure change of MWCNT-COOH caused by $SOCl_2$ treatment [32]. Besides, compared with raw MWCNT, the D-band and G-band of the functionalized MWCNTs (MWCNT-COOH and MWCNT-PCL) shifted towards higher wavenumbers by 6 and 9 cm^{-1}, respectively. This may originate from the covalent functionalization of organic moieties onto the surface of raw MWCNT.

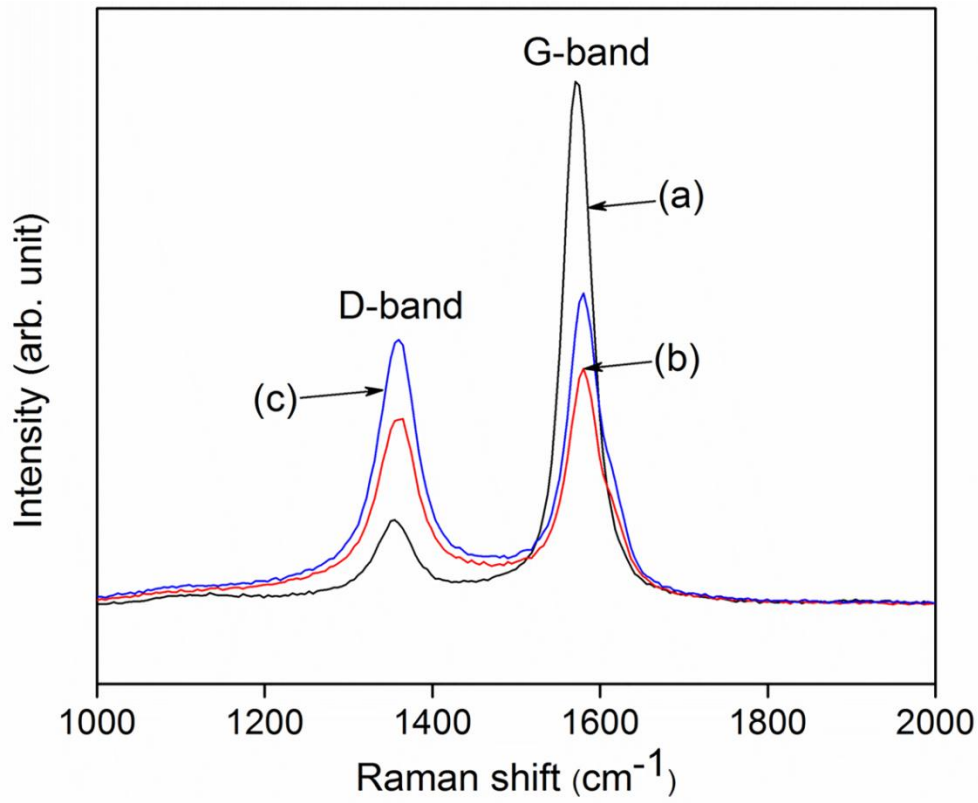

Figure 3.3 Raman spectra of raw MWCNT (a), MWCNT-COOH (b) and MWCNT-PCL (c)

The results of FTIR and Raman analysis are further supported by TEM and TGA tests. As shown in Figure 3.4a, the raw MWCNT presented a comparatively smooth and clean surface owning to its complete lattice structure of carbon network. But, the edges of MWCNT-COOH (Figure 3.4b) appeared to be very rough because of the attachment of carboxylic acid groups on their surfaces. In addition, it can be seen from Figure 3.4c that a core-shell structure consisting of a PCL layer as the shell and MWCNT as the core is formed for MWCNT-PCL, indicating that the MWCNT was coated by a layer of PCL chains. It is notable that the thickness of PCL layer wrapped on MWCNTs' surface is not uniform, which might be attributed to the inhomogeneous defect sites generated on MWCNTs' surface [33]. The TGA results also confirmed the successful functionalization of functional groups and PCL on the surface of MWCNTs. From the TGA curves of raw MWCNT, MWCNT-COOH, and MWCNT-PCL in Figure 3.5, the amounts of grafted functional groups and PCL on the surface of MWCNTs for MWCNT-COOH and MWCNT-PCL were estimated to be approximate 9 wt% and 16 wt%, respectively.

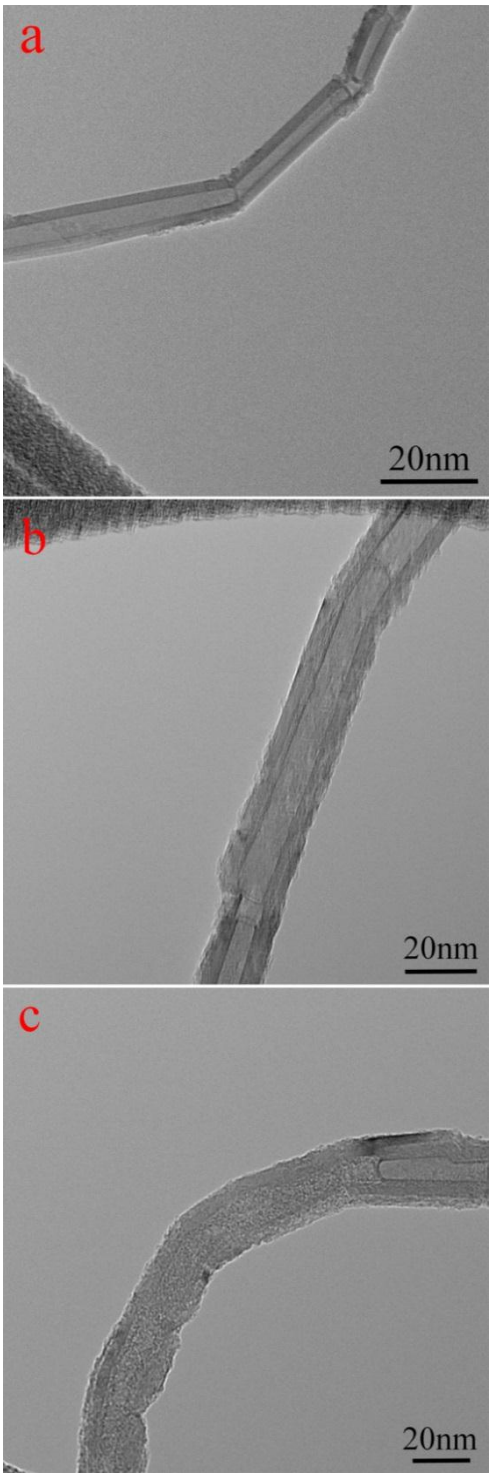

Figure 3.4 TEM images of raw MWCNT (a), MWCNT-COOH (b) and MWCNT-PCL (c)

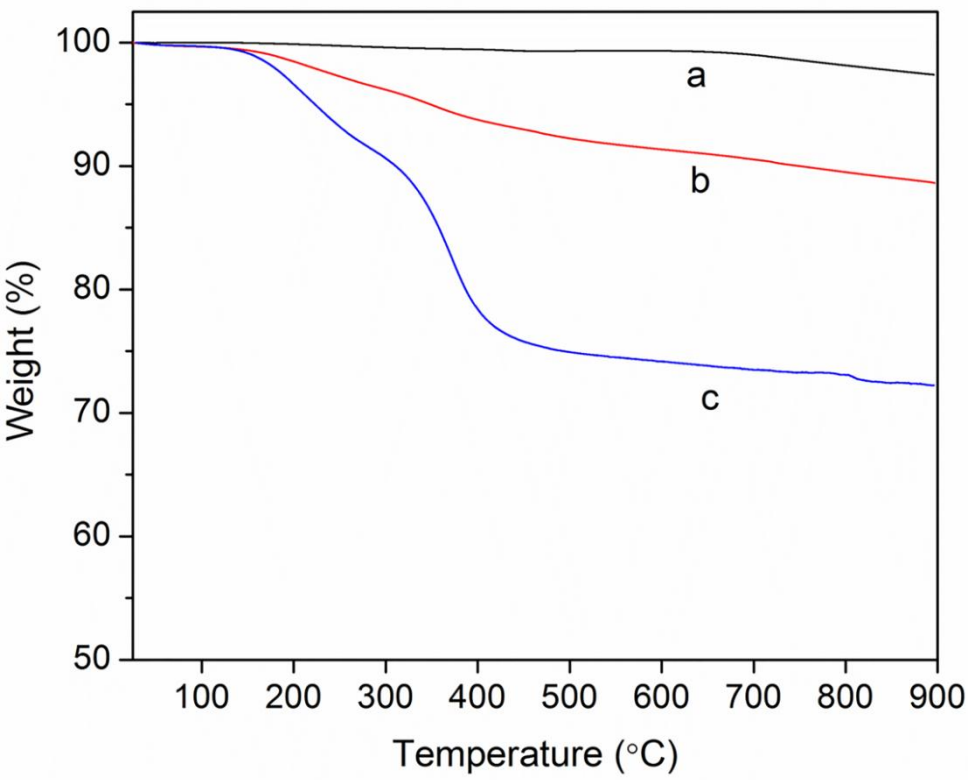

Figure 3.5 TGA curves of raw MWCNT (a), MWCNT-COOH (b) and MWCNT-PCL (c)

3.3.2 Interaction between MWCNTs and PU

For the MWCNTs/PU composites, the interfacial bonding between MWCNTs and the PU matrix was studied by FTIR analysis based on the shift of absorption peak of certain key group in the PU matrix. Figure 3.6 presents the FTIR spectra of pure PU, raw MWCNT/PU, MWCNT-COOH/PU and MWCNT-PCL/PU composites. The peak at 3332 cm^{-1} in Figure 3.6a was attributed to the N-H stretching vibration of the urethane linkages of PU. It can be observed that the N-H stretching peak shifted from 3332 cm^{-1} for pure PU and raw MWCNT/PU composite to lower wavenumbers 3326 cm^{-1} for

MWCNT-COOH/PU composite and 3323 cm^{-1} for MWCNT-PCL/PU composite. This revealed that the MWCNT-COOH/PU and MWCNT-PCL/PU composites were not just simple compounds of PU and MWCNTs but contained strong chemical interaction between them, while there was almost no chemical interaction between PU and raw MWCNT.

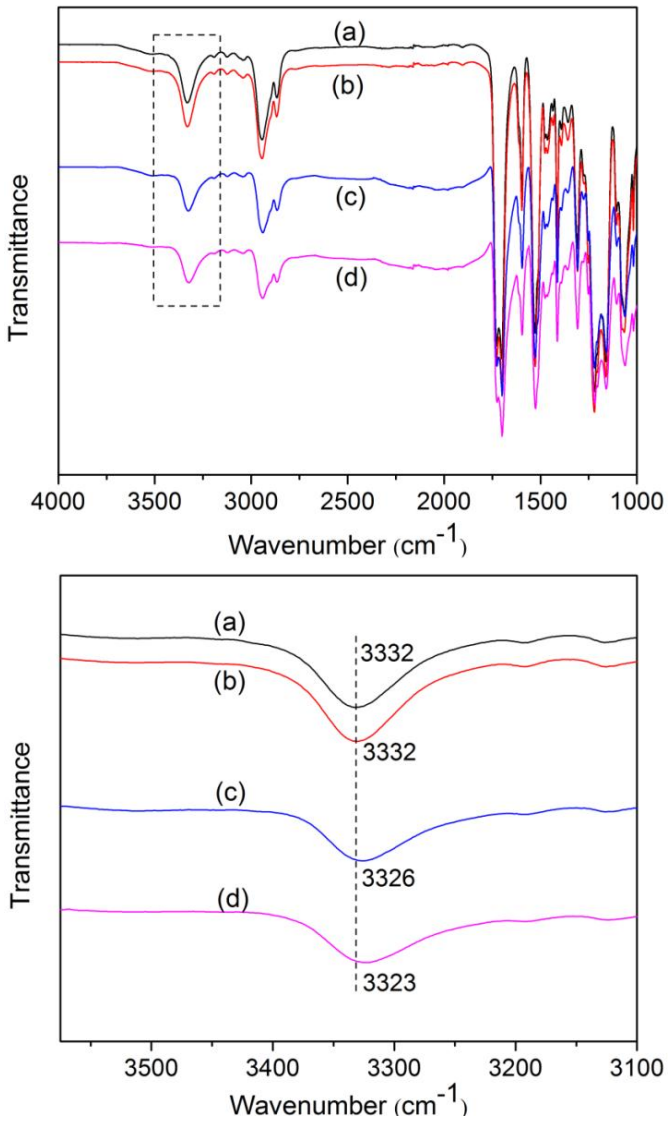

Figure 3.6 FTIR spectra of pure PU (a), raw MWCNT/PU composite (b), MWCNT-COOH/PU composite (c) and MWCNT-PCL/PU composite (d)

The red shift of the N-H stretching peak suggested that the N-H groups of the urethane linkages of PU became not "free" due to the addition of MWCNT-COOH and MWCNT-PCL. In order to explain the red shift, the hydrogen bonding between MWCNT-PCL and PU matrix was proposed because the PCL chains functionalized on MWCNTs' surface were very likely to interact with the N-H groups of PU. The possible hydrogen bonding between MWCNT-PCL and PU matrix is proposed in Figure 3.7. The situation in the MWCNT-COOH/PU composite was about the same. As is shown, the red shift of N-H stretching peak of MWCNT-PCL/PU composite was more prominent than that of MWCNT-COOH/PU composite. This may be because the PCL chains could provide more carbonyl groups, which were essential to the proposed hydrogen bonding, than the carboxylic acid groups. The hydrogen bonding may contribute to a better dispersion of functionalized MWCNTs in the PU matrix and more effective interfacial stress transfer between them. These suggestions were well supported by the observed dispersion of MWCNTs in the PU matrix and enhanced mechanical strength of composite films, as shown later.

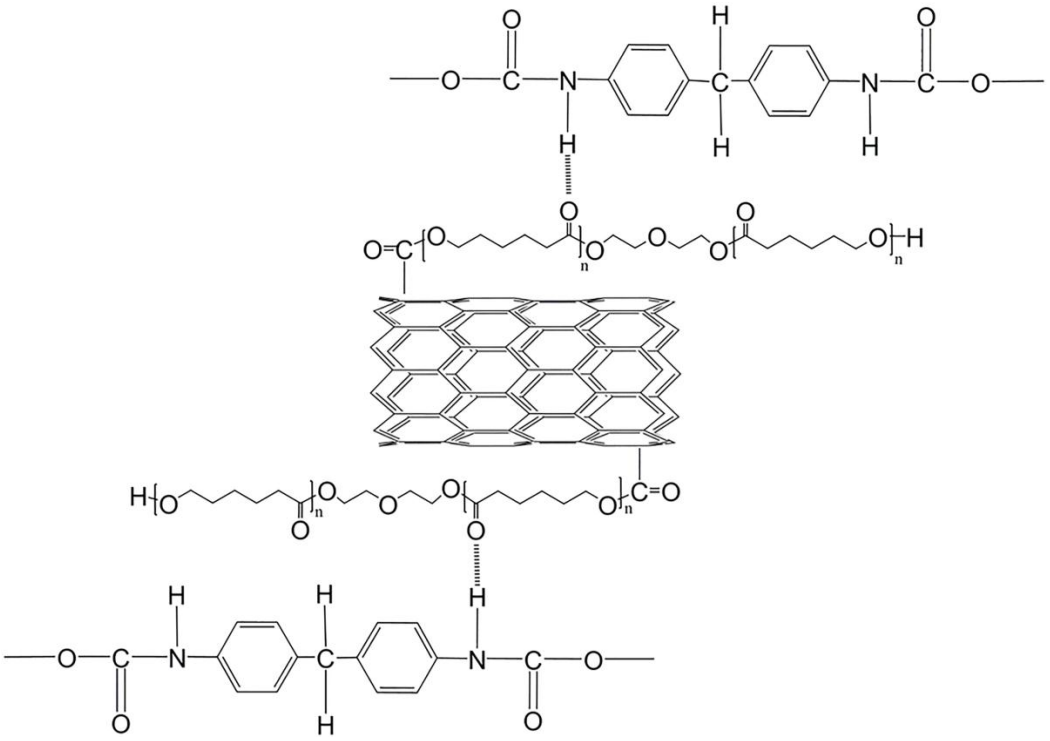

Figure 3.7 Schematic of hydrogen bonding between MWCNT-PCL and PU matrix

3.3.3 Dispersion of MWCNTs in PU

The dispersion of MWCNTs in a polymer matrix influences the properties of MWCNT/polymer composite greatly. Hence, FESEM and TEM were used to verify the dispersion of MWCNTs in the PU matrix. Figure 3.8 shows the FESEM images of the cross-sectional fractures of three studied composites: raw MWCNT/PU, MWCNT-COOH/PU and MWCNT-PCL/PU. A poor dispersion of raw MWCNTs in the PU matrix can be clearly observed in Figure 3.8a, with many large MWCNTs clusters in the matrix. Though prepared under exactly the same procedure, the MWCNT-COOH/PU composite (Figure 3.8b) displayed a better dispersion of MWCNTs with only a few small clusters.

Moreover, a homogeneous dispersion was achieved in the MWCNT-PCL/PU composite. The PU matrix was filled uniformly with MWCNT-PCL.

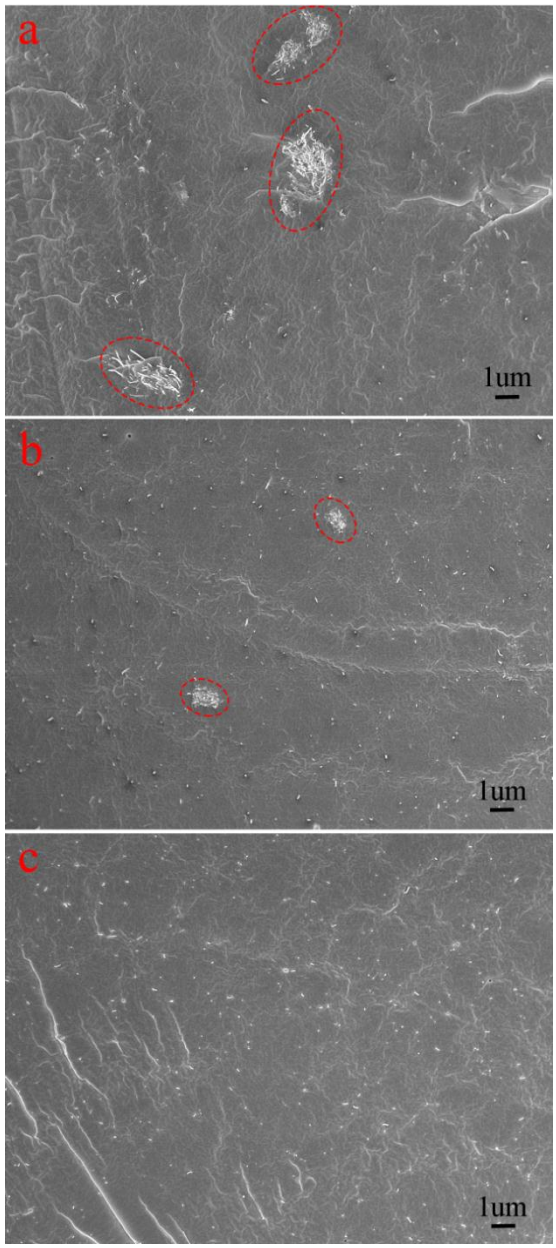

Figure 3.8 FESEM images of the cross-sectional fractures of raw MWCNT/PU composite (a), MWCNT-COOH/PU composite (b) and MWCNT-PCL/PU composite (c)

The improved dispersion of functionalized MWCNTs in the PU matrix was also confirmed by TEM, as shown in Figure 3.9. Since all the films were prepared by solution

casting, there was no preferred orientation for all types of MWCNTs. It can be clearly seen that MWCNT-PCL were distributed more uniformly in the matrix than MWCNT-COOH, while very large aggregates of raw MWCNTs were observed in the raw MWCNT/PU composite. The results indicated that the grafted carboxylic acid groups and PCL chains could significantly improve the dispersion of MWCNTs in the PU matrix. As confirmed with FTIR, the functional groups on MWCNTs' surface could form hydrogen bonding with the PU matrix, which reinforced the MWCNT-PU interface and weakened the van der Waals force among the MWCNTs. Compared with the MWCNT-COOH/PU composite, the better dispersion in MWCNT-PCL/PU composite may result from its stronger interfacial bonding, as discussed in the previous section.

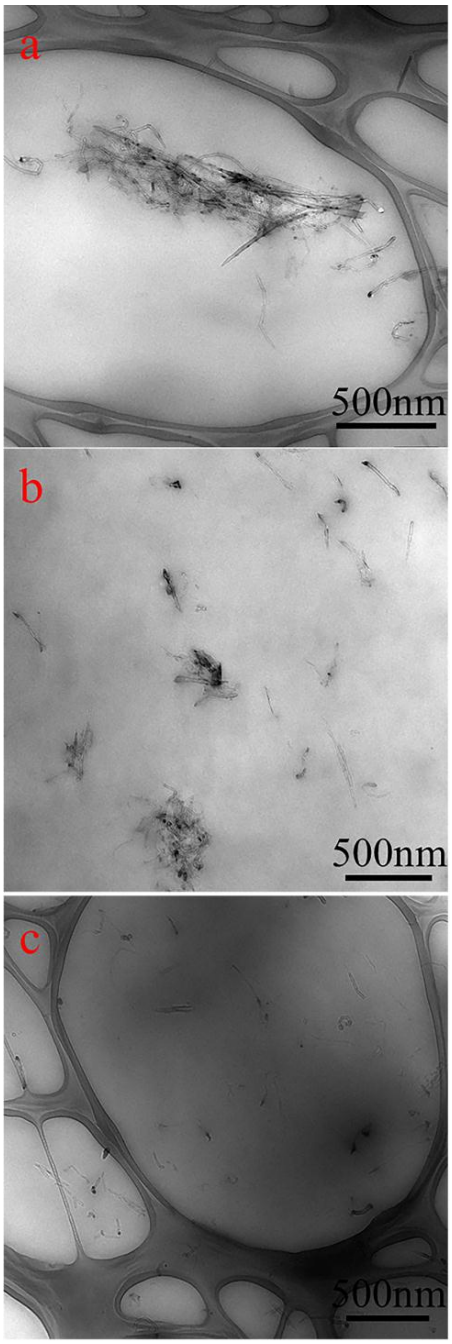

Figure 3.9 TEM images of raw MWCNT/PU composite (a), MWCNT-COOH/PU composite (b) and MWCNT-PCL/PU composite (c)

3.3.4 Mechanical performance of MWCNTs/PU composites

Mechanical properties of MWCNTs/PU composites were investigated employing tensile tests. Figure 3.10 exhibits the representative engineering stress-strain curves for pure PU as well as for three composites under study. All the film composites showed a nonlinear mechanical behavior, so the modulus was determined by taking the slope of the curve at low strains (0-8%), while the toughness was determined by calculating the area under the curve. Figure 3.11 presents detailed information about the tensile strength, modulus, elongation at break and toughness. In general, the improvement in mechanical properties of PU by the functionalized MWCNTs (MWCNT-COOH and MWCNT-PCL) was much more evident than by raw MWCNTs. The PU was even weakened with the addition of 1 wt% raw MWCNTs, showing a decrease of toughness by 13.8%. This was very likely attributed to the poor dispersion and lack of interfacial interaction between raw MWCNTs and the PU matrix. On the other hand, with 1 wt% loading, the functionalized MWCNTs significantly improved the mechanical properties of PU. Apparently, the highest improvement was achieved for the MWCNT-PCL/PU composite. Compared with pure PU, the tensile strength, modulus, elongation at break and toughness of the MWCNT-PCL/PU composite were 51.1%, 32.8%, 19.8% and 57.9% higher, respectively. The FESEM images demonstrate that MWCNT-PCL was homogeneously dispersed in the PU matrix, which was crucial to improving the mechanical properties. Besides, as confirmed with FTIR, the strong interfacial interaction between MWCNT-PCL and PU matrix was beneficial for the interfacial stress transfer. MWCNT-PCL showed a better enhancement effect than MWCNT-COOH, which may result from the similarity of

molecular structures of PCL and PU. With various functional groups in PCL, such as ester, ether and hydroxyl, MWCNT-PCL could form stronger interaction with PU matrix than MWCNT-COOH.

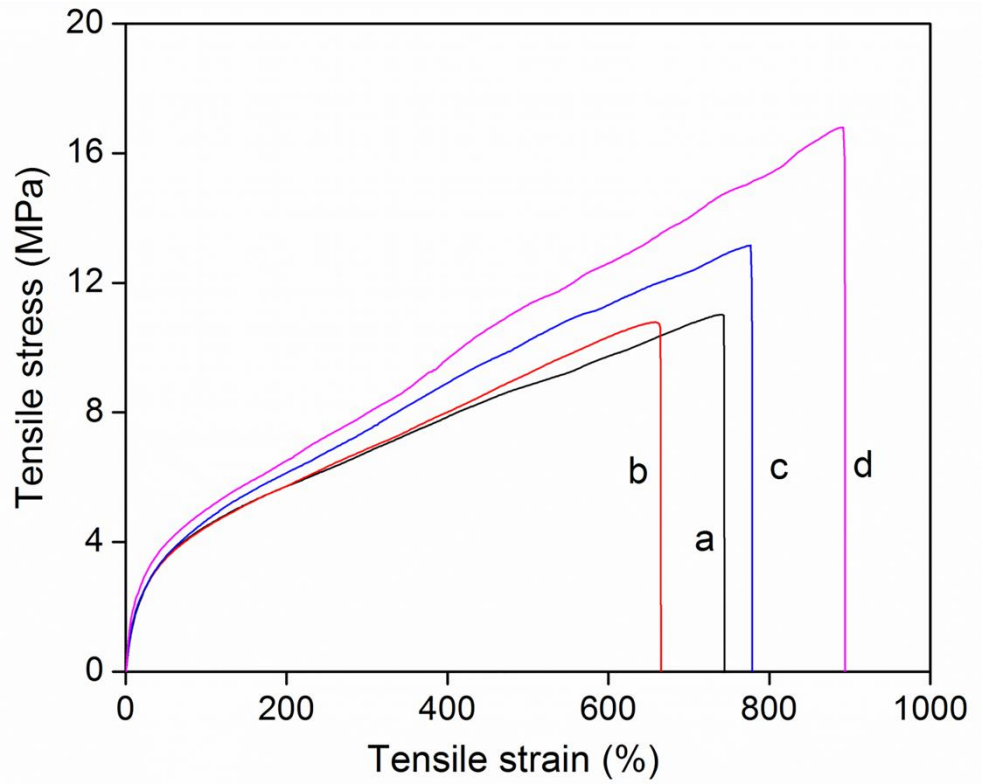

Figure 3.10 Typical engineering stress-strain curves: pure PU (a); raw MWCNT/PU composite (b); MWCNT-COOH/PU composite (c); MWCNT-PCL/PU composite (d)

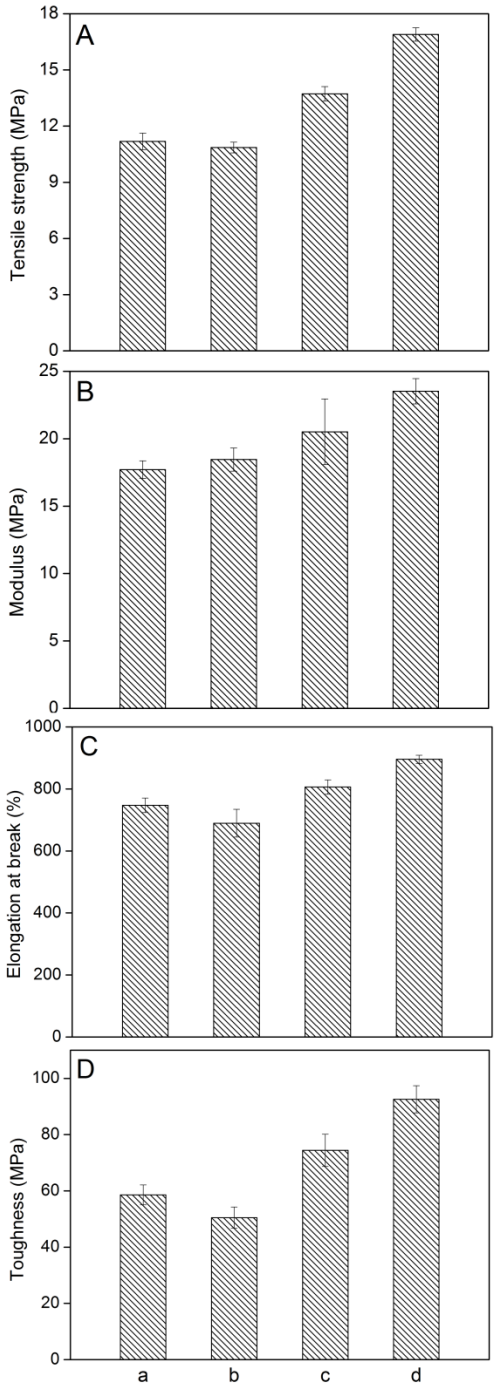

Figure 3.11 Tensile strength (A), modulus (B), elongation at break (C) and toughness (D): pure PU (a); raw MWCNT/PU composite (b); MWCNT-COOH/PU composite (c); MWCNT-PCL/PU composite (d)

3.3.5 Thermal stability of MWCNTs/PU composites

TGA thermograms of pure PU and three studied composites (Figure 3.12) demonstrate that the curves shifted towards higher temperature with the addition of raw MWCNT, MWCNT-COOH and MWCNT-PCL. In this work, the criteria for thermal stability were taken as the temperatures at which 2% ($T_{2\%}$) and 50% ($T_{50\%}$) weight-loss happened [13]. Compared with pure PU, $T_{2\%}$ of raw MWCNT/PU composite was about the same, while $T_{2\%}$ of MWCNT-COOH/PU and MWCNT-PCL/PU composites were increased by 22 ℃ and 38 ℃, respectively. For $T_{50\%}$, raw MWCNT/PU, MWCNT-COOH/PU and MWCNT-PCL/PU composites showed increments of 8 ℃, 13 ℃, and 35 ℃, respectively, as compared with pure PU. Obviously, the thermal stability of PU was significantly enhanced with the addition of MWCNTs, especially MWCNT-PCL. The increased thermal stability may result from high thermal conductivity of MWCNTs, which could promote heat dissipation in the PU matrix [34]. The interfacial bonding between functionalized MWCNTs and PU matrix may further promote the heat dissipation, thus delaying the decomposition of the functionalized MWCNTs/PU composites more effectively. In addition, the more uniform dispersion and stronger interfacial interaction in MWCNT-PCL/PU composite may contribute to its higher thermal stability compared to MWCNT-COOH/PU composite.

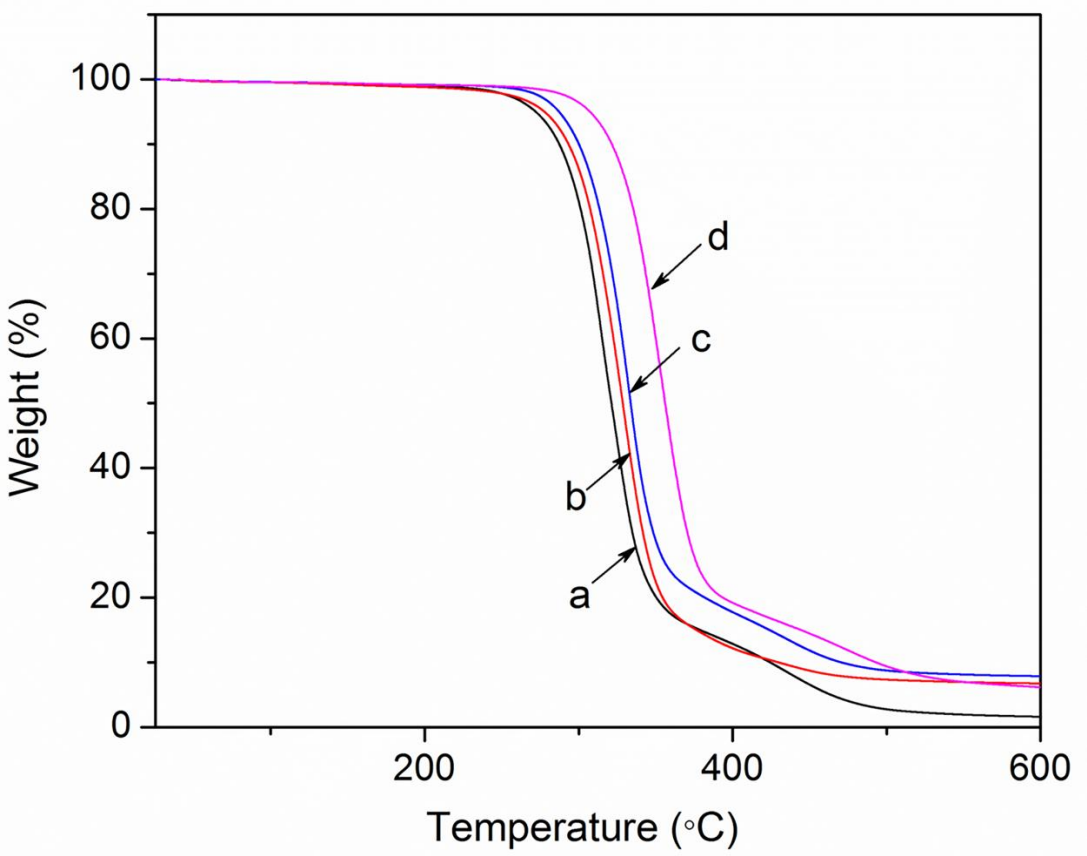

Figure 3.12 TGA thermograms: pure PU (a); raw MWCNT/PU composite (b); MWCNT-COOH/PU composite (c); MWCNT-PCL/PU composite (d)

3.4 Summary

In this work, polycaprolactone diol (PCL) was used as one of the components to synthesize PU, and at the same time PCL was also selectively used to functionalize MWCNTs, in order to achieve a high compatibility of functionalized MWCNTs with the PU matrix. Three types of MWCNTs/PU composites (namely, raw MWCNT/PU, MWCNT-COOH/PU and MWCNT-PCL/PU) with 1 wt% loading were prepared with a

solution mixing method. The successful functionalization of carboxylic acid groups and PCL chains on MWCNTs' surface was confirmed with FTIR, Raman, TEM and TGA tests. A uniform dispersion of MWCNTs in the PU matrix was achieved in the MWCNT-PCL/PU composite, as verified with FESEM and TEM. Tensile tests showed that the tensile strength, modulus, elongation at break and toughness of MWCNT-PCL/PU composite were significantly improved by 51.1%, 32.8%, 19.8% and 57.9%, respectively, as compared to pure PU. Regarding the thermal stability, $T_{2\%}$ and $T_{50\%}$ of MWCNT-PCL/PU composite were increased by 38 ℃ and 35 ℃, respectively, as compared to pure PU. Among pure PU and the three types of MWCNTs/PU composites, the highest reinforcing effect in both mechanical properties and thermal stability was found for the MWCNT-PCL/PU composite, which could be attributed to the homogeneous dispersion of MWCNT-PCL in the PU matrix and strong interfacial bonding between them. Since the monomer of a polymer is generally well compatible with the polymer itself, the approach based on the use of monomer-functionalized nanofillers to improve mechanical and thermal properties of polymer materials is very promising.

References

[1] Iijima S. Helical microtubules of graphitic carbon. Nature. 1991;354(6348):56-8.

[2] Baughman RH, Cui CX, Zakhidov AA, Iqbal Z, Barisci JN, Spinks GM, et al. Carbon nanotube actuators. Science. 1999;284(5418):1340-4.

[3] Esplandiu MJ, Bittner VG, Giapis KP, Collier CP. Nanoelectrode scanning probes from fluorocarbon-coated single-walled carbon nanotubes. Nano Letters. 2004;4(10):1873-9.

[4] Ajayan PM, Iijima S. Capillarity-induced filling of carbon nanotubes. Nature. 1993;361(6410):333-4.

[5] Balasubramanian K, Burghard M. Biosensors based on carbon nanotubes. Analytical and Bioanalytical Chemistry. 2006;385(3):452-68.

[6] Wang J. Carbon-nanotube based electrochemical biosensors: A review. Electroanalysis. 2005;17(1):7-14.

[7] Baughman RH, Zakhidov AA, de Heer WA. Carbon nanotubes - the route toward applications. Science. 2002;297(5582):787-92.

[8] Andrews R, Weisenberger MC. Carbon nanotube polymer composites. Current Opinion in Solid State and Materials Science. 2004;8(1):31-7.

[9] Sahoo NG, Cheng HKF, Li L, Chan SH, Judeh Z, Zhao JH. Specific Functionalization of Carbon Nanotubes for Advanced Polymer Nanocomposites. Advanced Functional Materials. 2009;19(24):3962-71.

[10] Clayton LM, Sikder AK, Kumar A, Cinke M, Meyyappan M, Gerasimov TG, et al. Transparent poly(methyl methacrylate)/single-walled carbon nanotube (PMMA/SWNT) composite films with increased dielectric constants. Advanced Functional Materials. 2005;15(1):101-6.

[11] Qian D, Dickey EC, Andrews R, Rantell T. Load transfer and deformation mechanisms in carbon nanotube-polystyrene composites. Applied Physics Letters. 2000;76(20):2868-70.

[12] Zhang XF, Liu T, Sreekumar TV, Kumar S, Moore VC, Hauge RH, et al. Poly(vinyl alcohol)/SWNT composite film. Nano Letters. 2003;3(9):1285-8.

[13] Zou YJ, Xiang CL, Yang LN, Sun LX, Xu F, Cao Z. A mediatorless microbial fuel cell using polypyrrole coated carbon nanotubes composite as anode material. International Journal of Hydrogen Energy. 2008;33(18):4856-62.

[14] Popov VN. Carbon nanotubes: properties and application. Materials Science and Engineering: R: Reports. 2004;43(3):61-102.

[15] Sun YP, Fu KF, Lin Y, Huang WJ. Functionalized carbon nanotubes: Properties and applications. Accounts of Chemical Research. 2002;35(12):1096-104.

[16] Terrones M. Science and technology of the twenty-first century: Synthesis, properties and applications of carbon nanotubes. Annual Review of Materials Research. 2003;33:419-501.

[17] Sahoo NG, Rana S, Cho JW, Li L, Chan SH. Polymer nanocomposites based on functionalized carbon nanotubes. Progress in Polymer Science. 2010;35(7):837-67.

[18] Oberdisse J, Hine P, Pyckhout-Hintzen W. Structure of interacting aggregates of silica nanoparticles in a polymer matrix: small-angle scattering and reverse Monte Carlo simulations. Soft Matter. 2007;3(4):476-85.

[19] Garg A, Sinnott SB. Effect of chemical functionalization on the mechanical properties of carbon nanotubes. Chemical Physics Letters. 1998;295(4):273-8.

[20] Ramanathan T, Fisher FT, Ruoff RS, Brinson LC. Amino-functionalized carbon nanotubes for binding to polymers and biological systems. Journal of Materials Chemistry. 2005;17(6):1290-5.

[21] Jung YC, Sahoo NG, Cho JW. Polymeric nanocomposites of polyurethane block copolymers and functionalized multi-walled carbon nanotubes as crosslinkers. Macromolecular Rapid Communications. 2006;27(2):126-31.

[22] Xiong JW, Zheng Z, Song WH, Zhou DS, Wang XL. Microstructure and properties of polyurethane nanocomposites reinforced with methylene-bis-ortho-chloroanilline-grafted multi-walled carbon nanotubes. Composites Part A: Applied Science and Manufacturing. 2008;39(5):904-10.

[23] Xiong JW, Zheng Z, Qin XM, Li M, Li HQ, Wang XL. The thermal and mechanical properties of a polyurethane/multi-walled carbon nanotube composite. Carbon. 2006;44(13):2701-7.

[24] Šebenik U, Krajnc M. Influence of the soft segment length and content on the synthesis and properties of isocyanate-terminated urethane prepolymers. International Journal of Adhesion and Adhesives. 2007;27(7):527-35.

[25] Coleman JN, Khan U, Blau WJ, Gun'ko YK. Small but strong: A review of the mechanical properties of carbon nanotube–polymer composites. Carbon. 2006;44(9):1624-52.

[26] Cho JW, Kim JW, Jung YC, Goo NS. Electroactive shape-memory polyurethane composites incorporating carbon nanotubes. Macromolecular Rapid Communications. 2005;26(5):412-6.

[27] Sahoo NG, Jung YC, Yoo HJ, Cho JW. Effect of functionalized carbon nanotubes on molecular interaction and properties of polyurethane composites. Macromolecular Chemistry and Physics. 2006;207(19):1773-80.

[28] Yun S, Im H, Kim J. The effect of different hard segments in polyurethane on the electrical conductivity of polyurethane grafted multi-walled carbon nanotube/polyurethane nanocomposites. Synthetic Metals. 2011;161(13-14):1361-7.

[29] Silverstein RM, Webster FX, Kiemle DJ. Spectrometric identification of organic compounds [electronic resource] / Robert M. Silverstein, Francis X. Webster, David J. Kiemle: Hoboken, NJ : John Wiley & Sons, c2005. 7th ed.; 2005.

[30] Chen XH, Wang HF, Zhong WB, Feng T, Yang XG, Chen JH. A scalable route to highly functionalized multi-walled carbon nanotubes on a large scale. Macromolecular Chemistry and Physics. 2008;209(8):846-53.

[31] Price BK, Hudson JL, Tour JM. Green chemical functionalization of single-walled carbon nanotubes in ionic liquids. Journal of the American Chemical Society. 2005;127(42):14867-70.

[32] Dettlaff-Weglikowska U, Skakalova V, Graupner R, Jhang SH, Kim BH, Lee HJ, et al. Effect of SOCl2 treatment on electrical and mechanical properties of single-wall carbon nanotube networks. Journal of the American Chemical Society. 2005;127(14):5125-31.

[33] Yang YK, Xie XL, Wu JG, Yang ZF, Wang XT, Mai YW. Multiwalled carbon nanotubes functionalized by hyperbranched poly(urea-urethane)s by a one-pot polycondensation. Macromolecular Rapid Communications. 2006;27(19):1695-701.

[34] Huxtable ST, Cahill DG, Shenogin S, Xue LP, Ozisik R, Barone P, et al. Interfacial heat flow in carbon nanotube suspensions. Nature Materials. 2003;2(11):731-4.

Chapter 4 Chemical functionalization of graphene oxide for improving mechanical and thermal properties of polyurethane composites*

Graphene oxide (GO) was chemically functionalized to prepare polyurethane (PU) composites with improved mechanical and thermal properties. In order to achieve a well exfoliated and stable GO suspension in an organic solvent (dimethylformamide, DMF), 4, 4'- methylenebis(phenyl isocyanate) and polycaprolactone diol, which were the two monomers for synthesizing PU, were selectively used to functionalize GO. The obtained functionalized GO (FGO) could form homogeneous dispersions in DMF solvent and the PU matrix, as well as provide a good compatibility with the PU matrix. The most efficient improvement of mechanical properties was achieved when 0.4 wt% FGO was added into the PU matrix, showing increases in tensile stress, elongation at break and toughness by 34.2%, 27.6% and 64.5%, respectively, compared with those of PU. Regarding the thermal stability, PU filled with 1 wt% FGO showed the largest extent of improvement with $T_{2\%}$ and $T_{50\%}$ (the temperatures at which 2% and 50% weight-loss happened) 16 ℃ and 21 ℃ higher than those of PU, respectively. The significant improvement in both mechanical properties and

thermal stability of FGO/PU composites should be attributed to the homogeneous dispersion of FGO in the PU matrix and strong interfacial interaction between them.

*The work in Chapter 4 is reprinted (adapted) with permission from Jing Q, Liu W, Pan Y, Silberschmidt VV, Li L, Dong Z. Materials & Design. 2015;85:808-14. Copyright 2015 Elsevier. Jing Q is the main contributor to this paper, responsible for the project design, experiments and paper writing. Liu W and Pan Y provided assistance during the experiments. Silberschmidt VV, Li L and Dong Z offered guidance and advices on experiments and paper writing.

4.1 Introduction

Research into graphene (refer to Section 2.2.1 for more details) has been one of the fastest growing areas due to its many fascinating properties such as ultrahigh thermal and electrical conductivity, excellent thermal stability, high specific surface area and remarkable mechanical strength [1-3]. Significant efforts have been put in developing multi-functional polymer composite materials using graphene as nanofiller for various applications, such as electromagnetic interference shielding materials, shape memory devices, drug release, actuators and infrared-triggered sensors [4-13]. To obtain defect-free, high-quality graphene sheets, the most widely used approaches are chemical vapor deposition [14, 15] and micromechanical cleavage of graphite [16]. Nevertheless, these approaches show a low production yield and are time consuming. In this situation, graphene oxide (GO), originated from the exfoliation of graphite oxide, has been extensively studied as an alternative to graphene. The established advantages of GO in production yield and cost [17] make it an attractive candidate as a nanofiller used in polymer composites.

GO (refer to Section 2.2.1 for more details) can be readily dispersed in water and form a stable colloidal suspension due to its high hydrophilicity [18-20]. However, the high hydrophilicity of GO could only benefit the fabrication of GO-based aqueous polymer composites. The exfoliation of GO in organic solvents is not favoured, presumably due to strong interlayer hydrogen bonds originated from those attached oxygen functional groups. The strong interactions between adjacent GO layers could prevent the penetration

of organic solvent molecules into the interlayer spaces, thus preventing full exfoliation of GO in organic solvents. Ruoff *et al.* [21] consider the hydrophilicity of GO as an obstacle to prepare high-performance GO-reinforced polymer composites in organic solvents. In their work, reactions between organic isocyanates and hydroxyl, carboxyl groups were taken advantage of to reduce the amount of hydrogen bond donor groups on GO sheets, thus weakening the strength of interlayer hydrogen bonding and hydrophilicity of GO. As a result, the isocyanate-treated GO can be fully exfoliated in some organic solvents, e.g., dimethylformamide (DMF), after a mild ultrasonication.

Thermoplastic polyurethane (PU) is an important class of polymers, which has been widely used in various applications such as foams, coatings, elastomers and adhesives. PU has a block copolymer structure, with polyol as soft segment and isocyanate and chain extender as hard segment. The molecular structure of PU could be easily adjusted to fulfil different property requirements [22]. It is commonly acknowledged that two factors should be mainly concerned in order to prepare high-performance nanofiller/polymer composites: (1) dispersion of nanofillers in the polymer matrix; (2) interfacial interactions between nanofillers and the matrix. The nanofillers tend to aggregate due to strong van der Waals forces among them, hindering their homogeneous dispersion in a polymer matrix. Besides, a lack of strong interfacial interactions between the nanofillers and matrix would greatly compromise the reinforcement effect of the nanofillers. One feasible and effective strategy to promote the reinforcement of composites is through chemical functionalization of nanofillers [23-26]. Among chemical functionalization methods, grafting molecules and/or polymer chains onto the surface of

graphene sheets was studied for many polymers [27-29]. The grafted molecules and/or polymer chains can enhance the dispersion of graphene sheets in the polymer matrix and interfacial interactions between them.

In this work, GO/PU composites were prepared via a solution mixing method. In order to obtain a homogeneous dispersion of GO in DMF, as well as a strong interfacial interaction between GO and PU, 4, 4′- methylenebis(phenyl isocyanate) (MDI) and polycaprolactone diol (PCL) were selectively used to functionalize GO. On one hand, MDI and PCL functionalization of GO was expected to improve the dispersion of GO in DMF, which could consequently improve the dispersion of GO in the PU matrix. On the other hand, since MDI and PCL were the monomers for synthesizing PU, a good compatibility between the functionalized GO (FGO) and the PU matrix was also expected, considering their structural similarity. Detailed characterizations of FGO were conducted and presented to confirm the successful functionalization of MDI and PCL on the GO surface. In addition, mechanical properties and thermal stability were tested to demonstrate the reinforcement effect of FGO on the composite materials.

4.2 Experimental

4.2.1 Materials

Graphene oxide (purity > 99%) was provided by XFNANO Materials Tech Co., Ltd. (Nanjing, China) which was synthesized from graphite powders using a common

Hummers method. PCL (average Mn ~530 g/mol and ~2000 g/mol), MDI (molecular weight 250.25 g/mol), 1,4-butanediol (BD, molecular weight 90.12 g/mol), and dibutyltin dilaurate (DBTDL) were all obtained from Sigma-Aldrich. DMF (Tritech Scientific), anhydrous DMF (Tritech Scientific) and anhydrous acetone (Tritech Scientific) were used as received.

4.2.2 Functionalization of GO

GO was vacuum freeze-dried to reduce the amount of stored water in its π–stacked structure [30] before using. In a typical operation, 300 mg GO was added into a round-bottom flask followed by 150 ml anhydrous DMF to form a colloidal suspension with the aid of an ultrasonication bath. Then, a 20 ml anhydrous DMF solution of MDI (5 g, 20 mmol) was mixed with the obtained suspension. The mixture was subsequently heated to 80 ℃ and kept for 24 h with magnetic stirring under a nitrogen atmosphere. After that, the mixture was poured into massive anhydrous acetone to coagulate into a solid. The solid was filtered, washed with additional anhydrous acetone and anhydrous DMF sequentially. Then, the resulting solid was immediately re-dispersed in 150 ml anhydrous DMF with the assistance of ultrasonication. Subsequently, a 20 ml anhydrous DMF solution of PCL (5 g, 9.4 mmol) was added and stirred for 36 h at 80 ℃ under nitrogen. After 36 h the reaction mixture was coagulated in massive anhydrous acetone to get a solid product. The product was further filtered, washed repeatedly with DMF to obtain FGO. The obtained FGO was then dispersed in DMF by ultrasonication to form a stable

stock suspension with a concentration of 0.71 mg/ml for later use. The schematic of FGO preparation is presented in Figure 4.1.

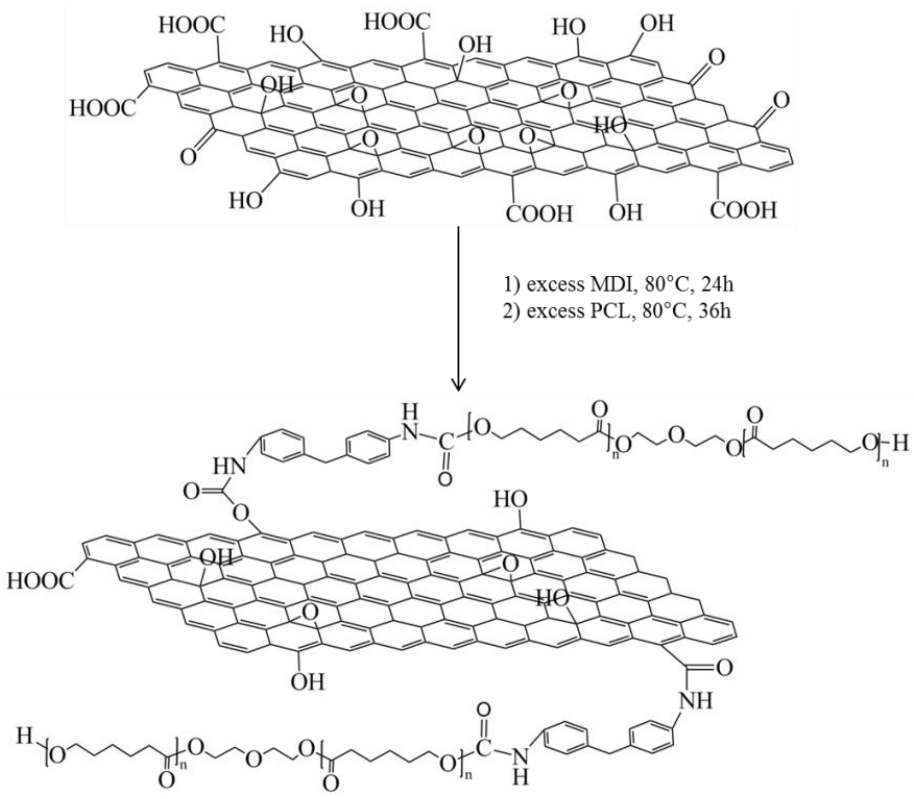

Figure 4.1 Schematic of FGO preparation

4.2.3 Preparation of FGO/PU composites

In this work, the prepolymerization method [31] was adopted to synthesize thermoplastic PU. MDI and PCL were used as monomers, with DBTDL and BD employed as the catalyst and chain extender, respectively. The feed molar ratio of MDI: PCL: BD was 6: 1: 5, corresponding to a hard segment content of 49.4 wt%. The solution mixing method was used to prepare a series of FGO/PU composites with different FGO contents - 0.1

wt%, 0.4 wt%, 0.7 wt% and 1 wt%. First, a certain volume of the as-prepared FGO/DMF stock suspension was added in a flask and then the synthesized PU (~5 g) was added into the suspension, based on the required FGO content in the composite. Considering different volumes of solvent in the series of FGO/DMF suspensions, additional DMF was added to ensure the same volume of solvent for each sample. After PU was completely dissolved with the assistance of magnetic stirring, a homogenizer was used at 9000 r/min for 15 min, followed by a bath ultrasonication for 40 min, to ensure homogeneity of the suspensions. Finally, the FGO/PU composite films were obtained through solution casting. The content of FGO in the composite was calculated based on the initial FGO amount in the stock suspension. As a control group, the GO/PU composite (0.4 wt%) was prepared according to the same procedure.

4.2.4 Characterization

FTIR spectroscopic measurements were performed using a FTIR Frontier (Perkin Elmer) equipped with an Attenuated Total Reflection (ATR). For the sample preparation, the powder sample was first mixed and ground with potassium bromide. Then, the mixture was pressed into a round transparent pellet using a pellet-forming die. The functionalization degree of FGO and thermal stability of the composite films were determined by thermo-gravimetric analysis (TGA Q500). The powder samples were first kept at 100 ℃ for 10 min to remove the absorbed water and then were heated to 600 ℃ at a speed of 10 ℃/min under nitrogen; the film samples were heated from 25 ℃ to 600 ℃ at a speed of 10 ℃/min under nitrogen. Powder X-ray diffraction (XRD) tests

were conducted using a Shimadzu X-ray diffractometer (Cu Kα) with step scanning (0.02 °, 0.6 s dwell time, 40 kV) over a 2θ range of 5-35 °. Field Emission Scanning Electron Microscopy (FESEM, JSM-7600F) was used to observe morphological features of GO and FGO. Before observation, the powder samples were sputtered with a thin layer of platinum using a sputter coater. Transmission Electron Microscopy (TEM) studies were conducted with a Carl Zeiss LIBRA®120 in-column energy filter TEM equipped with an integrated OMEGA filter. Leica Ultracut UCT was used to microtome the film samples in order to obtain flakes with a thickness of about 50-100 nm for TEM observation. Tensile Tester Instron 5567 (Instron, USA) was utilized to conduct the tensile tests. The film samples were cut according to ASTM D638, corresponding to a gauge length of 9.5 mm. The tensile tests were conducted at room temperature and five specimens were tested for each composite film.

4.3 Results and Discussion

4.3.1 Characterization of FGO and GO

The FTIR results are shown in Figure 4.2 for evaluation of the functionalization of GO. When organic isocyanates were used to functionalize GO, amides [32] and carbamate esters [33] would be formed derivatized with the carboxyl and hydroxyl groups, respectively. The typical features of GO are shown in Figure 4.2a. The peaks appearing at 3431 cm^{-1}, 1727 cm^{-1}, and 1060 cm^{-1} were associated with the O-H stretching, C=O stretching and C-O-C stretching, respectively. After treatment with MDI and PCL

sequentially, many new peaks appeared for FGO as compared with GO. The C=O stretching vibration of GO at 1727 cm^{-1} shifted towards a lower wavenumber and divided into two small peaks at 1698 cm^{-1} and 1670 cm^{-1}, corresponding to C=O stretching of the carbamate esters and amides, respectively. Together with the new peaks at 1598 cm^{-1} and 1310 cm^{-1}, which were due to N-H bending and C-N stretching, the reaction between the isocyanates and GO was confirmed [34]. Besides, the peaks at 2927 cm^{-1} and 2864 cm^{-1} were attributed to the asymmetrical and symmetrical stretching vibrations of $-CH_2-$ [35], and the peak at 757 cm^{-1} was attributed to the $-CH_2-$ bending vibration (4 or more $-CH_2-$) [34]. It is noteworthy that the peaks for the isocyanate group (-N=C=O), over a wavenumber range of 2275 - 2263 cm^{-1} [21], were not found in FGO, indicating that the -N=C=O groups of MDI reacted completely with the hydroxyl and carboxyl groups. The FTIR results confirmed that both MDI and PCL were covalently functionalized to the surface of GO.

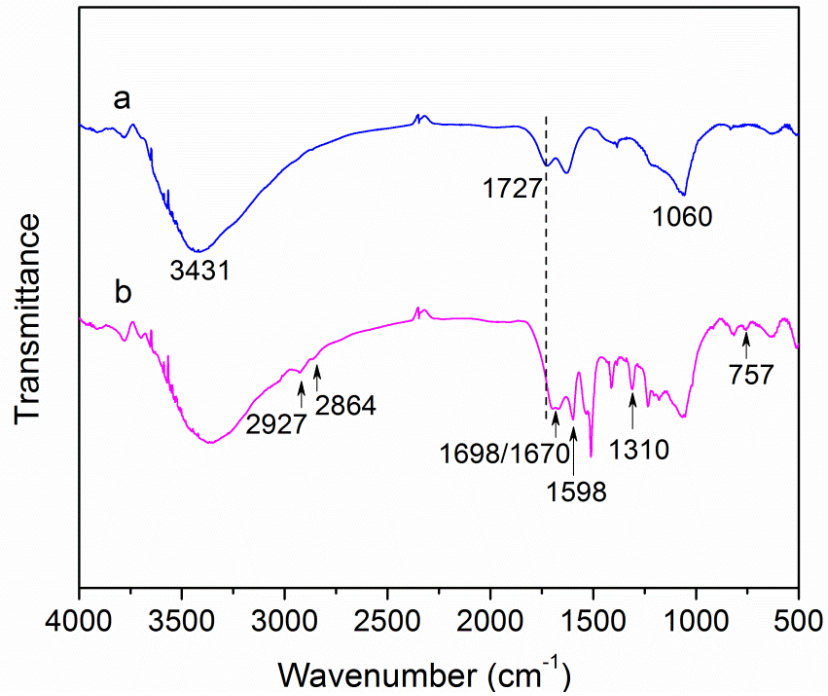

Figure 4.2 FTIR spectra of GO (a) and FGO (b)

The functionalization degree of FGO was determined by TGA tests. Figure 4.3 exhibits the TGA (A) and DTG (B) curves of GO (a), FGO (b) and PU (c). The samples were kept isothermal at 100 ℃ for 10 min to remove the absorbed water prior to heating [36]. It can be observed in Figure 4.3(A) that GO was not thermally stable. Its major mass loss appeared in the temperature range from 150 ℃ to 300 ℃, which was associated with the pyrolysis of the massive labile oxygen functional groups on its surface [37]. In contrast, the total mass loss process of FGO could be roughly divided into two major stages, based on the DTG curves. The first stage (100-250 ℃) should be due to pyrolysis of the residual oxygen functional groups from GO. It is clearly seen that the amount of oxygen functional groups in FGO was significantly decreased, presumably due to the following two reasons: first, the isocyanate groups from MDI would react with the hydroxyl and carboxyl groups on the surface of GO, as confirmed by the FTIR results, thus reducing GO to a certain extent; second, the solvothermal reduction could also play a role in decreasing the amount of oxygen functional groups. During the functionalization process, secondary amine groups would be formed after the reactions between MDI and carboxyl, hydroxyl groups of GO, as well as further reactions between MDI and PCL. The secondary amine groups were alkaline and able to donate electrons, thus acting as a reducing agent for GO [38]. Besides the DMF solvent also had a weak reducing ability [39, 40]. As a result, GO was partially reduced when subject to the relatively long time functionalization process. The second stage (250-450 ℃) exhibited a similar weight loss temperature range to that of the PU film, indicating that the mass loss at this stage was attributed to the thermal decomposition of covalently grafted MDI and PCL on the

surface of GO. As estimated from the TGA curves, FGO contained approximately 40 wt% of covalently functionalized MDI and PCL.

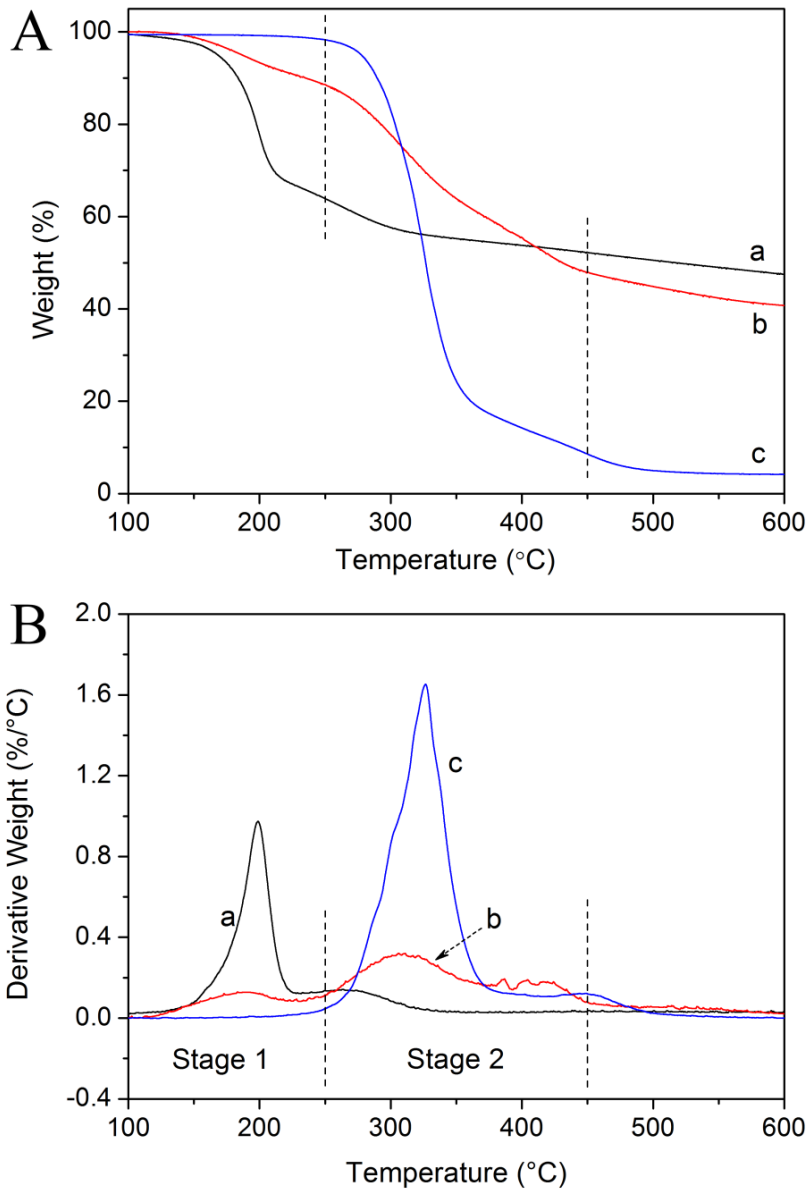

Figure 4.3 TGA (A) and DTG (B) curves of GO (a), FGO (b) and PU (c)

XRD tests were carried out to study the structural difference between GO and FGO. Figure 4.4 presents the XRD patterns of GO (a) and FGO (b) powders. The typical diffraction peak of GO was observed at approximately $2\theta = 10.8°$, corresponding to d-spacing of 0.82 nm. However, no characteristic intense diffraction peaks were observed for FGO, indicating that the covalent functionalization of GO by MDI and PCL could effectively prevent them from restacking. It is noteworthy that the broad peaks appearing at about 21° for both FGO and GO originated from the glass substrate used as sample holder in XRD tests [41].

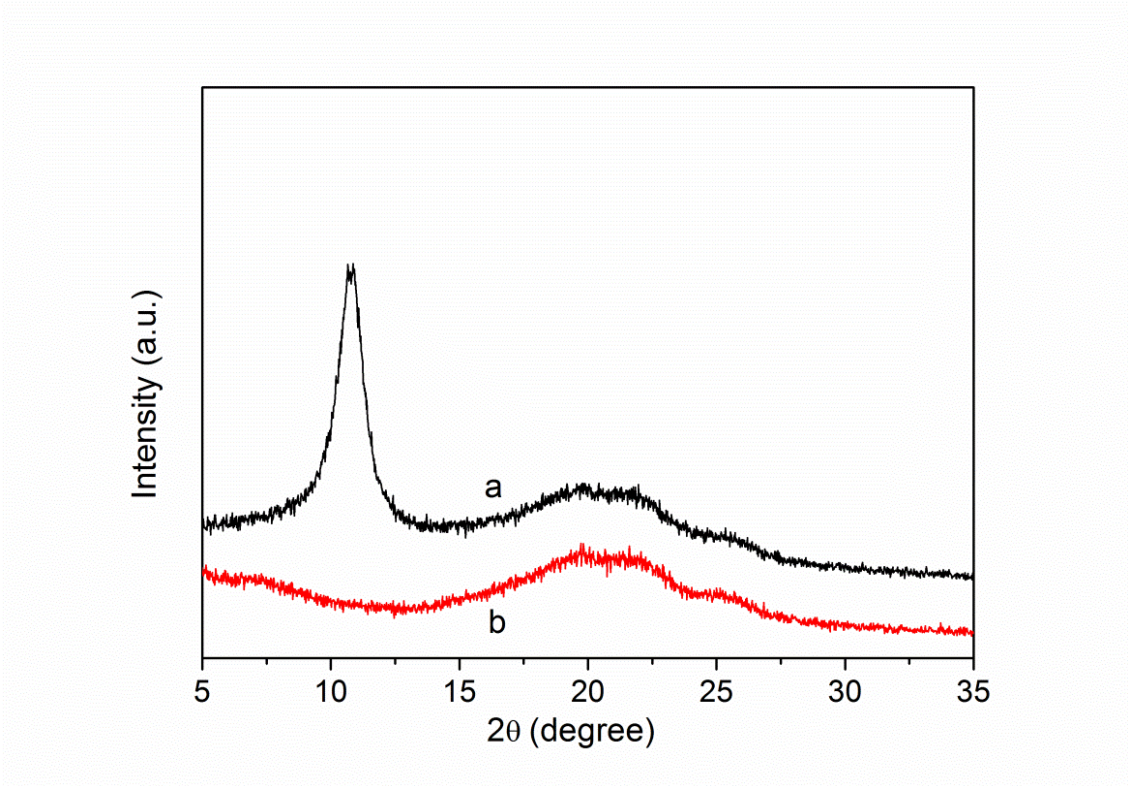

Figure 4.4 XRD patterns of GO (a) and FGO (b)

The FESEM images show the morphological features of GO and FGO. As can be seen in Figure 4.5, GO sheets exhibited wrinkled structures and smooth surfaces, while FGO

sheets presented comparatively rough surfaces and were covered by the covalently grafted MDI and PCL, as confirmed by the FTIR and TGA results.

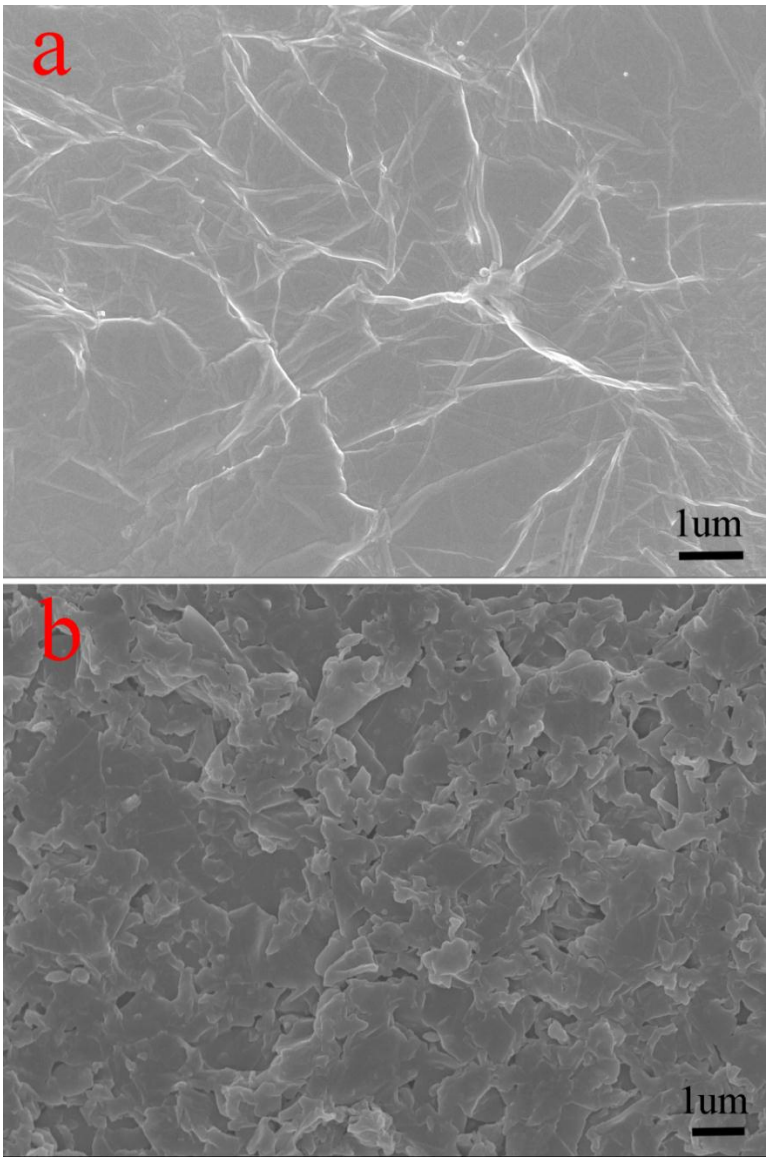

Figure 4.5 FESEM images of GO (a) and FGO (b)

4.3.2 Dispersions in solvent and PU matrix

Figure 4.6 presents digital photographs of GO (left) and FGO (right) dispersed in DMF (0.5 mg/ml): 5 min (a) and 14 days (b, c) after ultrasonication. As can be observed in Figure 4.6a, both GO and FGO formed homogeneous colloidal suspensions in DMF with the aid of ultrasonication. However, after 14 days, visible precipitates could be observed in the vial containing GO in DMF, whereas the suspension of FGO in DMF was stable and no visible precipitates were shown. Apparently, FGO exhibited a better dispersion ability in DMF than GO [21]. The massive oxygen functional groups on the surface of GO sheets could form strong interlayer hydrogen bonding, which could prevent the interlayers of GO from the permeation of organic solvent molecules. After the chemical functionalization of GO with MDI and PCL, the amount of available hydrogen bond donor groups decreased significantly, thus weakening the interlayer interactions of FGO, facilitating the exfoliation of FGO in DMF. Meanwhile, the covalently grafted MDI and PCL on the surface of FGO sheets could effectively prevent the graphene backbones from direct contact [37], which was also beneficial to the exfoliation of FGO in DMF.

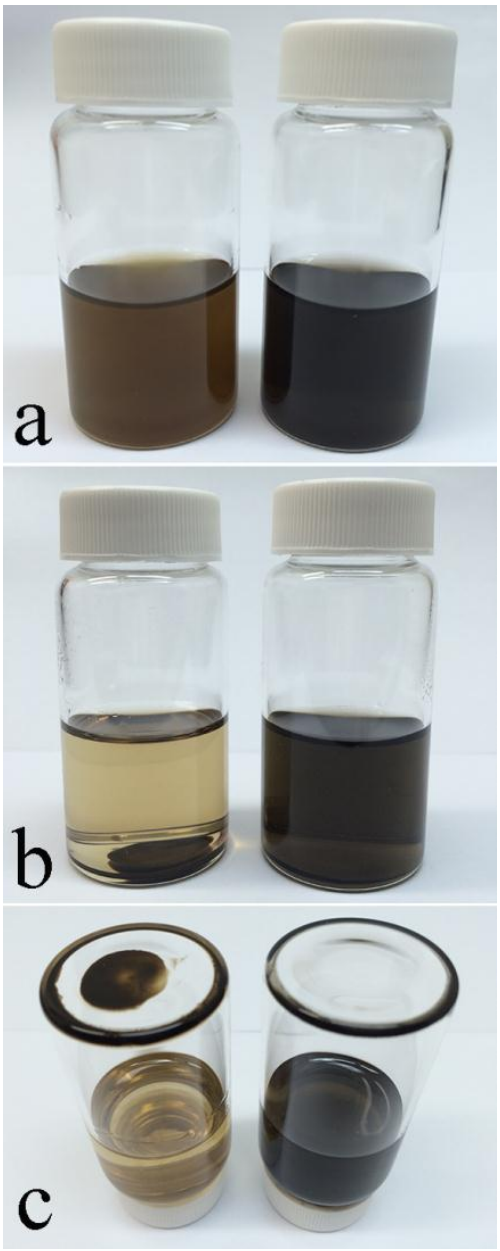

Figure 4.6 Digital photographs of GO (left) and FGO (right) dispersed in DMF (0.5 mg/ml): 5 min (a) and 14 days (b, c) after ultrasonication

The performance of a nanocomposite relies greatly on the dispersion state of nanofillers in the polymer matrix. As shown in Figure 4.7, the dispersions of GO and FGO in the PU matrix were observed by TEM. In the 0.4 wt% GO/PU composite, GO sheets could be

clearly observed, indicating their stacked structure, which was consistent with the XRD results. In contrast, the FGO sheets appeared obscure in the 0.4 wt% FGO/PU composite, indicating their improved exfoliation and dispersion in the PU matrix. From the TEM images, the better exfoliation and dispersion of FGO in the PU matrix than those of GO were confirmed. As shown above, FGO possessed a better dispersion ability in DMF than GO. Considering that the composites were prepared in DMF, the dispersion of FGO in the PU matrix should benefit from its good dispersion in DMF. Moreover, the covalently grafted MDI and PCL on the surface of FGO could improve the compatibility between FGO and the PU matrix, contributing to the better dispersion of FGO in the PU matrix.

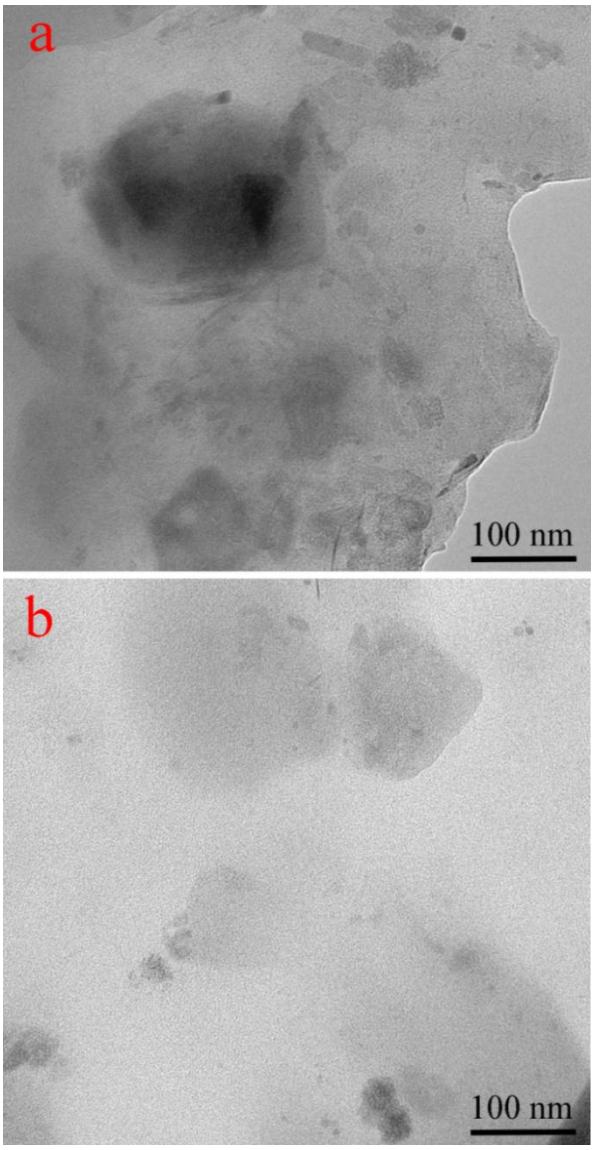

Figure 4.7 TEM images of 0.4 wt% GO/PU composite (a) and 0.4 wt% FGO/PU composite (b)

4.3.3 Mechanical properties

Figure 4.8 presents the typical engineering stress-strain curves for PU (a); 0.1 wt% FGO/PU (b); 0.4 wt% FGO/PU (c); 0.7 wt% FGO/PU (d); 1 wt% FGO/PU (e); 0.4 wt% GO/PU (f). The modulus and toughness were calculated using the same way as described

in Section 3.3.4. Figures 4.9 and 4.10 provide detailed information about the tensile strength, modulus, elongation at break and toughness. In general, the introduction of FGO into the PU matrix could significantly improve its mechanical properties. It can be seen that the most efficient improvement was achieved for the 0.4 wt% FGO/PU composite. Its tensile strength, elongation at break and toughness were 19.6 MPa, 1035.3% and 129.6 MPa, respectively, corresponding to increases by 34.2%, 27.6% and 64.5% compared with those of PU. Further addition of FGO into the PU matrix led to a decrease of these values, which was presumably due to the aggregation of FGO. Besides, the modulus of the FGO/PU composite increased gradually with increasing FGO content, reaching a peak of 29.6 MPa at 1 wt%. The significant improvements of mechanical properties in the FGO/PU composites were attributed to the improved dispersion of FGO in the PU matrix, as well as the interfacial interactions between them. The covalently grafted MDI and PCL on the surface of FGO could form hydrogen bonding with the PU matrix, resulting in an effective load transfer from the matrix to FGO under an external stress. Moreover, as can be seen in Figure 4.10, FGO exhibited a larger effect of reinforcement than GO at the same loading content (0.4 wt%) overall. The toughness and elongation at break for 0.4 wt% FGO/PU (129.6 MPa and 1035.3%) were 19.6% and 21.8% higher than those for 0.4 wt% GO/PU (108.4 MPa and 850.3%), respectively. It is interesting to find that the modulus of 0.4 wt% FGO/PU was smaller than that of 0.4 wt% GO/PU, which might be due to the covalently grafted MDI and PCL on the surface of FGO. Compared with GO, the grafted small molecules and soft chains on the surface of FGO could act as a “plasticizer” in the matrix, resulting in a lower stiffness yet higher toughness and ductility of the 0.4 wt% FGO/PU composite.

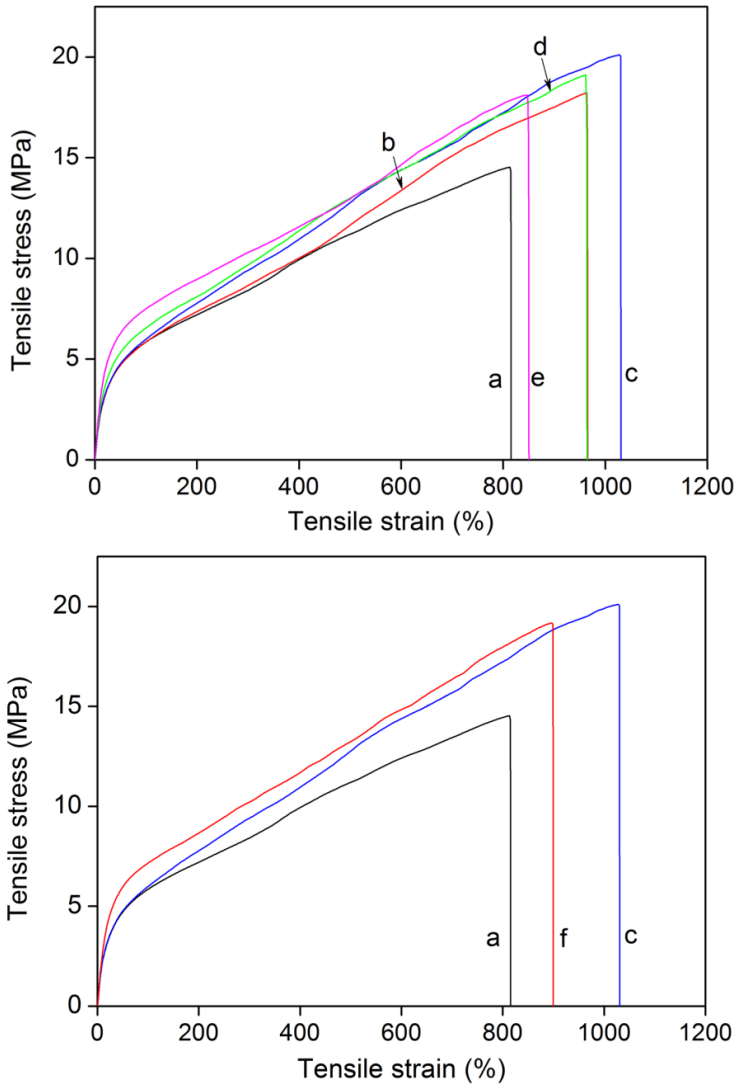

Figure 4.8 Typical engineering stress-strain curves: PU (a); 0.1 wt% FGO/PU (b); 0.4 wt% FGO/PU (c); 0.7 wt% FGO/PU (d); 1 wt% FGO/PU (e); 0.4 wt% GO/PU (f)

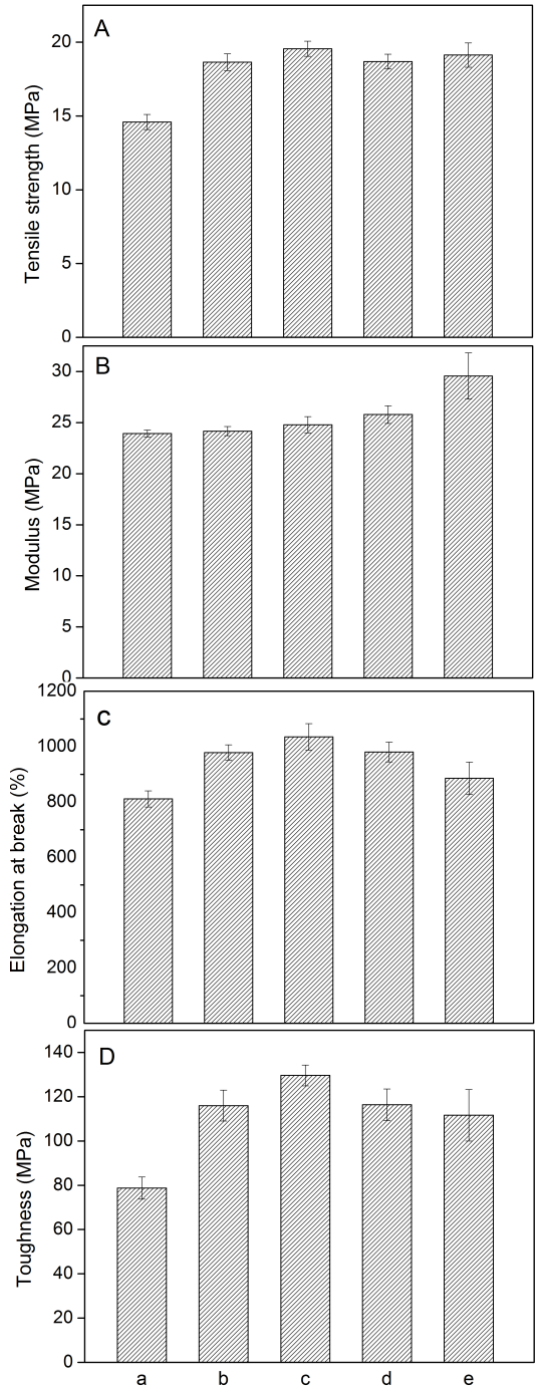

Figure 4.9 Tensile strength (A), modulus (B), elongation at break (C) and toughness (D): PU (a); 0.1 wt% FGO/PU (b); 0.4 wt% FGO/PU (c); 0.7 wt% FGO/PU (d); 1 wt% FGO/PU (e)

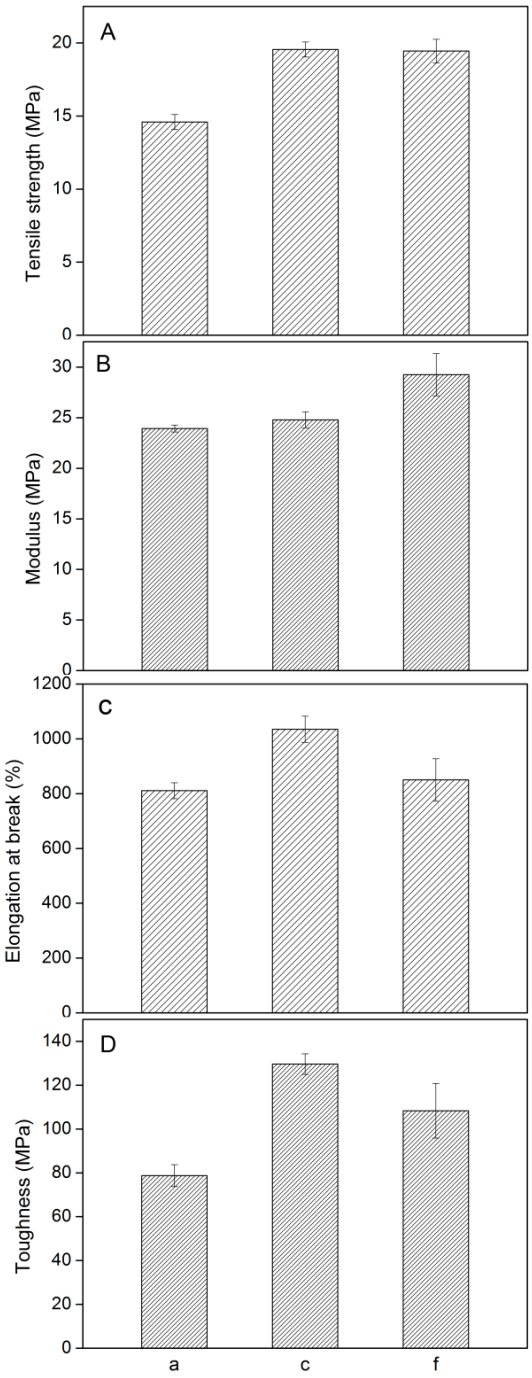

Figure 4.10 Tensile strength (A), modulus (B), elongation at break (C) and toughness (D): PU (a); 0.4 wt% FGO/PU (c); 0.4 wt% GO/PU (f)

4.3.4 Thermal stability

The thermal stability of FGO/PU composites was characterized by TGA, as shown in Figure 4.11. A magnified picture of a local part was inserted for better distinctness. It can be clearly seen that the curves shifted towards higher temperatures after adding FGO into the PU matrices. To assess the thermal stability, the temperatures corresponding to 2% ($T_{2\%}$) and 50% ($T_{50\%}$) weight-loss of the composites were taken as the criteria [42]. The largest improvement of thermal stability was achieved for the FGO/PU composite with 1 wt% FGO. The $T_{2\%}$ and $T_{50\%}$ of 1 wt% FGO/PU (271 ℃ and 348 ℃) increased by 16 ℃ and 21 ℃, respectively, as compared with those of PU (255 ℃ and 327 ℃). Apparently, the addition of FGO into the PU matrices could greatly improve the thermal stability of the composites, owing to the so-called "tortuous path" effect of graphene sheets, which delayed the escape of volatile degradation products and char formation as well [43].

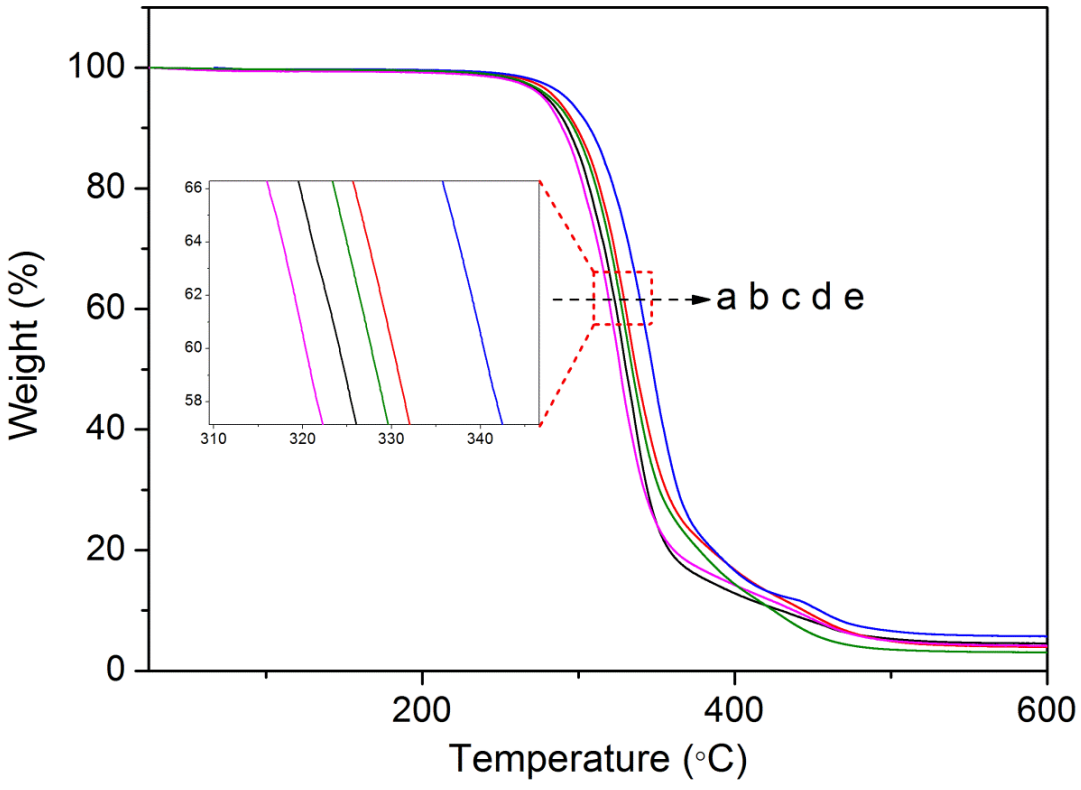

Figure 4.11 TGA curves with an inserted magnified image of a local part: PU (a); 0.1 wt% FGO/PU (b); 0.4 wt% FGO/PU (c); 0.7 wt% FGO/PU (d); 1 wt% FGO/PU (e)

4.4 Summary

In this work, GO was functionalized with the two monomers of PU: MDI and PCL, sequentially. The successful functionalization was confirmed by the FTIR, TGA, XRD and FESEM measurements. After the functionalization, the amount of oxygen functional groups on the surface of GO was reduced. The covalently grafted MDI and PCL on the surface of FGO could not only improve the exfoliation and dispersion of FGO in the DMF solvent and PU matrix, but also provide a good compatibility between FGO and the PU matrix. The most efficient improvement of mechanical properties was achieved when 0.4 wt% FGO was added into the PU matrix, resulting in the increases of tensile stress, elongation at break and toughness by 34.2%, 27.6% and 64.5%, respectively, compared with those of PU. Regarding the thermal stability, 1 wt% FGO/PU showed the largest reinforcement with $T_{2\%}$ and $T_{50\%}$ 16 ℃ and 21 ℃ higher than those of PU, respectively. A proper chemical functionalization of graphene sheets is crucial for their exfoliation and homogeneous dispersions in the organic solvent and polymer matrix, as well as a strong interfacial interaction between the graphene sheets and polymer matrix. The method using monomer-functionalized graphene oxide to prepare graphene-based polymer composite with enhanced performance is very promising.

References

[1] Geim AK. Graphene: Status and Prospects. Science. 2009;324(5934):1530-4.

[2] Park S, Ruoff RS. Chemical methods for the production of graphenes (vol 4, pg 217, 2009). Nature Nanotechnology. 2010;5(4):309-.

[3] Lee C, Wei XD, Kysar JW, Hone J. Measurement of the elastic properties and intrinsic strength of monolayer graphene. Science. 2008;321(5887):385-8.

[4] Eswaraiah V, Balasubramaniam K, Ramaprabhu S. One-pot synthesis of conducting graphene-polymer composites and their strain sensing application. Nanoscale. 2012;4(4):1258-62.

[5] Li CX, Adamcik J, Mezzenga R. Biodegradable nanocomposites of amyloid fibrils and graphene with shape-memory and enzyme-sensing properties. Nature Nanotechnology. 2012;7(7):421-7.

[6] Liang JJ, Wang Y, Huang Y, Ma YF, Liu ZF, Cai FM, et al. Electromagnetic interference shielding of graphene/epoxy composites. Carbon. 2009;47(3):922-5.

[7] Liang JJ, Xu YF, Huang Y, Zhang L, Wang Y, Ma YF, et al. Infrared-Triggered Actuators from Graphene-Based Nanocomposites. The Journal of Physical Chemistry C. 2009;113(22):9921-7.

[8] Xiao XC, Xie T, Cheng YT. Self-healable graphene polymer composites. Journal of Materials Chemistry. 2010;20(17):3508-14.

[9] Zhou T, Zhou XM, Xing D. Controlled release of doxorubicin from graphene oxide based charge-reversal nanocarrier. Biomaterials. 2014;35(13):4185-94.

[10] Shokrieh MM, Esmkhani M, Haghighatkhah AR, Zhao Z. Flexural fatigue behavior of synthesized graphene/carbon-nanofiber/epoxy hybrid nanocomposites. Materials & Design. 2014;62(0):401-8.

[11] Liu J, Cui L, Kong N, Barrow CJ, Yang W. RAFT controlled synthesis of graphene/polymer hydrogel with enhanced mechanical property for pH-controlled drug release. European Polymer Journal. 2014;50(0):9-17.

[12] Ma W-S, Wu L, Yang F, Wang S-F. Non-covalently modified reduced graphene oxide/polyurethane nanocomposites with good mechanical and thermal properties. Journal of Materials Science. 2014;49(2):562-71.

[13] Yang L, Wang F, Han H, Yang L, Zhang G, Fan Z. Functionalized graphene oxide as a drug carrier for loading pirfenidone in treatment of subarachnoid hemorrhage. Colloids and Surfaces B: Biointerfaces. 2015;129(0):21-9.

[14] Dato A, Radmilovic V, Lee Z, Phillips J, Frenklach M. Substrate-free gas-phase synthesis of graphene sheets. Nano Letters. 2008;8(7):2012-6.

[15] Reina A, Jia XT, Ho J, Nezich D, Son HB, Bulovic V, et al. Large Area, Few-Layer Graphene Films on Arbitrary Substrates by Chemical Vapor Deposition. Nano Letters. 2009;9(1):30-5.

[16] Novoselov KS, Geim AK, Morozov SV, Jiang D, Zhang Y, Dubonos SV, et al. Electric field effect in atomically thin carbon films. Science. 2004;306(5696):666-9.

[17] Park S, Ruoff RS. Chemical methods for the production of graphenes. Nature Nanotechnology. 2009;4(4):217-24.

[18] Erickson K, Erni R, Lee Z, Alem N, Gannett W, Zettl A. Determination of the Local Chemical Structure of Graphene Oxide and Reduced Graphene Oxide. Advanced Materials. 2010;22(40):4467-72.

[19] Szabo T, Tombacz E, Illes E, Dekany I. Enhanced acidity and pH-dependent surface charge characterization of successively oxidized graphite oxides. Carbon. 2006;44(3):537-45.

[20] Titelman GI, Gelman V, Bron S, Khalfin RL, Cohen Y, Bianco-Peled H. Characteristics and microstructure of aqueous colloidal dispersions of graphite oxide. Carbon. 2005;43(3):641-9.

[21] Stankovich S, Piner RD, Nguyen ST, Ruoff RS. Synthesis and exfoliation of isocyanate-treated graphene oxide nanoplatelets. Carbon. 2006;44(15):3342-7.

[22] Šebenik U, Krajnc M. Influence of the soft segment length and content on the synthesis and properties of isocyanate-terminated urethane prepolymers. International Journal of Adhesion and Adhesives. 2007;27(7):527-35.

[23] Loh KP, Bao QL, Ang PK, Yang JX. The chemistry of graphene. Journal of Materials Chemistry. 2010;20(12):2277-89.

[24] Dreyer DR, Park S, Bielawski CW, Ruoff RS. The chemistry of graphene oxide. Chemical Society Reviews. 2010;39(1):228-40.

[25] Jing Q, Law JY, Tan LP, Silberschmidt VV, Li L, Dong Z. Preparation, characterization and properties of polycaprolactone diol-functionalized multi-walled carbon nanotube/thermoplastic polyurethane composite. Composites Part A: Applied Science and Manufacturing. 2015;70(0):8-15.

[26] Ahmadi-Moghadam B, Sharafimasooleh M, Shadlou S, Taheri F. Effect of functionalization of graphene nanoplatelets on the mechanical response of graphene/epoxy composites. Materials & Design. 2015;66, Part A(0):142-9.

[27] Pan YZ, Bao HQ, Sahoo NG, Wu TF, Li L. Water-Soluble Poly(N-isopropylacrylamide)-Graphene Sheets Synthesized via Click Chemistry for Drug Delivery. Advanced Functional Materials. 2011;21(14):2754-63.

[28] Salavagione HJ, Gomez MA, Martinez G. Polymeric Modification of Graphene through Esterification of Graphite Oxide and Poly(vinyl alcohol). Macromolecules. 2009;42(17):6331-4.

[29] Liu LH, Lerner MM, Yan MD. Derivitization of Pristine Graphene with Well-Defined Chemical Functionalities. Nano Letters. 2010;10(9):3754-6.

[30] Jung I, Dikin D, Park S, Cai W, Mielke SL, Ruoff RS. Effect of Water Vapor on Electrical Properties of Individual Reduced Graphene Oxide Sheets. The Journal of Physical Chemistry C. 2008;112(51):20264-8.

[31] Cho JW, Kim JW, Jung YC, Goo NS. Electroactive shape-memory polyurethane composites incorporating carbon nanotubes. Macromolecular Rapid Communications. 2005;26(5):412-6.

[32] Blagbrough IS, Mackenzie NE, Ortiz C, Scott AI. The Condensation Reaction between Isocyanates and Carboxylic-Acids - a Practical Synthesis of Substituted Amides and Anilides. Tetrahedron Letters. 1986;27(11):1251-4.

[33] March J, Smith MB. March's advanced organic chemistry : reactions, mechanisms and structure. Hoboken, N.J: Wiley; 2007.

[34] Silverstein RM, Webster FX, Kiemle DJ. Spectrometric identification of organic compounds [electronic resource] / Robert M. Silverstein, Francis X. Webster, David J. Kiemle: Hoboken, NJ : John Wiley & Sons, c2005. 7th ed.; 2005.

[35] Yun S, Im H, Kim J. The effect of different hard segments in polyurethane on the electrical conductivity of polyurethane grafted multi-walled carbon nanotube/polyurethane nanocomposites. Synthetic Metals. 2011;161(13-14):1361-7.

[36] Yang LP, Yee WA, Phua SL, Kong JH, Ding H, Cheah JW, et al. A high throughput method for preparation of highly conductive functionalized graphene and conductive polymer nanocomposites. RSC Advances. 2012;2(6):2208-10.

[37] Wu C, Huang XY, Wang GL, Wu XF, Yang K, Li ST, et al. Hyperbranched-polymer functionalization of graphene sheets for enhanced mechanical and dielectric properties of polyurethane composites. Journal of Materials Chemistry. 2012;22(14):7010-9.

[38] Fan X, Peng W, Li Y, Li X, Wang S, Zhang G, et al. Deoxygenation of exfoliated graphite oxide under alkaline conditions: a green route to graphene preparation. Advanced Materials. 2008;20(23):4490-3.

[39] Zhou D, Cheng Q-Y, Han B-H. Solvothermal synthesis of homogeneous graphene dispersion with high concentration. Carbon. 2011;49(12):3920-7.

[40] Pastoriza-Santos I, Liz-Marzán LM. Synthesis of silver nanoprisms in DMF. Nano Letters. 2002;2(8):903-5.

[41] Kondoh K, Kawabata K, Serikawa T, Kimura H. Structural Characteristics and Crystallization of Metallic Glass Sputtered Films by Using Zr System Target. Research Letters in Materials Science. 2008;2008:4.

[42] Sahoo NG, Cheng HKF, Li L, Chan SH, Judeh Z, Zhao JH. Specific Functionalization of Carbon Nanotubes for Advanced Polymer Nanocomposites. Advanced Functional Materials. 2009;19(24):3962-71.

[43] Cao Y, Feng J, Wu P. Preparation of organically dispersible graphene nanosheet powders through a lyophilization method and their poly(lactic acid) composites. Carbon. 2010;48(13):3834-9.

Chapter 5 Effect of graphene oxide enhancement on large-deflection bending performance of thermoplastic polyurethane elastomer*

Thermoplastic polyurethane (PU) elastomers are used as shoe-sole materials due to many excellent properties but their inelastic deformation is a serious deficiency for such applications. Hence, graphene oxide (GO) was introduced into the synthesized thermoplastic PU to produce a GO/PU composite material with enhanced properties. Plastic behavior of this composite was assessed in cyclic tensile tests, demonstrating reduction of irreversible deformations with the addition of GO. Additionally, in order to evaluate mechanical performance of PU and the GO/PU composite under conditions of large-deflection bending typical for shoe soles, finite-element simulations with Abaqus/Standard were conducted. An elastic-plastic finite-element model was developed to obtain detailed mechanical information for PU and the GO/PU composite. The numerical study demonstrated that the plastic area, final specific plastic dissipation energy and residual height for PU specimens were significantly larger than those for the GO/PU composite. Besides, the addition of GO into the PU matrix greatly delayed the onset of plastic deformation in PU in a large-deflection bending process. The

average residual height and final specific plastic dissipation energy for PU were approximately 5.6 and 17.7 times as large as those for the studied GO/PU composite. The finite-element analysis provided quantification of the effect of GO enhancement on the large-deflection bending performance of PU for regimes typical for shoe soles and can be used as a basis for optimization of real composite products.

*The work in Chapter 5 is reprinted (adapted) with permission from Jing Q, Liu Q, Li L, Dong Z, Silberschmidt VV. Composites Part B: Engineering. 2016;89:1-8. Copyright 2016 Elsevier. Jing Q is the main contributor to this paper, responsible for the project design, experiments and paper writing. Liu Q provided assistance during the experiments. Li L, Dong Z and Silberschmidt VV offered guidance and advices on experiments and paper writing.

5.1 Introduction

As an alternative to graphene, graphene oxide (GO) is also an attractive nanofiller candidate for development of advanced polymer composite material thanks to its established advantages in the production yield and cost [1]. GO, obtained from the exfoliation of graphite oxide, owns the same framework as graphene and contains numerous oxygen functional groups. Thermoplastic polyurethane (PU) is an important class of polymers, widely used in various applications such as foams, coatings, elastomers and adhesives. PU has a block copolymer structure, with polyol as soft segment and isocyanate and chain extender as hard segment. The molecular structure of PU could be easily adjusted to fulfil different property requirements [2]. Thermoplastic PU elastomers have been used in many sporting applications such as ski tips, ski boots, fins for surfboards, goggles and inline skates. They have been introduced in athletic footwear since the 1970's, and are mostly used as outsole materials for rugby, American football, golf, soccer shoes, and so on [3]. Thermoplastic PU elastomers offer a high level of performance as shoe-sole materials in several aspects. With regard to physical properties, they exhibit good low-temperature performance, great scratch and cut resistance, good resistance to seawater and microbial attack, outstanding flex properties and strong abrasion resistance [4, 5]. They could also be easily coloured and made into different shapes, which is critical for a footwear industry. In addition, they could be produced with matt and glossy areas moulded together [6]. These materials also show great ability to bond with other materials in a shoe thanks to a reactive nature of the urethane linkage. However, it was widely reported that many thermoplastic PU

elastomers were not pure elastic but also exhibiting plasticity [7-9], a deficiency for shoe-sole materials.

Based on the results in Chapter 4, the enhancement effect of FGO on the mechanical properties of PU was significant especially under high strains, while GO exhibited advantages under low strains. In this study, GO was added into a PU matrix to prepare a GO/PU composite via a solution mixing method. The effect of GO on plastic properties of PU was investigated experimentally by means of cyclic tensile tests. Apparently, extending analysis of material's behavior to cases of in-service conditions typical to those of real-life products is very challenging, especially when non-linear factors are considered. This necessitates the use of numerical simulations that has advantages in terms of comprehensive information presented and low costs when compared to parametric experimental studies. Here, in order to study the mechanical performance of PU and GO/PU composite under large-deflection bending typical to shoe soles, the finite-element analysis with Abaqus/Standard was conducted. An elastic-plastic finite-element model was developed to obtain detailed mechanical information for PU and the GO/PU composite and quantify the enhancement effect of GO on the large-deflection bending performance of PU. Results of numerical analysis for the in-service behavior, such as stress concentration and equivalent plastic strain, are useful for the product optimization.

5.2 Experimental

5.2.1 Materials

Graphene oxide (purity > 99%) was provided by XFNANO Materials Tech Co., Ltd. (Nanjing, China) which was synthesized from graphite powders using a common Hummers method. Polycaprolactone diol (PCL, average Mn ~2000 g/mol), 4,4′-methylenebis(phenyl isocyanate) (MDI, molecular weight 250.25 g/mol), 1,4-butanediol (BD, molecular weight 90.12 g/mol), and dibutyltin dilaurate (DBTDL) were all obtained from Sigma-Aldrich. Dimethylformamide (DMF, Tritech Scientific) were used as received.

5.2.2 Preparation of PU and GO/PU composite

In this work, the prepolymerization method [10] was adopted to synthesize thermoplastic PU elastomer (refer to Section 4.2.3 for more details). The solution mixing method was used to prepare a GO/PU composite. First, 20 mg GO was dispersed in 50 ml DMF to form a colloidal suspension with the aid of an ultrasonication bath. Then 4.98 g of the synthesized PU was added into the suspension, corresponding to a 0.4 wt% of GO in the GO/PU composite. After PU was completely dissolved with the assistance of magnetic stirring, a homogenizer was used at 9000 r/min for 15 min, followed by a bath ultrasonication for another 40 min, to ensure homogeneity of the suspension. Finally, a 0.4 wt% GO/PU composite film was obtained by solution casting. As a control group, the pure PU film was prepared according to the same procedure without any addition of GO.

5.2.3 Cyclic tensile tests

Cyclic tensile tests were carried out using an Instron 5569 universal testing machine (Instron, USA). Specimens for tests were prepared based on ISO 527 standard, corresponding to a gauge length of 20 mm. The specimen was loaded to a fixed level of engineering strain of 40% and then unloaded to a position with a force magnitude of 0.05 N. The loading-unloading cycle was repeated 50 times, with both the loading and unloading processes performed at a crosshead speed of 50 mm/min, equivalent to a strain rate of 0.042 s^{-1}. All the tests were conducted at room temperature, and three specimens were tested for each material.

5.3 Experimental results and discussion

In its service as a shoe-sole material, the thermoplastic PU elastomer is exposed to various conditions such as repetitive large-deflection bending. So it is important to understand the material's mechanical response to loading-unloading cycles. The data obtained in cyclic tensile tests is presented in Figure 5.1, exhibiting typical engineering stress-strain curves for PU and the obtained GO/PU composite. It can be clearly seen that PU is not completely elastic within the applied range of engineering tensile strain (40%). An unrecoverable strain was yielded immediately after the first loading-unloading cycle, which is referred to as plastic strain (ε_p). For both materials, the difference between the first and the second loading curves was evident. However, that difference became smaller

and smaller for the subsequent loading-unloading cycles, becoming eventually nearly undistinguishable. Compared with PU, the GO/PU composite showed smaller plastic strain after each loading-unloading cycle, indicating a reduced extent of plasticity.

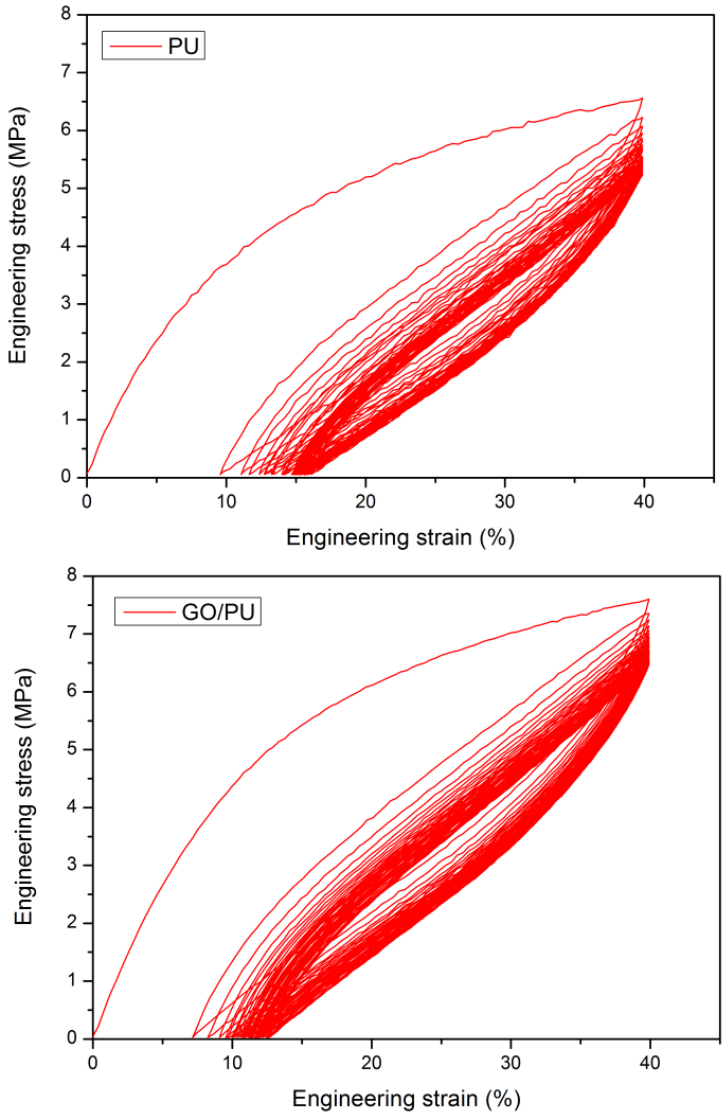

Figure 5.1 Typical engineering stress-strain curves of cyclic tensile tests for PU and GO/PU composite

The process of accumulation of plastic strain is presented in Figure 5.2 providing the values after each cycle (up to 50 cycles) for PU and the GO/PU composite. The plastic strain in PU could be clearly observed; it was attributed to irreversible deformation of its hard segments under external force [9]. The lower value of irreversible strain, which served as an indicator of plasticity, for the GO/PU composite demonstrated that the addition of GO into the PU matrix could effectively reduce plasticity of the thermoplastic PU elastomer. A similar effect was often observed in the shape memory property studies of PU-based nanocomposites, where the addition of nanofillers was able to reduce plasticity of PU [11-13]. A widely accepted reason for reduced plasticity was that nanofillers could inhibit the process of irreversible deformation of hard segments due to interactions between them. As for the studied GO/PU composite, the hydrogen bonding between the oxygen functional groups of GO and urethane linkages of PU could play a significant role in reducing the extent of plasticity of PU [14-16]. Besides, it is apparent that the plastic strain for each material experienced a fast increase at the initial few cycles, becoming nearly stable afterwards. Finally, the plastic strain reached 16.1% and 12.7% for PU and the GO/PU composite, respectively, after 50 loading-unloading cycles.

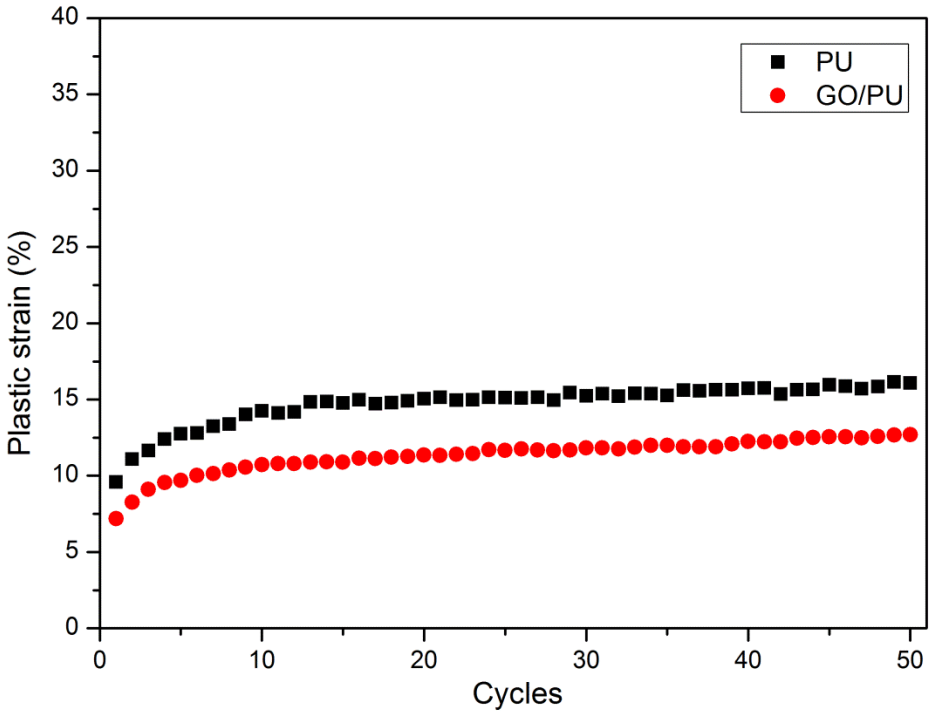

Figure 5.2 Plastic strains after each loading-unloading cycle for PU and GO/PU composite

5.4 Finite-element modelling

For a material exposed to large-deflection bending deformation, as in a case of a shoe sole, the study of relevant mechanical features such as distributions of stresses and plastic deformations as well as plastic dissipation energy are fairly complicated due to non-linear mechanical behavior and non-uniform deformation. The most suitable tool to overcome this is a computational method based on finite-element analysis (FEA) that can obtain comprehensive and detailed information of the studied mechanical behavior at costs lower than that for detailed experimental analysis. In this study, quasi-static finite-element analysis was performed using commercial FE software Abaqus/Standard to evaluate the large-deflection bending performance of the two materials.

5.4.1 Modelling strategy

An elastic-plastic finite-element model was employed to study the mechanical behavior of PU and the GO/PU composite material. As shown previously, plastic strain of each material reached a nearly stable state after 50 loading-unloading cycles. In this study, the modelling was developed based on the stabilized level of plastic strain. The first step was to convert the original engineering stress-strain data into the true stress-strain data using the traditional formulae:

$$\sigma_{True} = \sigma_{Eng} \times (1 + \varepsilon_{Eng}) \quad (1)$$

$$\varepsilon_{True} = \ln(1 + \varepsilon_{Eng}) \quad (2)$$

where σ_{Eng}, ε_{Eng}, σ_{True} and ε_{True} are the engineering stress and strain, and true stress and strain, respectively.

The value of true plastic strain after 50 loading-unloading cycles ($\varepsilon_{P\text{-}50}$) was taken to calculate the elastic modulus for Abaqus input. As the total true strain (ε_{Total}) could be divided into its elastic component (ε_e) and plastic component (ε_p) [17, 18], as

$$\varepsilon_{Total} = \varepsilon_e + \varepsilon_p \quad (3)$$

So the elastic modulus (E) could be obtained from the following relation,

$$E = \frac{\sigma_{\text{ref}}}{\varepsilon_{ref} - \varepsilon_{p-50}} \tag{4}$$

where ε_{ref} is the true strain equivalent to the pre-defined 40% engineering strain, σ_{ref} is the true stress corresponding to the engineering strain of 40% in the first loading-unloading cycle. The Poisson's ratio was taken as 0.3. For input of plastic behavior into Abaqus, a tabular form for the data on true yield stress and corresponding true plastic strain was used. As illustrated in Figure 5.3, for certain point M ($\varepsilon_{M,}$ σ_M) on the first loading curve, its true yield stress equaled to the true stress (σ_M). And the corresponding true plastic strain ($\varepsilon_{P(M)}$) was calculated based on the following formula:

$$\varepsilon_{P(M)} = \varepsilon_M - \frac{\sigma_M}{E} \tag{5}$$

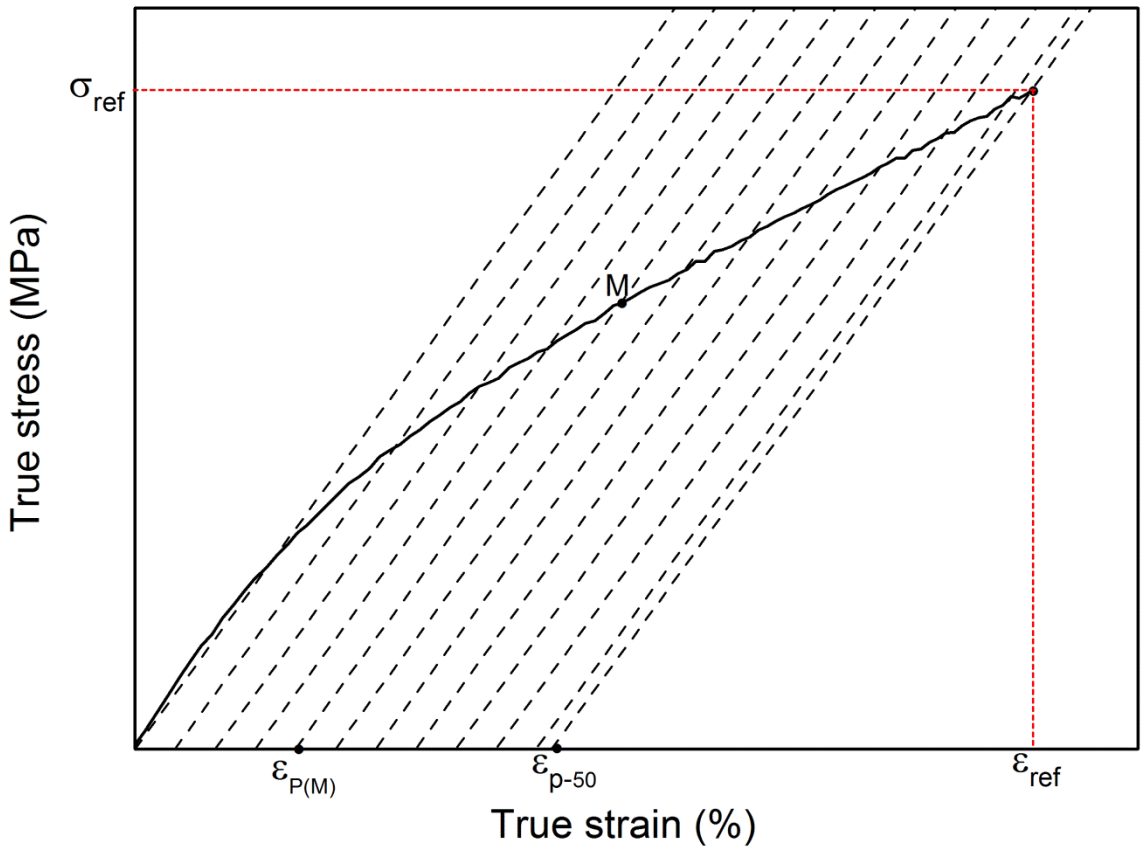

Figure 5.3 Schematic of the calculation of true plastic strain

5.4.2 Geometry and boundary conditions

A FE model as shown in Figure 5.4 was developed to simulate large-deflection bending deformation of a shoe sole, whose geometry was simplified as a flat specimen with a length, width and height of 24.0 cm, 8.5 cm and 2.0 cm, respectively. Besides, an analytical rigid plane was created to simulate the ground that the shoe sole will contact with. A pressure of 1 MPa was applied at the first quarter of the top surface (AC in Figure 5.4) of the sole model, while the bottom surface was in contact with the ground. Other boundary conditions, applied in a local cylindrical coordinate system, included: (i)

constrained translations at Point B; (ii) anticlockwise rotation of surface EF; (iii) all translations and rotations of the ground were constrained. A contact between the bottom surface of the material and the ground was defined as follows: (i) small sliding formulation; (ii) node-to-surface discretization method; (iii) 0.2 degree of smoothing for master surface; (iv) selectively use supplementary contact points. For the normal behaviour of the interaction, it was controlled with: (i) "Hard" contact for pressure-overclosure; (ii) Augmented Lagrange (Standard) constraint enforcement method; (iii) allow separation after contact; (iv) default contact stiffness value; (v) 1 for stiffness scale factor.

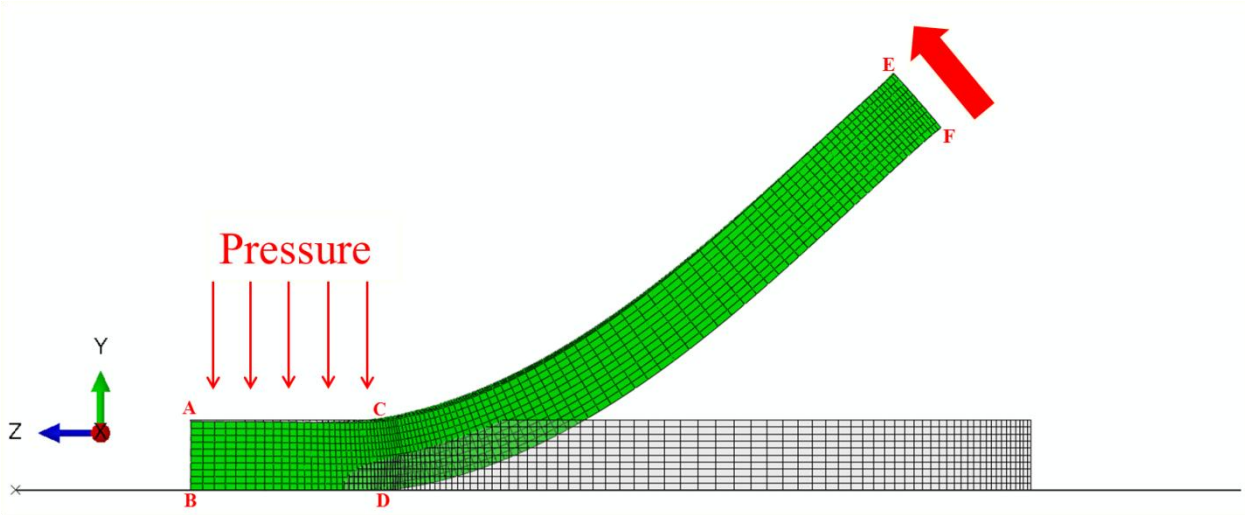

Figure 5.4 FE model for simulation of bending of shoe sole

5.4.3 Mesh

The modelled sole was meshed with 8-noded linear hexahedral elements of type C3D8R, using a structured meshing technique. Prior to performing simulations, the mesh convergence was studied with different mesh densities. The mesh densities ranged from a total of 1440 elements (minimum element length of 1.6 mm) to a total of 25200 elements (minimum element length of 0.7 mm). As is shown in Figure 5.5, the residual height (refer to section 5.5.3) increased with the increasing total element numbers and solution convergence was achieved. The final model, containing a total of 18900 elements and 22154 nodes (minimum element length of 0.7 mm), was chosen for computationally effective simulations.

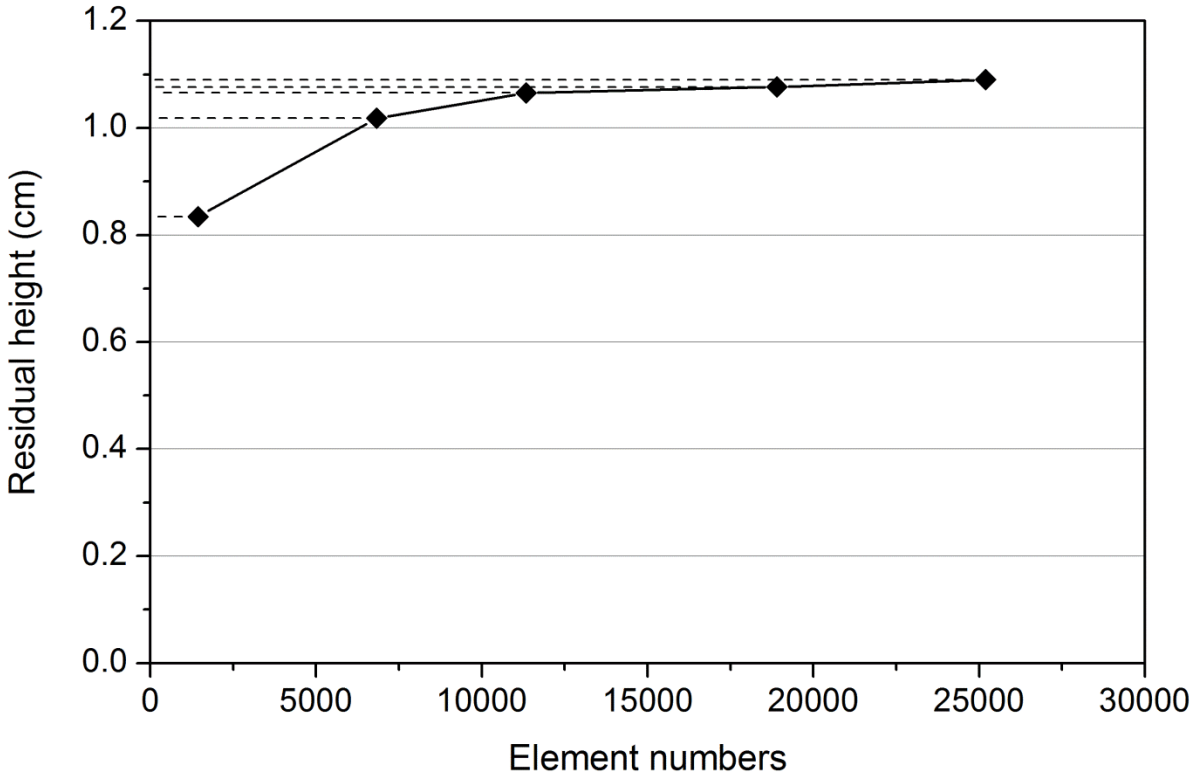

Figure 5.5 Residual height sensitivity to total element numbers

5.5 Simulation results and discussion

5.5.1 Uniaxial tensile tests

In order to verify the accuracy of the constructed elastic-plastic model, a quasi-static finite-element simulation of uniaxial tensile test was performed using the Abaqus/Standard. The true stress-strain curves of PU and the GO/PU composite from both experimental studies and finite-element simulation are presented in Figure 5.6. As can be seen, the data obtained in FE analysis was highly consistent with those from our experiments, demonstrating that the constructed elastic-plastic model was able to adequately describe the mechanical behavior of the studied materials, which was the basis for the subsequent simulations.

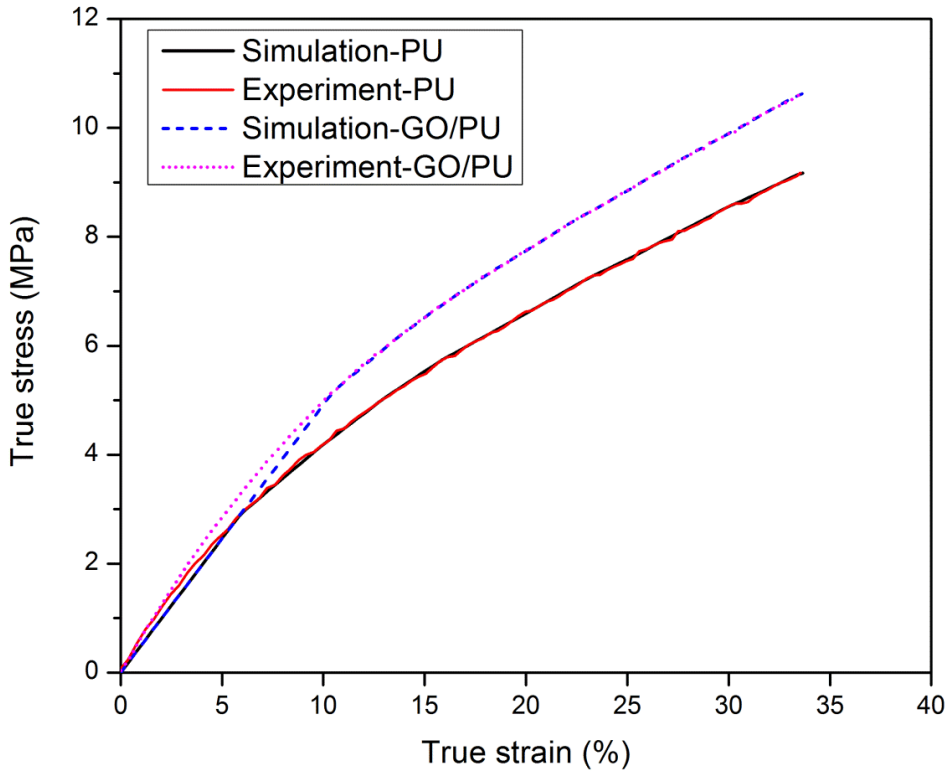

Figure 5.6 True stress-strain curves of PU and GO/PU from experiment and simulation

5.5.2 Stress distribution

The results of finite-element simulations for distribution of the von Mises stress in the model are presented in Figure 5.7 for two viewing angles both for PU and the GO/PU composite for the highest level of deflection. It is obvious that von Mises stress was mostly concentrated in the bending part of the model. The bottom surface of the bending part showed higher stress concentration than the top surface, because it was subjected to larger deformation. Besides, the GO/PU composite exhibited higher levels of von Mises stress compared with those in PU. From inspection, the maximum von Mises stress for PU and the GO/PU composite was found to be 5.36 MPa and 6.05 MPa, respectively. The detailed information of von Mises stress distribution obtained from the simulation results can be very useful for product optimization, either by changing the material or adjusting the geometry, when extending analysis to in-service behavior of real products.

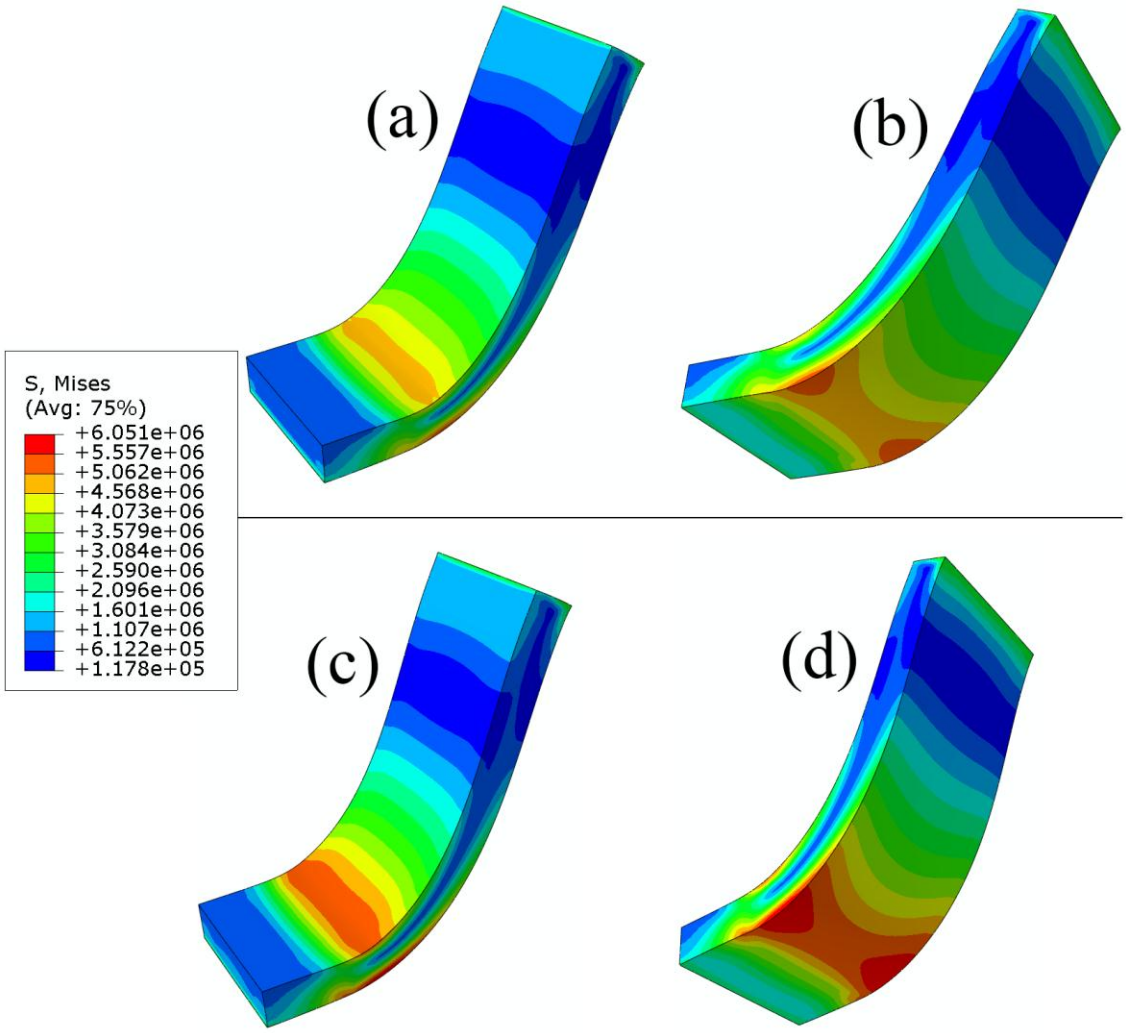

Figure 5.7 Contour of von Mises stress (in Pa) distribution for two viewing angles for PU (a, b) and GO/PU composite (c, d) at highest level of deflection

5.5.3 Residual Height

After reaching the maximum deformation, the boundary condition applied on surface EF (Figure 5.4) was released and the model of sole returned to a position where no further displacement would happen. Due to the onset of plasticity, the initial state could not be

reached after unloading in high-deflection bending. In Figure 5.8a, the contours of equivalent plastic strain (PEEQ) of the side surface for PU and the GO/PU composite are presented. Apparently, both models could not return to their original shapes, exhibiting unrecoverable deformations. The distance between the bottom edge F (Figure 5.4) and the ground was noted as 'residual height' and recorded along with the simulation time. Obviously, the residual height for PU was more significant than that of the GO/PU composite. Additionally, a larger zone of plastic deformation was observed in PU (as indicated by the PEEQ contour), which was consistent with the results for residual-height difference. The height-time history output for PU and the GO/PU composite is shown in Figure 5.8b (time was a mere parameter in this quasi-static study). Both curves exhibited a plateau after unloading (from time of 2.0), indicating that the model experienced no further deformation afterwards and proving completion of the 'unbending' process for each material. Meanwhile, a direct quantitative comparison between the residual heights of PU and the GO/PU composite could be observed through the curves (detailed information is included in Table 5.2).

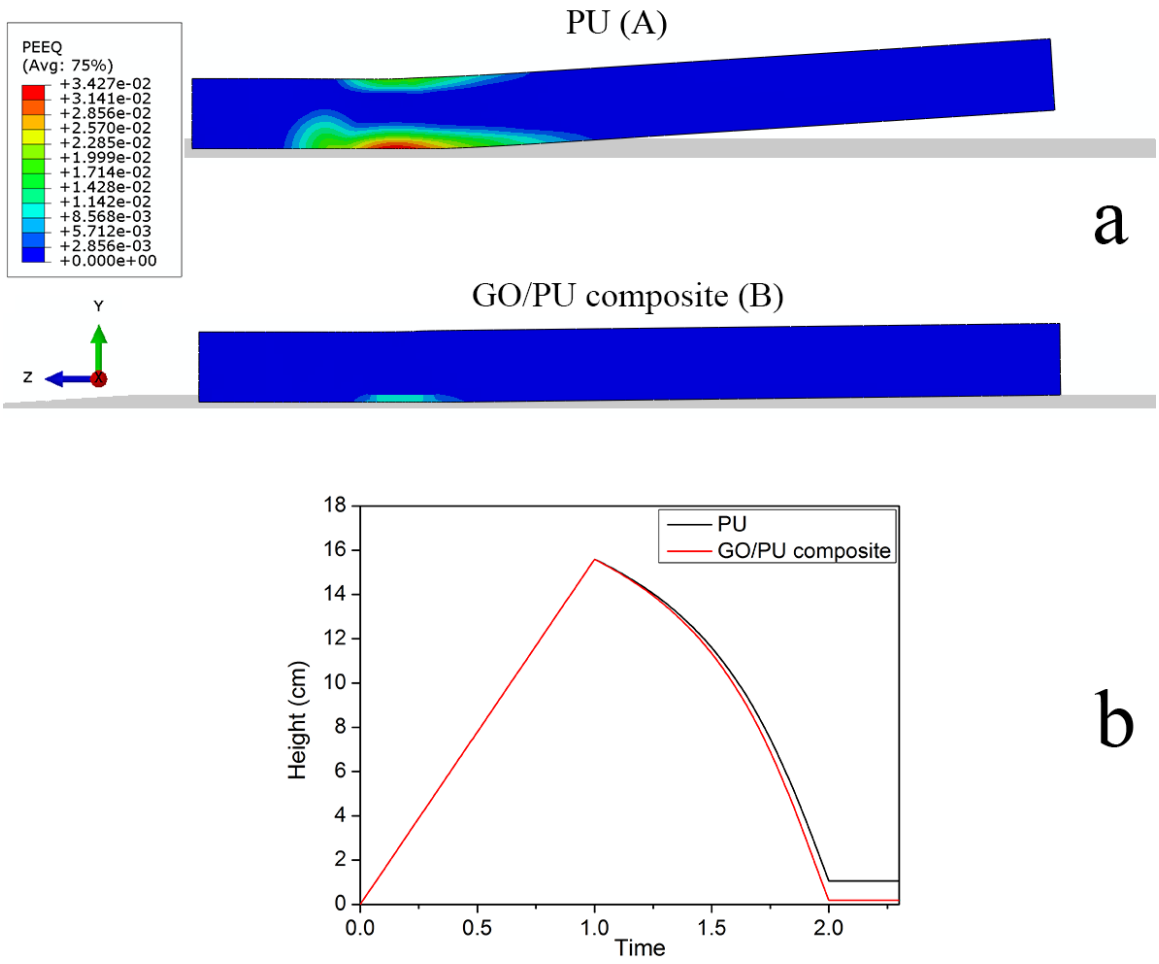

Figure 5.8 (a) Contours of equivalent plastic strain (PEEQ) of side surfaces for PU (A) and GO/PU composite (B) (b) Height-time curves for PU and GO/PU composite

5.5.4 Plastic zone

A separate study focussed on the size of plastic zone: Figure 5.9 shows the contours of equivalent plastic strain (PEEQ) of the top and bottom surfaces for pure PU and the GO/PU composite. It is obvious that PU has much larger plastic areas for all the three

surfaces – side surface (Figure 5.8a-A), top surface (Figure 5.9-C) and bottom surface (Figure 5.9-D).

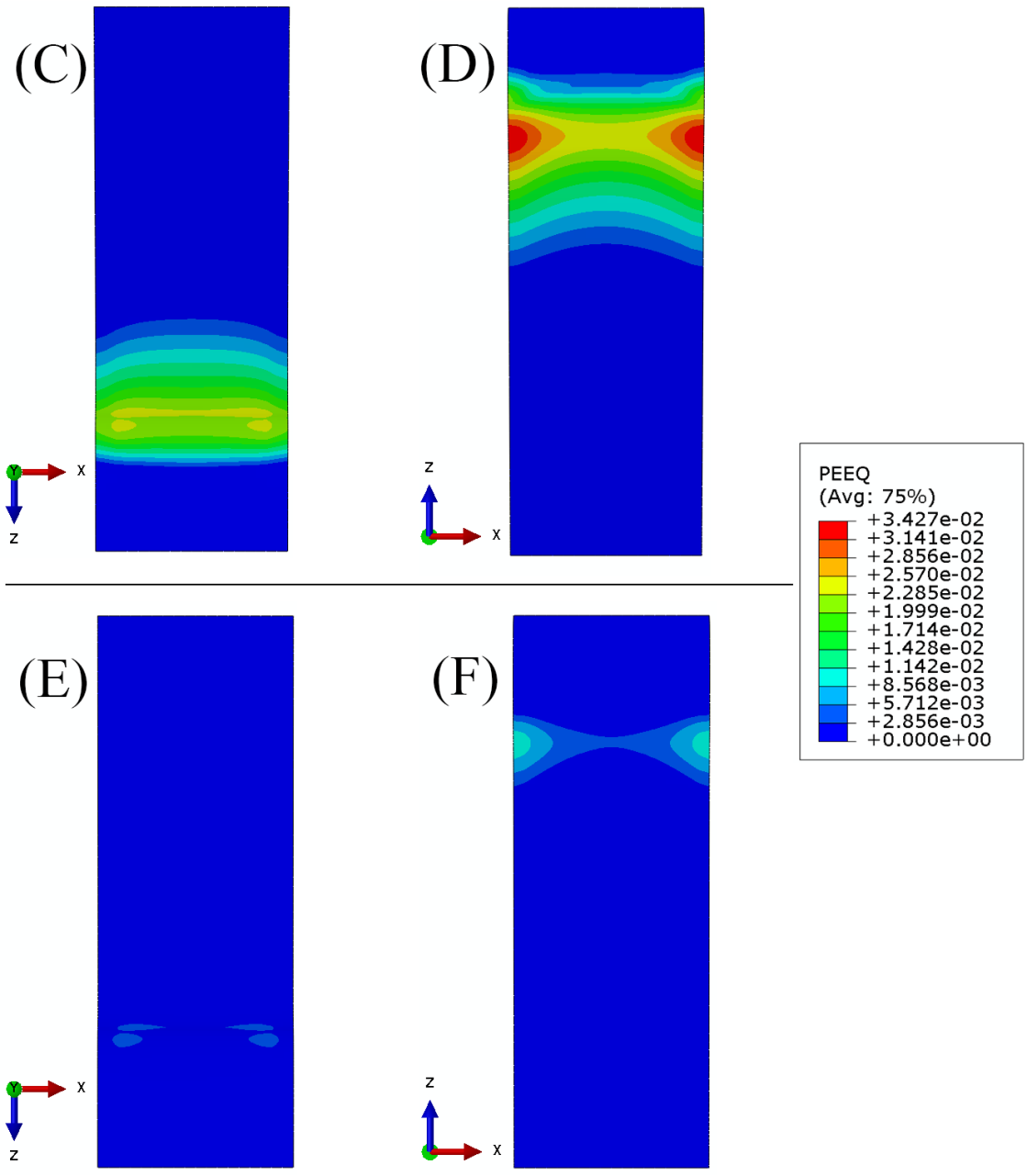

Figure 5.9 Contours of equivalent plastic strain (PEEQ) of top surfaces (C, E) and bottom surfaces (D, F) for PU (C, D) and GO/PU composite (E, F)

In order to quantitatively describe the difference of plastic areas for the two studied materials, the areas with plastic deformation (i.e. colours of PEEQ contours) were measured with the software Photoshop and expressed as numbers of pixels, as shown in Table 5.1. Obviously, the initial total areas of the three surfaces were the same for both materials. After the loading-unloading process of the model in the simulation, the total area and plastic areas were measured for all three surfaces. Then, the fraction of plastic area after unloading was obtained by dividing the plastic area with the respective total area (due to irreversible deformation the latter differed from the initial total area). The respective fractions for the side, top and bottom surfaces for PU were 12.6, 21.3 and 4.7 times as large as those for the GO/PU composite.

Table 5.1 Areas measured based on PEEQ contour

	Initial total area (pixels)	Total area after unloading (pixels)	Plastic area (pixels)	Plastic area fraction (%)
PU				
Side surface	165200	187312	28197	15.1
Top surface	181830	175802	44806	25.5
Bottom surface	181830	177669	58776	33.1
GO/PU				
Side surface	165200	188072	2227	1.2
Top surface	181830	180345	2167	1.2
Bottom surface	181830	180678	12630	7.0

5.5.5 Specific plastic dissipation energy

Numerical simulations allow calculating other important mechanical features that can be hardly obtained in experimental tests: Figure 5.10 shows evolution of specific plastic dissipation energy in PU and the GO/PU composite in a loading-unloading cycle. At the initial stage of loading, there was no plastic dissipation of energy, indicating that this stage was completely elastic. Then, plastic dissipation energy started to arise and reached its peak at the highest deflection. Finally, during the unloading process, the specific plastic dissipation energy kept constant till the end of this process, since there was no further plastic deformation induced. Compared with PU, the GO/PU composite exhibited a significantly lower value of the final specific plastic dissipation energy (detailed information is given in Table 5.2). More importantly, the point, from which the curve started to climb, revealed the point of bending process corresponding to the onset of plastic deformation. Observed from the data, the PU started to yield at a height of 8.73 cm, while that process was delayed to a height of 13.56 cm for the GO/PU composite. This information is very helpful for the design of shoe soles allowing to reduce plastic deformation, or even to avoid it completely.

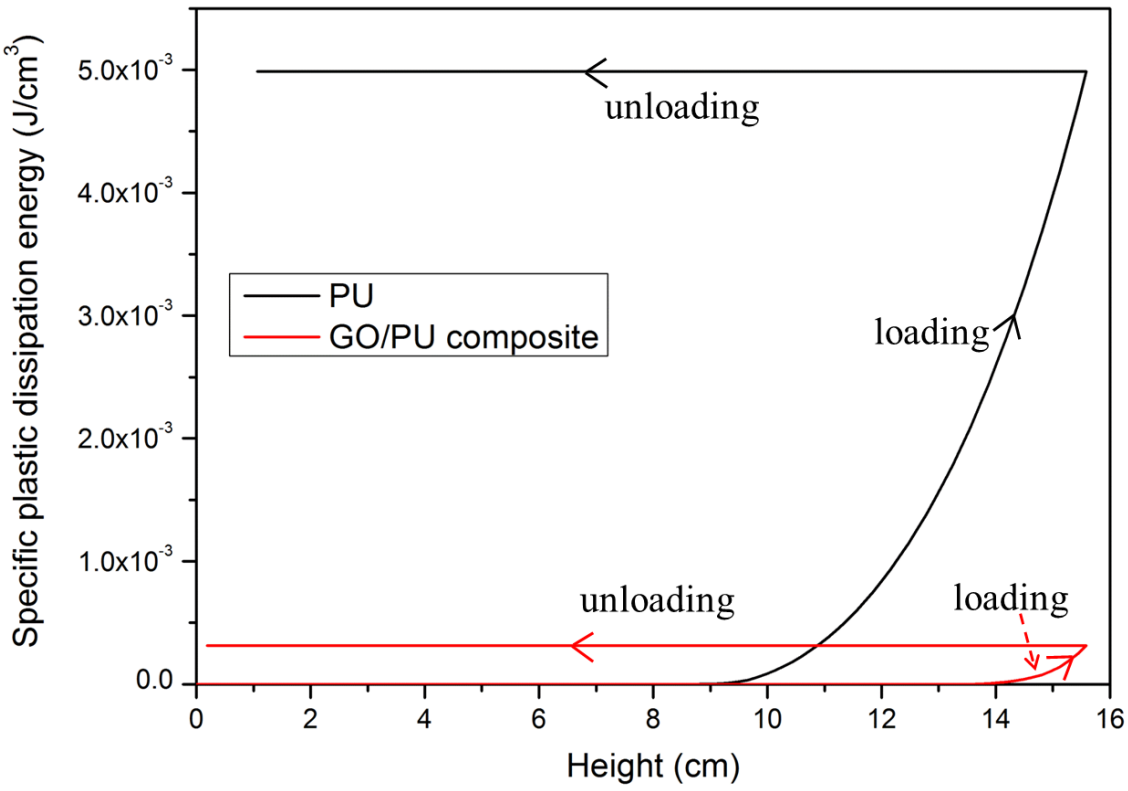

Figure 5.10 Evolution of specific plastic dissipation energy with deflection (height) for PU and GO/PU composite

Three specimens of the two studied materials were analysed in the experimental cyclic tensile tests, as well as in the subsequent finite-element simulations based on the stress-strain curves obtained for each specimen. The values of residual height and final specific plastic dissipation energy are listed in Table 5.2 together with their averages. As can be seen, the average residual height for the PU model was 1.07 cm, approximately 5.6 times as large as that for the model of the GO/PU composite. The average final specific plastic dissipation energy for PU was 5.17×10^{-3} J/cm^3, almost 17.7 times as large as that for the studied composite.

Table 5.2 Residual height and final specific plastic dissipation energy of three specimens for each material: PU and GO/PU composite

	Residual Height (cm)	Final specific plastic dissipation energy (J/cm^3)
PU-1	1.08	4.99×10^{-3}
PU-2	1.24	6.17×10^{-3}
PU-3	0.89	4.37×10^{-3}
Average	1.07	5.17×10^{-3}
GO/PU-1	0.20	3.13×10^{-4}
GO/PU-2	0.18	2.73×10^{-4}
GO/PU-3	0.20	2.92×10^{-4}
Average	0.19	2.92×10^{-4}

5.6 Summary

GO, containing massive oxygen functional groups on its surfaces and edges, was used as the nanofiller to prepare a GO/PU composite. Based on the experimental cyclic tensile tests, the level of plastic strains for both PU and the GO/PU composite became nearly stable after 50 loading-unloading cycles, and the extent of plasticity of PU was demonstrated to be reduced with the addition of GO. Additionally, in order to study the mechanical performance of PU and the GO/PU composite under conditions of large-deflection bending deformation, typical for shoe soles, the finite-element analysis was conducted with Abaqus/Standard. An elastic-plastic finite-element model was developed to obtain the detailed mechanical information for pure PU and the composite. Both

experiment and simulation results of the uniaxial tensile tests were highly consistent, thus verifying the accuracy of the constructed model. From the performed numerical simulations of the large-deflection bending for both materials, it was found that the von Mises stress was mostly concentrated at the bending part of the model, and the GO/PU composite exhibited higher von Mises stress overall compared with that in PU. More importantly, the plastic area, final specific plastic dissipation energy and residual height for PU were significantly larger than those of the GO/PU composite. Besides, the addition of GO into the PU matrix greatly delayed the onset of plastic deformation in PU in the large-deflection bending process. Simulations of three specimens of each material based on experimentally obtained stress-strain data, demonstrated that the average residual height for PU was 1.07 cm, i.e. approximately 5.6 times as large as that for the GO/PU composite. The average final specific plastic dissipation energy for PU was 5.17×10^{-3} J/cm^3, almost 17.7 times as large as that for the GO/PU composite. The detailed mechanical information from the finite-element analysis quantitatively revealed the enhancing effect of GO on the large-deflection bending performance of PU and can be used for design and optimization of shoe soles of real products.

References

[1] Park S, Ruoff RS. Chemical methods for the production of graphenes. Nature Nanotechnology. 2009;4(4):217-24.

[2] Šebenik U, Krajnc M. Influence of the soft segment length and content on the synthesis and properties of isocyanate-terminated urethane prepolymers. International Journal of Adhesion and Adhesives. 2007;27(7):527-35.

[3] Ames KA. Elastomers for shoe applications. Rubber chemistry and technology. 2004;77(3):413-75.

[4] Camargo RE, Roberts CM, Limerkens N. Thermoplastic Polyurethanes: New Material Options for High Performance Footwear. Polyurethanes Conference 2000: proceedings of the Polyurethanes Conference 2000: October 8-11, 2000, Boston, Massachusetts: American Plastics Council; 2000. p. 49.

[5] Inc CC. UTECH Asia '99: Conference Book of Papers : the International Polyurethanes Conference & Exhibition for Asia-Pacific : March 16-18, 1999, Suntec City, Singapore: Crain Communications; 1999.

[6] Salm W. Almost like flying. Kunststoffe-Plast Europe. 1999;89(7):118-20.

[7] Buckley CP, Prisacariu C, Martin C. Elasticity and inelasticity of thermoplastic polyurethane elastomers: Sensitivity to chemical and physical structure. Polymer. 2010;51(14):3213-24.

[8] Prisacariu C. Polyurethane elastomers: from morphology to mechanical aspects: Springer Science & Business Media; 2011.

[9] Christenson EM, Anderson JM, Hiltner A, Baer E. Relationship between nanoscale deformation processes and elastic behavior of polyurethane elastomers. Polymer. 2005;46(25):11744-54.

[10] Cho JW, Kim JW, Jung YC, Goo NS. Electroactive shape-memory polyurethane composites incorporating carbon nanotubes. Macromolecular Rapid Communications. 2005;26(5):412-6.

[11] Park J, Kim B. Infrared light actuated shape memory effects in crystalline polyurethane/graphene chemical hybrids. Smart Materials and Structures. 2014;23(2):025038.

[12] Choi JT, Dao TD, Oh KM, Lee H-i, Jeong HM, Kim BK. Shape memory polyurethane nanocomposites with functionalized graphene. Smart Materials and Structures. 2012;21(7):075017.

[13] Deka H, Karak N, Kalita RD, Buragohain AK. Biocompatible hyperbranched polyurethane/multi-walled carbon nanotube composites as shape memory materials. Carbon. 2010;48(7):2013-22.

[14] Han S, Chun BC. Preparation of polyurethane nanocomposites via covalent incorporation of functionalized graphene and its shape memory effect. Composites Part A: Applied Science and Manufacturing. 2014;58:65-72.

[15] Prisacariu C, Scortanu E. Sensitivity to the physical and chemical structure of hard-segment-reinforced polyurethane elastomers with variable percentage of hydrogen bonding. Journal of Applied Polymer Science. 2011;122(6):3544-50.

[16] Park J, Dao T, Lee H-i, Jeong H, Kim B. Properties of Graphene/Shape Memory Thermoplastic Polyurethane Composites Actuating by Various Methods. Materials. 2014;7(3):1520-38.

[17] Bonet J, Wood RD. Nonlinear continuum mechanics for finite element analysis: Cambridge university press; 1997.

[18] Shabana A. Computational continuum mechanics. 2008. Cambridge University Press, New York.

Chapter 6 Conclusions and recommendations for future work

6.1 Conclusions

In this project, polyurethane (PU)-based composites with improved mechanical properties and thermal stability were prepared via a solution mixing method with addition of carbon nanomaterials: multi-walled carbon nanotubes (MWCNTs) and graphene oxide (GO). MWCNTs and GO were specifically functionalized based on their particular physical structures and chemical properties, as well as the PU matrix. As a result, a better compatibility between nanofillers and the PU matrix was achieved.

As for the MWCNTs, polycaprolactone diol (PCL) - one of the monomers of PU - was selected to covalently functionalize MWCNTs, resulting in MWCNT-PCL, with carboxylic acid groups functionalized MWCNTs (MWCNT-COOH) and raw MWCNTs served as control. Both MWCNT-COOH and MWCNT-PCL improved dispersion of nanofillers in the PU matrix and interfacial bonding between them at 1 wt% loading content. The MWCNT-PCL/PU composite showed the largest extent of improvement in both mechanical properties and thermal stability. Performed tensile tests showed that the tensile strength, modulus, elongation at break and toughness of MWCNT-PCL/PU composite were significantly improved by 51.1%, 32.8%, 19.8% and 57.9%, respectively, as compared to pure PU. Regarding thermal stability, $T_{2\%}$ and $T_{50\%}$ of MWCNT-PCL/PU

composite were increased by 38 ℃ and 35 ℃, respectively, as compared to pure PU. These remarkable improvements for the MWCNT-PCL/PU composite were attributed to the homogeneous dispersion of MWCNT-PCL in the PU matrix and strong interfacial interactions between them.

As for GO, 4, 4′-methylenebis (phenyl isocyanate) (MDI) and PCL - the two monomers of PU - were covalently grafted onto GO, resulting in the functionalized GO (FGO). After the functionalization, the GO was partially reduced. The covalently grafted MDI and PCL on the surface of FGO could not only improve the dispersions of FGO in the DMF solvent and PU matrix, but also provide a good compatibility between FGO and the PU matrix. The most efficient improvement of mechanical properties was achieved when 0.4 wt% FGO was added into the PU matrix, resulting in the increases of tensile stress, elongation at break and toughness by 34.2%, 27.6% and 64.5%, respectively, compared with those of PU. At the same loading content, the 0.4 wt% FGO/PU composite showed lower stiffness yet higher toughness and ductility compared with the 0.4 wt% GO/PU composite. Besides, the 1 wt% FGO/PU composite showed the largest reinforcement of thermal stability, with $T_{2\%}$ and $T_{50\%}$ 16 ℃ and 21 ℃ higher than those of PU, respectively. The achieved homogeneous dispersion of FGO in the PU matrix and strong interfacial interactions between them could contribute to the improvement in mechanical properties and thermal stability of FGO/PU composites.

The method employing monomer-functionalized nanomaterials to reinforce PU was demonstrated to be very effective based on the studies involved with MWCNTs and GO.

It is also expected to be applicable to other nanomaterials and different types of PU. Moreover, since the monomer of a polymer is generally well compatible with the polymer itself, this method is promising for preparing many other polymer composites as well.

The finite-element analysis (FEA) with Abaqus/Standard software was conducted to study the mechanical performance of PU and its composite under conditions of large-deflection bending, typical for shoe soles. Based on the results of the previous study, the enhancing effect of FGO on the mechanical properties of PU was significant, especially under high strains, while GO exhibited advantages under low strains. In this work, the GO/PU composite was further studied and the effect of GO enhancement on the large-deflection bending performance of PU was revealed. Based on the experimental cyclic tensile studies, the level of plastic strains for both PU and the GO/PU composite became nearly stable after 50 loading-unloading cycles, and the extent of plasticity of PU was demonstrated to reduce with the addition of GO. In addition, an elastic-plastic finite-element model was developed for numerical simulations, and the results showed that the plastic area, final specific plastic dissipation energy and residual height for PU were significantly larger than those for the GO/PU composite. Besides, the addition of GO into the PU matrix greatly delayed the onset of plastic deformation in PU in the large-deflection bending process. The average residual height and final specific plastic dissipation energy for PU were approximately 5.6 and 17.7 times as large as those for the studied GO/PU composite. The FEA results can be used for design and optimization of shoe soles of real products.

6.2 Recommendations for future work

6.2.1 Carbon nanomaterials/PU composites prepared via melt processing

Applying the melt processing method to prepare polymer-based composites is of great interest for industrial production because it is environmentally friendly and economical thanks to the absence of solvents. This simple and common method is particularly useful for thermoplastic polymers, e.g. PU. During melt processing, nanomaterials are mechanically dispersed in the polymer matrix under high temperature using a high shear force compounder or mixer [1]. The shear force could break up aggregates of nanomaterials and contribute to their dispersion in the polymer matrix. However, it is also reported that high-intensity shears may cause fracture of nanomaterials. And, a short processing time may be inefficient for high levels of dispersion [2]. So it is important to optimize the melt processing conditions including time, temperature and screw speed. Besides, the covalently functionalized MWCNTs or GO, as prepared in our project, is capable to provide a good compatibility with the PU matrix, which is crucial for the dispersion of nanomaterials, especially when no solvent is involved. With effective functionalization of nanomaterials, we can expect not only a better dispersion state but also a higher loading content in the polymer matrix.

6.2.2 Tribological properties of composites

The tribological properties of polymer composites have attracted considerable attention due to their importance for various applications, such as ultra-light weight aerospace

structures, gears, bearings, bullet-proof helmets and shoe soles etc. The presence of carbon nanomaterials in the polymer matrix has been reported to enhance the tribological performance of the polymer. They could effectively impede the propagation process of microcracks, leading to improved wear resistance of the composite material. In particular, graphene nanofillers present outstanding self-lubricant features owing to the exclusive graphitic layers, easy shear capability on the atomically smooth surface and remarkably high strength [3, 4]. Graphene has shown a huge potential to be applied as high-performance lubricant for polymers. For example, it was reported by Xiaojun *et al*. [5] that a small amount of GO in the epoxy matrix could significantly improve the wear resistance of epoxy. Zhixin *et al*. found that the tribological performance of ultra-high-molecular-weight PE was remarkably enhanced with the addition of GO [6]. Hence, tribological properties of the PU-based composites reinforced by GO are worthy to be further studied.

6.2.3 Further simulation

Obviously, pressure of feet applied on the shoe sole is not even, and this needs to be considered for shoe sole design. The future simulation work may develop a model reflecting a real shape of a shoe sole, with unevenly distributed pressure in the model. Such a distribution of pressure is supposed to have a significant effect on the large-deflection bending behavior of the studied materials. Also, viscous properties of materials need to be included in the simulation so as to achieve a more accurate visco-elastic-plastic model. Besides, viscosity of materials can be characterized with dynamic

mechanical analysis (DMA) and included in the numerical analysis to evaluate the dynamic performance of materials. With dynamic modelling, the influence of bending rate (i.e. walking/running), weight of individual, etc. can be studied, thus providing more comprehensive and applicable information for design and optimization of shoe sole products.

References

[1] Andrews R, Jacques D, Minot M, Rantell T. Fabrication of carbon multiwall nanotube/polymer composites by shear mixing. Macromolecular Materials and Engineering. 2002;287(6):395-403.

[2] Borse NK, Kamal MR. Estimation of stresses required for exfoliation of clay particles in polymer nanocomposites. Polymer Engineering & Science. 2009;49(4):641-50.

[3] Berman D, Erdemir A, Sumant AV. Graphene: a new emerging lubricant. Materials Today. 2014;17(1):31-42.

[4] Lee C, Li Q, Kalb W, Liu X-Z, Berger H, Carpick RW, et al. Frictional characteristics of atomically thin sheets. Science. 2010;328(5974):76-80.

[5] Shen X-J, Pei X-Q, Fu S-Y, Friedrich K. Significantly modified tribological performance of epoxy nanocomposites at very low graphene oxide content. Polymer. 2013;54(3):1234-42.

[6] Tai Z, Chen Y, An Y, Yan X, Xue Q. Tribological behavior of UHMWPE reinforced with graphene oxide nanosheets. Tribology Letters. 2012;46(1):55-63.

APPENDIX: List of Publications

Journal

1. **Jing Q**, Law JY, Tan LP, Silberschmidt VV, Li L, Dong Z. Preparation, characterization and properties of polycaprolactone diol-functionalized multi-walled carbon nanotube/thermoplastic polyurethane composite. Composites Part A: Applied Science and Manufacturing. 2015;70:8-15.
2. **Jing Q**, Liu W, Pan Y, Silberschmidt VV, Li L, Dong Z. Chemical functionalization of graphene oxide for improving mechanical and thermal properties of polyurethane composites. Materials & Design. 2015;85:808-14.
3. **Jing Q**, Liu Q, Li L, Dong Z, Silberschmidt VV. Effect of graphene oxide enhancement on large-deflection bending performance of thermoplastic polyurethane elastomer. Composites Part B: Engineering. 2016;89:1-8.

Conference

4. **Jing Q**, Silberschmidt VV, Li L, Dong Z. Improved dispersion of multi-walled carbon nanotubes in polyurethane via chemical functionalization. 1st International Conference in Sports Science & Technology. Singapore. 2014.